Faculdade de Engenharia da Universidade do Porto
Instituto de Ciências Biomédicas Abel Salazar

Assessing reactive astrogliosis in Parkinson's brain with astroglial tracers BU99008 and Deprenyl

Filipa Monteiro Neves Rocha

Mestrado em Bioengenharia Molecular

Supervisor: Amit Kumar, PhD

Institutional advisor: Professor Carlos Reguenga, PhD

Junho 2023

© Filipa Monteiro Neves Rocha, 2023

Assessing reactive astrogliosis in Parkinson's brain with astroglial tracers BU99008 and Deprenyl

Filipa Monteiro Neves Rocha

Mestrado em Bioengenharia Molecular

The work presented in this thesis was fully developed at the following institution:

Karolinska Institutet, Stockholm, Sweden



Karolinska Institutet

Funding

This study was financially supported by the Swedish Foundation for Strategic Research (SSF; RB13-0192), the Swedish Research Council (projects 2017-02965, 2017-06086,2020-01990), the Stockholm County Council -Karolinska Institute regional agreement on medical training and clinical research (ALF grant), the Swedish Brain Foundation, the Swedish Alzheimer Foundation, the Foundation for Old Servants, Gun and Bertil Stohne's Foundation, Magnus Bergvall's Foundation, the Swedish Dementia Foundation, the Center for Innovative Medicine (CIMED) Region Stockholm, Åhlens Foundation, the Alzheimer Association USA (AARF -21-848395), Loo and Hans Osterman Foundation for Medical Research, and the Recherche sur Alzheimer Foundation (Paris, France).

Resumo

A doença de Parkinson (DP) é a segunda doença neurodegenerativa mais comum e estima-se que, até 2040, afetará cerca de 12.9 milhões de pessoas em todo o mundo. Neurodegeneração, deposição de *Lewy Bodies (LBs)* e neuroinflamação são características prominentes da doença.

A neuroinflamação, mediada por células da glia, desempenha um papel importante no desenvolvimento e progressão das doenças neurodegenerativas e, na DP, está associada à neurodegeneração e à formação de *LBs*, realçando a importância deste processo. Os astrócitos, células da glia fundamentais para a homeostease do cérebro, como resposta à lesão cerebral, tornam-se reactivos, envolvendo-se num processo caracterizado por alterações bioquímicas, morfológicas, metabólicas e fisiológicas – **astrogliose reativa**.

Deste modo, vários marcaradores astrocíticos têm revelado uma forte correlação com patologias neurodegenerativas, levando alguns destes a ser propostos como biomarcadores ideais para tomografia por emissão de positrões (PET) cerebral. Entre estes, a monoaminoxidase (MAO)-B e os receptores ou locais de ligação da imidazolina-2 (I_2BS) que se encontram sobreexpressos nos astrócitos em múltiplas regiões cerebrais.

Avanços na imagiologia por PET levaram ao desenvolvimento de radiotraçadores específicos, capazes de visualizar a astrogliose reativa, permitindo que este processo seja estudado em pacientes. O **Deprenyl** e o **BU99008**, que se ligam, respetivamente, a MAO-B e aos I_2BS, têm vindo a revelar potencial para analisar este mecanismo com precisão. No entanto, não foram realizados ainda estudos de validação pré-clínica ou de imagiologia *postmortem* utilizadando estes marcadores astrocíticos de PET em DP.

Posto isto, o presente estudo abordou esta lacuna na área, avaliando o comportamento de ligação de Deprenyl e de BU99008 em tecido cerebral *postmortem* de pacientes de DP e de controlos cognitivamente saudáveis (CN). Foram efetuados ensaios de ligação de radioligandos (saturação, competição e distribuição regional) e estudos de imagiologia cerebral *postmortem*, utilizando secções cerebrais congeladas em autoradiografias.

Os estudos de saturação mostraram que a densidade máxima de ligação ao recetor (Bmax) de ^{3}H-BU99008 no caudado da DP é 3 vezes superior à de CN, porém, relativamente inferior no córtex frontal. Em contraste, ^{3}H-Deprenyl mostrou um Bmax 1,2 vezes superior no córtex frontal de DP, em comparação com CN e um valor comparável no caudado.

Os ensaios comparativos e de competição de ^{3}H-BU99008 e ^{3}H-Deprenyl revelaram múltiplos locais de ligação com diferentes afinidades (SHA - super elevada, HA - elevada e LA – baixa afinidade) nos cérebros de DP e CN. Ambos mostraram maior % de ligação (86%-100%) a um local de ligação HA, o que foi corroborado pelos resultados de estudos de competição entre - ^{3}H-BU990008 vs. *unlabeled* Deprenyl e ^{3}H-Deprenyl vs. *unlabeled* BU99008, nos quais não se observou *displacement* deste local de ligação.

A avaliação do padrão de distribuição regional de ^{3}H-BU99008 mostrou uma ligação mais pronunciada (~50% mais elevada) no caudado dos casos de DP. A autoradiografia utilizando ^{3}H-BU99008 demonstrou um aumento de ligação de 78% no caudado e de 81% no córtex temporal dos casos de DP, em comparação com os CN. Foi identificada, apesar de baixa, uma proporção de ligação *off target* na autoradiografia com bloqueio prévio da MAO-B, possivelmente causada pelo I_2BS na MAO-B. Porém, deteteram-se valores elevados e consistents de ligação em DP em todas as regiões avaliadas, comparando com os CN destacando o caudado, que apresentou a maior diferença nos valores de ligação (~462%; CN: 37,3 fmol/mg vs DP: 210 fmol/mg). Nos ensaios de distribuição regional com ^{3}H-Deprenyl observaram-se diferenças inconsistentes entre grupos, no entanto, a autoradiografia revelou uma ligação globalmente mais elevada em todas as regiões analisadas de DP em comparação com CN, com maior destaque para as regiões corticais (~17-27% de aumento de ligação).

Em conclusão, o ^{3}H-BU99008 e o ^{3}H-Deprenyl podem detetar múltiplos locais de ligação com diferentes afinidades em cérebros de DP e CN, com a percentagem mais elevada de ligação ao local de ligação de elevada afinidade (HA - nM). Os diferentes padrões regionais de ligação sugerem a possibilidade de ^{3}H-BU99008 e ^{3}H-Deprenyl refletirem subpopulações/subtipos distintos de astrócitos reativos. Mais importante ainda, ^{3}H-BU99008 e ^{3}H-Deprenyl demonstraram um aumento de ligação nos cérebros *postmortem* de DP de uma forma dependente da região, em comparação com os cérebros da CN, o que sugere níveis elevados de astrogliose reativa nas fases finais da DP e realça a importância de uma abordagem *multi-tracer* para compreender o papel da astrogliose reativa nestas doenças complexas.

Abstract

Parkinson's disease (PD) is the second most common neurodegenerative disease, and it is estimated that it will affect at least 12.9 million people worldwide by 2040. Neurodegeneration, deposition of Lewy bodies (LBs) and neuroinflammation are the most prominent hallmarks of the disease.

Neuroinflammation, mediated by glial cells, plays a major role in the progression, and spread of neurodegenerative diseases and, in PD, is associated with neurodegeneration and LBs formation, highlighting the importance of this process in PD pathology. Astrocytes, the key homeostatic glial cells in the brain, as a response to brain damage, become reactive, engaging in a process characterized by biochemical, morphological, metabolic, and physiological changes - **reactive astrogliosis**.

Various astrocytic markers have been shown to be correlated with neurodegenerative pathologies and some have been proposed as diagnostic biomarkers ideal for brain Positron emission tomography (PET) imaging. Amongst these, monoaminoxidase (MAO)-B and Imidazoline-2 receptors or binding sites (I_2BS) have shown overexpression in astrocytes in multiple brain regions, suggesting potential as markers of reactive astrogliosis.

PET imaging breakthroughs have been achieved by developing specific radiotracers that can accurately detect reactive astrogliosis, allowing this process to be further studied in living patients. Both **Deprenyl** and **BU99008**, which target MAO-B and I_2BS respectively, have shown potential to accurately detect reactive astrogliosis. Nonetheless, to the best of our knowledge, no preclinical validation and *postmortem* imaging studies have been performed before using these astrocytic PET tracers in PD brains.

This thesis addressed this gap in biomarkers research by evaluating and determining the binding behavior of Deprenyl, and BU99008 on *postmortem* brain tissue from PD and cognitively healthy controls (CN). We performed specialized radioligand binding assays

(saturation, competition, and regional distribution) and *postmortem* brain imaging studies, using small frozen brain sections autoradiography in PD and CN brains.

Saturation binding studies showed that the maximal binding receptor density (Bmax) of ^{3}H-BU99008 in the caudate of PD brains was 3-fold higher than CN but relatively lower in the frontal cortex. In contrast, ^{3}H-Deprenyl showed a 1.2-fold higher Bmax in frontal cortex of PD brains as compared to CN and almost comparable binding in the caudate.

Competition and comparative assays revealed multiple binding sites with different affinities (SHA – super high, HA – high and LA – low affinity) in both PD and CN brains. Interestingly, both tracers showed most binding (86%-100%) to a main HA site, which was corroborated by comparative competition assays - ^{3}H-BU990008 vs. unlabeled Deprenyl and ^{3}H-Deprenyl vs. unlabeled BU99008, where no displacement at these sites was observed.

Regional distribution assessment using ^{3}H-BU99008 showed more pronounced binding (~50% increase) in the caudate of PD brains. Autoradiography using ^{3}H-BU99008 demonstrated increased binding in the caudate by 78%, and in the temporal cortex by 81%, of PD brains in comparison with CN. A small proportion of off-target binding sites for ^{3}H-BU99008, possibly caused by the known I_2BS on MAO-B, was identified in the autoradiography studies with pre-blockage using MOA-B inhibitor. However, the ^{3}H-BU99008 higher binding was still detectable and consistent in all assessed PD brain regions as compared to CN with caudate showing the most prominent increase (~462%; CN- 37.3 fmol/mg vs PD- 210 fmol/mg). In regional distribution binding studies with ^{3}H-Deprenyl inconsistent differences between groups were observed but autoradiography revealed an overall higher binding in all assessed regions of PD brains compared to CN with a higher difference in the cortical regions (~17-27%).

In conclusion, ^{3}H-BU99008 and ^{3}H-Deprenyl can detect multiple binding sites with different affinities in both PD and CN brains, with the highest % of binding to HA binding site (nM range). Different regional binding patterns suggest that ^{3}H-BU99008 and ^{3}H-Deprenyl might be targeting distinct subpopulations/subtypes of reactive astrocytes. Most importantly, ^{3}H-BU99008 and ^{3}H-Deprenyl demonstrated increased binding in *postmortem* PD brains in a region-dependent manner as compared to CN brains, which suggests high levels of reactive astrogliosis at end stages of PD and highlight the importance of multi-tracer approach in understanding the role of reactive astrogliosis in these complex disorders.

Acknowledgements

This thesis was a personal and professional adventure. This journey would not have been possible without the help and support of many people around me who I would like to acknowledge.

Firstly, I would like to express my gratitude to Dr. Amit Kumar for sharing his knowledge, which greatly broadened my experience and confidence but mostly for believing in me. As my supervisor, was greatly important to have his help, close guidance and understanding, allowing me to share ideas and theories, to make mistakes and learn from them.

I also want to thank all members of the group for creating a constant supportive environment, for all their time and patience and for the warm and kind atmosphere. Mona-Lisa, Miriam, Sira, I am truly grateful I had you by my side.

I am also thankful to Professor Agneta Nordberg and NVS division at KI for the opportunity to work in a gold standard university and in such an incredible group.

To all my friends with special attention on Gui, Ana Sofia, Ri, Maria, Carol, Carolina, Inês, Cate, Matilda and Sen. You were a bigger part of this thesis than you think, not only for your emotional support but for your friendship, for all the conversation about life, fears, resolutions and for your company and good energy. I know I can always count on you as much as you can count on me.

To ANEEB and absolutely everyone that was part of my path in this beautiful association. You inspired me to do better, to never give up, to trust myself. You showed me my best qualities and without even realizing made me work on my flaws. Bárbara, you taught me to find a balance between a soft, warm kind heart and an assertive attitude. Mariana, with you I learned about hard work, sacrifice, and the importance of always being available to the ones who need us.

Obviously, I cannot find words to express how grateful I am for my family. To my parents, for believing in me, allowing me to pursuit my ambitions, to motivate me to dream big and high, always. Without them, would not be the person I am today and would never have gone to Sweden. To my mum, to fight my battles with me, as they were hers with all her strength, motivation, and determination. For always being available for me, no matter what or when. To my dad, for teaching

me the spirit of hard work, but showing me that the most important is to balance it with family and quality time with the ones you love.

To my sister, my Tiz, my best friend in the entire world, for simply being the kindest heart, the purest mind, and the strongest person I have ever met. With her, I learned, and I am still learning to search for a better version of myself. In the middle of all our differences, we have grown in the strengths that bring us closer and closer every day and I could not be prouder of the person she has become. I cannot wait to see what life holds for you and for Diogo. Both of you absolutely deserve the best in the world and be certain of this: I will always be right next to you to celebrate your victories with all my heart.

Last, but not least, to my dear João Pedro for being my rock, for being with me when something went wrong and for celebrating with genuine happiness my accomplishments and successes. For being the biggest supporter of my decisions, even the harder ones (as coming to Stockholm), for patiently listening to me complain about home sickness, life dramas and nonsenses and for always having the best and most reliable pep talk. For reminding me constantly of the braveness I sometimes forget I have and about everything I am capable of. For his contagious smile, positive words that kept me going through bad days and for making even the smallest moments unforgettable. I admire you more and more every day. I am truthfully lucky.

To all,

Obrigada,

Filipa Monteiro Neves Rocha.

“The people who are crazy enough to think they can change the world are the ones who do.” - Steve Jobs.

Contents

Chapter 1 19

1. Introduction 19
   1.1 - From normal ageing to neurodegenerative diseases 19
   1.2 - Parkinson's Disease 19
   1.3 - Neuroinflammation 31
   1.4 - Astrocytes & Astrogliosis 33
   1.5 - Biomarkers 35
   1.6 - Astrocytic Markers 36
   1.7 - PET Imaging 40
   1.8 - Summary and Motivation 46
   1.9 - Research aims and strategy 46

Chapter 2 47

2. Materials & Methods 47
   1.1 Chemicals 47
   1.2 Methods 48

Chapter 3 55

3. Results 55
   3.1 Saturation Binding Studies 55
   3.2 Competition Binding Studies 58
   3.1 Regional Distribution Binding Studies 62
   3.2 Autoradiography studies 64

Chapter 4 71

4. Discussion 71

Chapter 5 77

5. Conclusions 77

References 80

Supplementary Data 102

List of Figures

Figure 1.1 - Projection of number of individuals with PD 1990-2040 (Dorsey & Bloem, 2018). 20

Figure 1.2 - Illustration of PD loss of dopaminergic neurons that project from SNpc (Midbrain) to the striatum (Broski et al., 2014). 23

Figure 1.3 – Depigmentation of the substantia nigra in Parkinson's brain (A) and normal brain appearance (B) (adapted from Triarhou, 2013). 23

Figure 1.4 - Comparison of the Lewy and MSA α-synuclein filament folds (Y. Yang et al., 2022) 24

Figure 1.5 - Lewy bodies from multiple *postmortem* PD brains in SN (A, C, F) and in the dorsal vagal nucleus (E). Hematoxilina & eosina-stained section (adapted from Wakabayashi et al., 2007). 25

Figure 1.6 – Sex differences in symptomatology and risk factors of PD patients 26

Figure 1.7 - - Braak Staging scale – scheme of the LBs deposition evolution throughout the Braak stages (Georgiopoulos, 2019). 29

Figure 1.8 -Protoplasmic Astrocytes (A); Fibrous Astrocytes (B) adapted from (Verkhratsky et al., 2021). 33

Figure 1.9 - Non-reactive/ resting astrocytes vs reactive astrocytes - GFAP marked (A) and respective illustration (B) (Pekny et al., 2014). 34

Figure 1.10 - Levels of MAO-B in PD and CN brains, adapted from (Tong et al., 2017). 39

Figure 1.11 - The 'first (early)' and 'second (late)' wave of reactive astrogliosis in AD pathology adapted from (Kumar et al., 2023) (A) and from (Fontana et al., 2023) (B). 42

Figure 2.1- Cryostat with small frozen *postmortem* brain tissue mounted and prepared to be sectioned. 49

Figure 2.2 - Illustration shows the subcellular fractionation protocol for the preparation of P1 nuclear, P2 synaptosomal/membrane and S2 microsome/cytosolic proteins fractions from brain homogenates. 50

Figure 2.3 - Illustration of Saturation binding assay protocol steps. 51

Figure 2.4 - Illustration of Competition binding assay protocol steps. 51

Figure 2.5 - Illustration of Regional distribution binding assay protocol steps. 52

Figure 3.1 - ^{3}H-BU99008 Saturation Binding Assay in CN and PD brains. This study was performed in Frontal Cortex (A, B) brain homogenates from one CN and one PD case and

in Caudate nucleus (C,D) in one CN and two PD cases, using increasing concentrations of ^{3}H-BU99008 (0-40nM). A,B,C,D show saturation binding curves for CN (82yo) and PD (83,68yo) cases, respectively, along with the corresponding Scatchard plot. The second binding site presented was drawn manually. Data are presented as means ± SEM of three experiments in duplicate. Kd- dissociation constant; Bmax - density of binding sites. 56

Figure 3.2 - ^{3}H-Deprenyl Saturation Binding Assay in CN and PD brains. This study was performed in Frontal Cortex (A, B) brain homogenates from one CN and three PD case and in Caudate nucleus (C,D) in one CN and three PD cases, using increasing concentrations of ^{3}H-Deprenyl (0-40nM). A,B,C,D show saturation binding curves for CN (82yo) and PD (66,68,83yo) cases, respectively, along with the corresponding Scatchard plot. Data are presented as means ± SEM of two experiments in duplicate. Kd- dissociation constant; Bmax - density of binding sites. 57

Figure 3.3 - ^{3}H-BU99008 competition binding assay with unlabeled BU99008 in Frontal Cortex (A) and Caudate nucleus (B) brain homogenates of two CN (82 and 89 years old) cases. A single concentration of ^{3}H-BU99008 (1nM) was used along with increasing concentrations of BU99008 (10^{-5}-10^{-14}). Data are presented as means ± SEM of three experiments in duplicate for each CN and PD. IC50 – half-maximal inhibitory concentration. 58

Figure 3.4 - ^{3}H-Deprenyl competition binding assay with unlabeled Deprenyl in Frontal Cortex (A) and Caudate nucleus (B) brain homogenates of three CN (82, 82, 77 years old) and two PD (82 and 89 years old) cases. A single concentration of ^{3}H-Deprenyl (3nM) was used along with increasing concentrations of Deprenyl (10^{-5}-10^{-14}). Data are presented as means ± SEM of three experiments in duplicate for each CN and PD. IC50 – half-maximal inhibitory concentration. 59

Figure 3.5 - ^{3}H-BU99008 competition binding assay with unlabeled Deprenyl in Frontal Cortex (A) and Caudate nucleus (B) brain homogenates of one CN (82 years old) and one PD (83 years old) case. A single cocentration of ^{3}H-BU99008 (1nM) was used along with increasing concentrations of Deprenyl (10^{-5}-10^{-14}). Data are presented as means ± SEM of three experiments in duplicate for each CN and PD. IC50 – half-maximal inhibitory concentration. 60

Figure 3.6 - ^{3}H-Deprenyl competition binding assay with unlabeled BU99008 in Frontal Cortex (A) and Caudate nucleus (B) brain homogenates of one CN (82 years old) and one PD (83 years old) case. A single cocentration of ^{3}H-Deprenyl (3nM) was used along with increasing concentrations of BU99008 (10^{-5}-10^{-14}). Data are presented as means ± SEM of three experiments in duplicate for each CN and PD. IC50 – half-maximal inhibitory concentration. 60

Figure 3.7 - Affinities of the various binding sites revealed for ^{3}H-BU99008 competition assays with unlabeled BU99008 and Deprenyl in *postmortem* CN and PD brain tissue in FC and Caudate nucleus. When two binding sites are detected the proportion (%) of each site is presented next to its affinity. SH- Super high-affinity binding sites, SHA- super high-affinity, HA- high-affinity, LA- low-affinity binding sites. 61

Figure 3.8 – Affinities of the various binding sites revealed for ^{3}H-Deprenyl competition assays with unlabeled Deprenyl and BU99008 in *postmortem* CN and PD brain tissue in FC and Caudate nucleus. When two binding sites are detected the proportion (%) of each site is presented next to its affinity. SH- Super high-affinity binding sites. SHA- super high-affinity, HA- high-affinity, LA- low-affinity bind sites. 61

Figure 3.9 - ^{3}H-BU99008 regional distribution binding in *postmortem* homogenates of CN and PD individuals in four brain regions (FC, TC, Caud. Nuc., Put.), using a single concentration of ^{3}H-BU99008 of 1nM and 1 μM of unlabeled BU99008 to determine NSP binding. The graph (left side) shows a comparison between the specific binding results of CN and PD cases for each evaluated region and respective quantitative results are presented on the table (right side). Data are presented as box and whiskers plots and each point represents a

mean of three experiments performed in duplicate for each case. FC – Frontal Cortex, TC – Temporal Cortex, Caud Nuc – Caudate nucleus, Put – Putamen. 62

Figure 3.10 - ^{3}H-Deprenyl regional distribution binding in *postmortem* homogenates of CN and PD individuals in four brain regions (FC, TC, Caud. Nuc., Put.), using a single concentration of ^{3}H-Deprenyl of 3nM and 1 μM of unlabeled Deprenyl to determine NSP binding. The graph (left side) shows a comparison between the specific binding results of CN and PD cases for each evaluated region and respective quantitative results are presented on the table (right side). Data are presented as box and whiskers plots and each point represents a mean of three experiments performed in duplicate for each case. FC – Frontal Cortex, TC – Temporal Cortex, Caud Nuc – Caudate nucleus, Put – Putamen. 63

Figure 3.11 - ^{3}H-BU99008 autoradiography on small frozen brain sections (20μm) for PD and CN cases. The figure displays the result of a total binding of 1nM of ^{3}H-BU99008 and non-specific binding of 1 μM unlabeled BU99008 (identified as NSP in white). Standards are representative of the binding scale: + = 2915-2957 fmol/mg, − = 0.83-0.85 fmol/mg. The autoradiography color/brightness threshold level was set on 50629 from the raw images (16 bits: 0–65,535 (color scale). Regions of interest as shown in the figures were drawn manually using Multigauge software to calculate the specific, non-specific and total binding values in fmol/mg. NA – not available. 65

Figure 3.12 - Semiquantitative analysis of Autoradiography presented in figure above (Figure 3.11) (A) and percentage of increase of the specific binding in PD compared to CN, reflecting the results of the autoradiography presented in Figure 3.11 (B). 65

Figure 3.13 - ^{3}H-BU99008 autoradiography on small frozen brain sections (20μm) for PD and CN cases with pre-incubation with 1 μM unlabeled Deprenyl. The figure displays the result of the posterior total binding of 1nM of ^{3}H-BU99008 and Non-specific binding of 1 μM unlabeled BU99008 (identified as NSP in white). Standards are representative of the binding scale: + = 2915 fmol/mg, − = 0.83 fmol/mg. The autoradiography color/brightness threshold level was set on 50629 from the raw images (16 bits: 0–65,535 (color scale). Regions of interest as shown in the figures were drawn manually to calculate the specific, non-specific, and total binding values in fmol/mg. NA – Not available. 67

Figure 3.14 - Semiquantitative analysis of Autoradiography presented in figure above (Figure 3.14) (A); percentage of increase of the specific binding in PD compared to CN, reflecting the results of the autoradiography presented in Figure 3.14 (B); percentage of increase of the specific binding in PD and CN presented in autoradiography Figure 3.11, compared to the previous autoradiography ^{3}H-BU99008 against BU99008 – Figure 3.9 (C). 67

Figure 3.15 - ^{3}H-Deprenyl autoradiography on small frozen brain sections (20μm) for PD and CN cases. The figure displays the result of a total binding of 3nM of ^{3}H-Deprenyl and Non-specific binding of 1 μM unlabeled Deprenyl (identified as NSP in white). Standards are representative of the binding scale: + = 2913–2959 fmol/mg, − = 0.83-0.85 fmol/mg. The autoradiography color/brightness threshold level was set on 50629 from the raw images (16 bits: 0–65,535 (color scale). Regions of interest as shown in the figures were drawn to calculate the specific, non-specific and total binding values in fmol/mg. NA – Not available. 68

Figure 3.16 - Semiquantitative analysis of Autoradiography presented in figure above (Figure 3.15) (A); percentage of increase of the specific binding in PD compared to CN, reflecting the results of the autoradiography presented in Figure 3.15 (B). 69

Figure 3.17 - Analysis of age and sex-influence on binding of ^{3}H-BU99008 and ^{3}H-Deprenyl. ^{3}H-BU99008 autoradiography results compared with age of the individuals per each assessed brain region (A);^{3}H-Deprenyl autoradiography results compared with age of the individuals per each assessed brain region (B); ^{3}H-BU99008 autoradiography results separated by sex of the individuals per each assessed brain region (C); ^{3}H-Deprenyl Autoradiography results separated by sex of the individuals per each assessed brain region (D). 70

List of Tables

Table S. 1 - ^{3}H-BU99008 autoradiography - Total, Non-specific and specific binding (fmol/mg) in PD and CN cases. 103

Table S. 2 - ^{3}H-BU99008 in the presence of unlabeled Deprenyl autoradiography - Total, Non-specific and specific binding (fmol/mg) in PD and CN cases. 104

Table S. 3 - ^{3}H-Deprenyl autoradiography - Total, Non-specific and specific binding (fmol/mg) in PD and CN cases 104

Abbreviations

AD	Alzheimer's Disease
ALS	Amyotrophic Lateral Sclerosis
ATN	A – Amyloid-ß; T – Tau; N – Neurodegeneration
ATP	Adenosine triphosphate
Aß	Amyloid-ß
Bmax	Density of binding sites
BS	Braak Stage
Caud Nuc	Caudate nucleus
CBD	Corticobasal Degeneration
CN	Cognitively healthy control(s)
CNS	Central Nervous System
CSF	Cerebrospinal fluid
D1	Dopamine recpetor(s) 1
D2	Dopamine receptor(s) 2
DA	Dopamine
DED	Deprenyl
FC	Frontal Cortex
FDA	Food and Drug Administration
FDG	Fluorodeoxyglucose
FTD	Frontotemporal Dementia
GFAP	Glial fibrillary acidic protein
H&Y	Hoehn and Yahr
HA	High affinity
HD	Huntington's disease
I_2BS	Imidazoline-2 binding site(s)
I_2R	Imidazoline-2 recpetor(s)
IC50	Half-maximal inhibitory concentration
IF	Intermediate filament
IL	Interleukin
Kd	Dissociation constant
LA	Low affinity

LBD	Lewy-Bodies disease
LBs	Lewy bodies
LN	Lewy neurites
MAO	Monoaminoxidase
MCI	Mild cognitive impairment
MDS	International Parkinson and Movement Disorder Society
MMSE	Mini-Mental State Examination
MoCA	Montreal Cognitive Assessment
MRI	Magnetic resonance imaging
MSA	Multiple system atrophy
NA	Not available
NSP	Non-specific
PD	Parkinson's Disease
PDD	Parkinson's Disease Dementia
PET	Positron emission tomography
PIB	Pittsburgh Compound B
Put.	Putamen
RBD	Rapid eye movement behavior disorder
REM	Rapid eye movement
RT	Room temperature
SHA	Super high affinity
SN	Substantia Nigra
SNpc	Substantia Nigra pars compacta
SPECT	Single-photon emission computed tomography
TC	Temporal Cortex
TCS	Transcranial brain sonography
TNF	Tumor necrosis factor
UPDRS	Unified Parkinson's Disease Rating Scale
αSyn	α-synuclein

Chapter 1

1. Introduction

1.1 - From normal ageing to neurodegenerative diseases

Ageing is a natural and inevitable process which causes individuals to experience progressive impact on physical and mental abilities. Aged-related physiological consequences in the brain lead to molecular changes – mitochondrial dysfunction, protein aggregation, cellular senescence, neurodegeneration, DNA damage, more telomere attrition, genetic and epigenetic alterations, structural and functional changes with a gradual decline in specific faculties (e.g., processing speed, memory, etc.). Thus, elderly present increased inherent tendency to develop a panoply of comorbidities (Harada et al., 2013; Hou et al., 2019).

Neurodegenerative diseases such as Alzheimer's Disease (AD), Huntington's disease (HD), Frontotemporal Dementia (FTD), Lewis-Bodies disease (LBD), Parkinson's Disease (PD) are associated with neuronal dysfunction and/or loss. Although ageing is a primary risk factor to develop most of these conditions, the mechanism behind the switch from normal cognitive ageing to substantial neurological functional loss, cognitive deficits, or/and motor disabilities that characterize these severe pathologies and lead to either physical disability, cognitive deficits, or both remains elusive (Hou et al., 2019).

1.2 - Parkinson's Disease

1.2.1 Epidemiology

PD is a progressive movement disorder and it's the second most common neurodegenerative disease globally, after AD, and, among all neurological diseases, PD is the one showing the fastest growing rate (Dorsey & Bloem, 2018).

The Global Burden of Disease indicates that, by 2040, 12.9 million people will suffer from PD **(Figure 1.1)**. However, given the constantly increasing longevity and the close link between age and neurodegeneration, this number is highly likely to increase, leading researchers to define the disease as a pandemic. This designation also aims to highlight the importance to investigate the disease, develop accurate diagnostic strategies, improve therapies and provide access to high quality health care (Dorsey & Bloem, 2018).

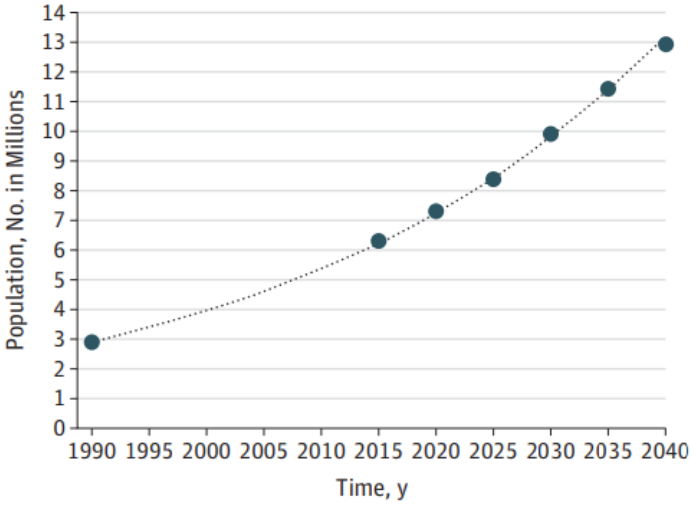


Figure 1.1 - Projection of number of individuals with PD 1990-2040 (Dorsey & Bloem, 2018).

PD incidence peaks at the ages between 85 and 89 years, whereas the risk of developing the pathology begins to increase exponentially around 60 years and declines at 90 years old (Driver et al., 2009). In spite of that, there are also cases of early onset PD patients, who show an overall decrease in life expectancy. Life expectancy was mostly reduced in cases with ages between 25 and 40 years, but also in cases up to 65 years, which might be caused by the prolonged disease duration, that leads patients to reach severe stages with significant disability (Ishihara et al., 2007).

PD patients are divided into two categories: familial and sporadic cases. Majority of the cases are idiopathic and around 5-15% are hereditary (Ascherio & Schwarzschild, 2016; Balestrino & Schapira, 2020). The etiology of idiopathic cases is still unclear, however the familial cases are known to be associated with genetic mutations and 90 genetic risk factors have been linked with the development of PD. Some of the identified mutations are LRRK2,

PARK2, PARK7/DJ-1, PINK1, GBA or the *SNCA* gene (Nalls et al., 2019; Nuytemans et al., 2010; Smith & Schapira, 2022; Takahashi-Niki et al., 2004).

As mentioned before, age is the biggest risk factor, although external factors such as exposure to pesticides, metals, solvents, stress, caffeine consume, smoking habits, diet and physical activity can alter the risk of developing the disease, showing that environmental components should be considered in risk management (Ascherio & Schwarzschild, 2016; Marras et al., 2019).

1.2.2 Symptoms and clinical phenotypes

Clinically, PD is a heterogenous disease, mostly characterized by an asymmetric slowly progressive onset of parkinsonism, which causes a wide array of symptoms that worsen as long as the disease progresses (Balestrino & Schapira, 2020).

The symptoms can be divided in *two categories*: motor and nonmotor symptoms.

1) Motor symptoms normally manifest asymmetrically and include resting tremor, bradykinesia/ hypokinesia, gait problems and muscular rigidity. Resting tremors mostly affect the upper limbs but also the legs and less frequently the head. Bradykinesia/ hypokinesia, which is the slowness and impairment of voluntary and involuntary movements, affects automatic and habitual daily actions such as swinging the arms during walking, eye blinking, or swallowing saliva. Gait problems lead to frequent falls, difficulties in turning the body, in initiating movements, and, in severe situations, freezing – a stage of incapacity to walk. Muscular rigidity causes a feeling of stiffness and a reduced ability to relax limb muscles. Dopaminergic system seems to root these symptoms, as dopamine-replacing medication (as Levodopa) effectively reduces rigidity and normalizes the abnormal stretch responses (Irwin et al., 2013).

2) Common nonmotor symptoms are mood changes, fatigue, olfactory problems, constipation, sleep disorders, pain, behavioral issues, among others. The speech and communication skills are affected despite presentation of intellectual capacity. Together, these can highly impact the patient´s quality of life (Martinez-Martin et al., 2011). The prodromal phase of PD may start years before average diagnosis or typical symptomatic manifestation. Rapid eye movement (REM) sleep behavior disorder (RBD) – sleep disorder involving unpleasant dreams with vocal sounds, violent movements with arms and legs can possibly start 12 to 14 years before disease identification, constituting the strongest clinical predictor (Postuma et al., 2012). Other nonmotor symptoms for instance constipation, orthostatic hypotension, urinary

urge, erectile dysfunction, depression, daytime somnolence, hyposmia, regardless of being early indicators of possible development of the disease, the fact that these symptoms overlap with other non-related conditions doesn't allow clinicians to directly correlate/diagnose with PD (Greenland & Barker, 2018; Postuma et al., 2012).

1.2.3 Neuropathological features

PD is clinicopathologically complex and heterogenous. The predominant pathologic features of PD are neuronal dopaminergic loss and α-synuclein (αSyn) abnormal accumulation. Specifically, there is loss of neurons that are part of the Nigrostriatal pathway, which projects from the Substantia nigra (SN) pars compacta (SNpc) in the midbrain - the first region to be show neuronal alterations - to the striatum (putamen & caudate nucleus) (Broski et al., 2014). In addition, other pathological changes are present including oxidative stress, mitochondrial dysfunction, disrupted axonal transport, and neuroinflammation (Poewe et al., 2017).

Nigrostriatal degeneration causes a depletion of dopamine (DA) available for neurotransmission in the Striatum, since DA is released from SN to the basal ganglia, leading to biochemical imbalance **(Figure 1.2).** Consequently, this causes motor dysfunction, given that basal ganglia play a key role in controlling body's movements. Clinical symptoms typically begin after the patient loses 40%-60% of the dopaminergic neurons (Broski et al., 2014).

A compensatory mechanism induces upregulation of dopamine receptors D1 and D2. DA receptors can be divided into 5 categories, all with important functions and related to movements, emotions, among others. D1 controls memory, attention, locomotion and D2 receptor is associated with attention, sleep, memory, movements. Currently available medication tries to tackle multiple of these difficulties: D1 and D2 receptors agonist (ex: bromocriptine), increase/ replacement of dopamine levels (ex: levodopa), inhibit dopamine degradation (ex: selegiline) (Bhatia et al., 2023).

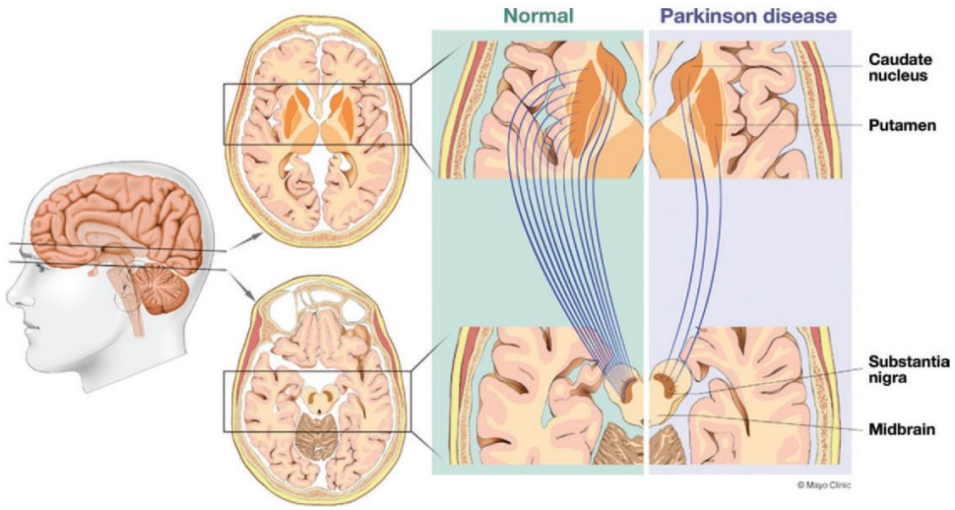


Figure 1.2 - Illustration of PD loss of dopaminergic neurons that project from SNpc (Midbrain) to the striatum (Broski et al., 2014).

Despite main loss of dopaminergic neurons, there is also a pronounced involvement (in motor and pathological features, as neurodegeneration) of many other systems, as glutamatergic, cholinergic, adenosinergic, noradrenergic, serotonergic and histaminergic neurons (Kalia et al., 2013; Perez-Lloret & Barrantes, 2016).

Macroscopically, the brain of a PD patient presents depigmentation in the SN and brainstem **(Figure 1.3)** due to loss of dopaminergic neuromelanin-containing neurons and mild atrophy in the frontal cortex (FC) (Dickson, 2012; Triarhou, 2013).

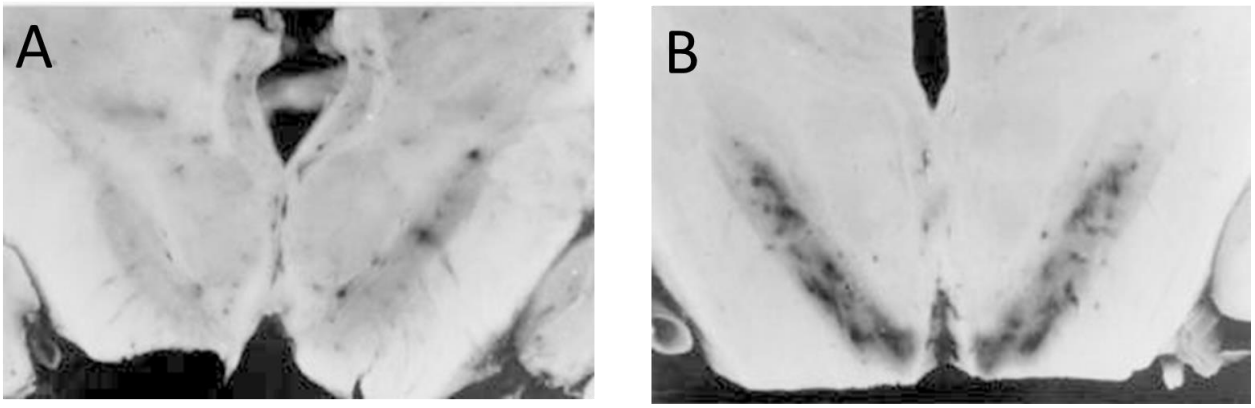


Figure 1.3 - Depigmentation of the substantia nigra in Parkinson's brain **(A)** and normal brain appearance **(B)** (adapted from Triarhou, 2013).

1.2.4 α-synuclein & Lewy Body formation

αSyn is a 140-amino-acid protein, that is encoded by the *SNCA* gene on chromosome 4q21, it is localized in the presynaptic nerve terminal and despite its biological function not being fully understood, shows involvement in synaptic-vesicle transport (Vekrellis et al., 2011).

αSyn is a small and intrinsically disordered protein, that is highly expressed in various tissues, but mostly in the brain. In normal physiological conditions the protein can be found in different conformations: monomers, and a variety of oligomers, including helically folded tetramer, which maintain a dynamic balanced equilibrium in the neuronal cytoplasm (Breydo et al., 2012; Theillet et al., 2016).

Synucleinopathies are a group of neurodegenerative diseases which one of the core pathological features is αSyn deposition - PD, Parkinson's disease dementia (PDD) and Dementia Lewy Bodies (DLB) and Multiple system atrophy (MSA).

In these pathologies, the oligomerization of αSyn leads to the formation of large, insoluble, neurotoxic fibrils known as Lewy bodies (LBs). Post translational modifications, such as phosphorylation, of αSyn may influence its toxicity and propensity to aggregate (Zhang et al., 2019), but how monomers convert into oligomers and cause pathology remains unclear. Evidences point to mediation of binding of αSyn to lipid membranes as a key factor (Killinger et al., 2019).

Cryogenic electron microscopy (CryoEM) studies (preprint) report that PD, PDD and DLB present similar α-synuclein filaments and MSA filaments are markedly different **(Figure 1.4)**, showing distinct molecular conformations of assembled α-synuclein within the synuclopathies (Y. Yang et al., 2022).

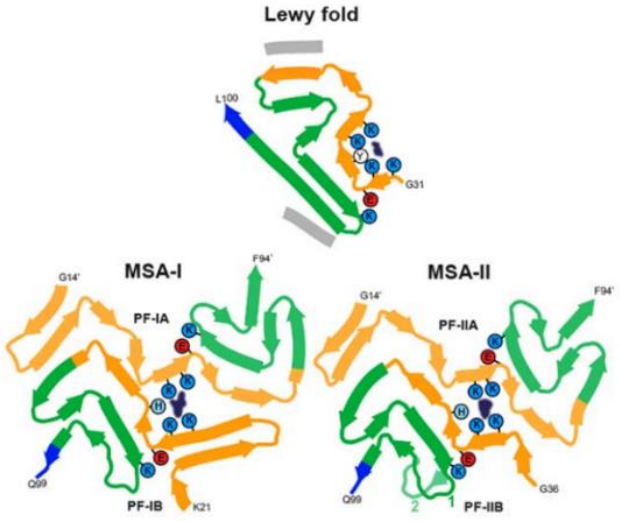


Figure 1.4 - Comparison of the Lewy and MSA α-synuclein filament folds (Y. Yang et al., 2022)

Besides α-synuclein, LBs contain other molecular components, mainly proteins, for example tau, ubiquitin, parkin, heat shock proteins (HSPs), oxidized and nitrated proteins, cytoskeletal and phosphorylated proteins. These are found enclosed in a granular and fibrillar core surrounded by α-synuclein **(Figure 1.5)** (Xia et al., 2008). Organelles, lysosomes, mitochondria, vesicles, and lipid membranes can also be found in LBs (Koga et al., 2021).

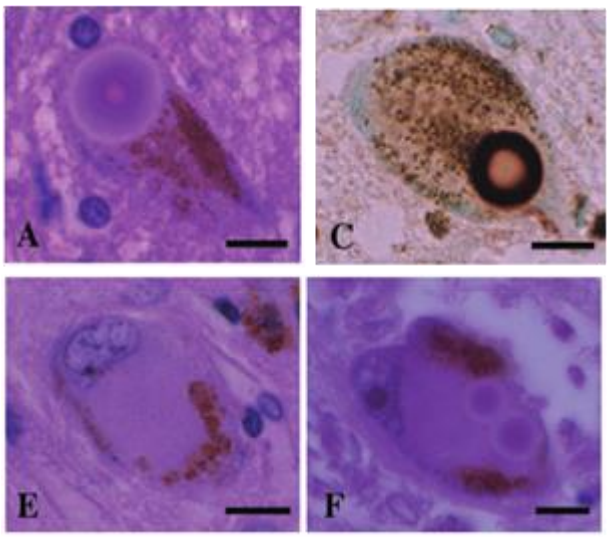


Figure 1.5 - Lewy bodies from multiple *postmortem* PD brains in SN **(A, C, F)** and in the dorsal vagal nucleus **(E)**. Hematoxilina & eosina-stained section (adapted from Wakabayashi et al., 2007).

In PD, αSyn forms pathological LBs and Lewy neurites (LN) aggregates that appear in early stages of the disease, first in the lower brainstem, later ascend to limbic and cortical regions (Vekrellis et al., 2011).

PD studies highlight that LBs contribute to neurodegeneration and the spreading of the LBs by transferring pathogenic α-syn aggregates between neurons and from neurons to astrocytes, promotes neurotoxicity and worsens disease burden (Irwin et al., 2013).

1.2.5 Sex differences

Women show a faster progression rate, a higher mortality but twice lower probability of even developing the disease, highlighting that gender is an important risk factor and sex differences can divide individuals with PD in two different sub-profiles (Cerri et al., 2019).

Sex-related discrepancies have been attributed to women's longer lifespan, distinct pathogenic mechanisms, phenotypical differences, and hormonal impact (Cerri et al., 2019).

Estrogens presence can increase striatal dopamine levels, consequently delaying symptomatic PD development and explaining lower and later incidence in females (Haaxma

et al., 2007). In addition, estrogens have anti-inflammatory effects and mitigate memory decline by modulating neuroinflammation, through the reduction of NF-κB activity, according to an animal study (Yun et al., 2018).

Furthermore, medication and therapies such as deep brain stimulation show distinct levels of efficiency between sexes, women present greater levodopa bioavailability, which is further supported by lower levodopa clearance levels (Kumagai et al., 2014) and present differences in the dopaminergic system (such as higher D1:D2 ratio), which might lead to different treatment response (Cullity et al., 2019).

Concerning motor manifestation, despite later start in females, with specific characteristics such as reduced rigidity and tremor, are more often and come associated with milder motor deterioration and striatal degeneration (Haaxma et al., 2007). Male, on the other hand, show gait complications significantly later and higher postural instability (Kim et al., 2018).

Non-motor symptoms such as fatigue, restless legs, constipation, pain, loss of taste or smell, weight change and excessive sweating are more severe and common in women, as well as more severe and persistent depression and anxiety (Broen et al., 2018; Haaxma et al., 2007). On the contrary, male sex tend to develop more aggressive RBD (Zhou et al., 2015).

In conclusion, sex-related differences **(Figure 1.6)** and its characterization should be factored in while diagnosing, prescribing treatment, evaluating progress, and mainly assessing symptom patterns.

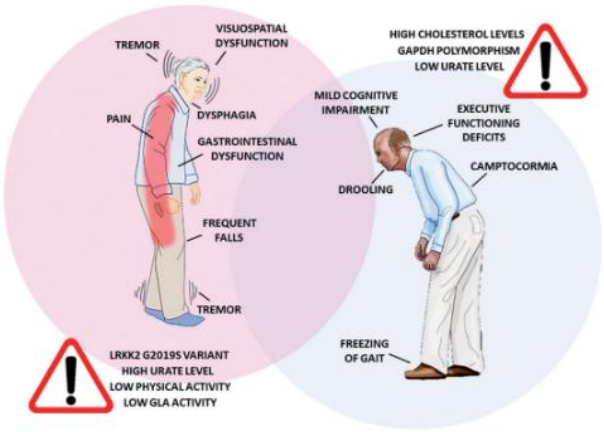


Figure 1.6 – Sex differences in symptomatology and risk factors of PD patients

1.2.6 Diagnosing Criteria

The definitive diagnosis of PD relies on *postmortem* histologic confirmation of intraneural Lewy body inclusions in the SN. Nowadays, there is no conclusive screening, test or exam which, isolated, can diagnose early and accurately the disease. Diagnosis is mostly based on the clinical manifestation of symptoms, which can occur years after the disease has started (Broski et al., 2014).

Often individuals with a PD diagnosis find out later that they suffer from a different condition that mimics Parkinson's. To avoid misdiagnosing, there are many well-established scales and defined guidelines that aim to systematize the process and allow reproducible results across centers and large applicability (Postuma et al., 2015).

The official International Parkinson Disease and Movement Disorder Society (MDS) diagnostic criteria defines a step by step tool to be followed by clinicians (MDS-PD Criteria), aiming to reflect the most current understanding of PD and significantly reduce the failure to recognize other pathologies, as parkinsonian disorders, secondary parkinsonism, or absence of any of the mentioned conditions (Postuma et al., 2015).

According to MDS-PD criteria, PD diagnosis is based on the presence or not of 3 categories of symptoms. Absolute **exclusion criteria**, such as cerebellar abnormalities, Downward vertical supranuclear gaze palsy, Parkinsonian features restricted to the lower limbs, no response to levodopa. The presence of this features allows to rule out PD. **Red flag features** (rapid balance loss, stagnation of motor symptoms, absence of nonmotor signs despite 5 years of disease duration, severe autonomic failure) require additional factors to be counterbalanced, so do not lead to a conclusion alone. **Supportive criteria** (positive response to dopamine replacement medication, shaking or tremor in a limb while resting, stiffness or rigidity of the member: arms, legs or trunk, present frequent falls or troubles with balance) which raise confidence in the final diagnosing decision (Postuma et al., 2015).

A patient must have no absolute exclusion criteria, two supportive criteria and no red flags feature to attribute a **PD diagnosis**. If the subject presents no absolute exclusion criteria but red flags, counterbalanced with supportive features, then the diagnosis is **probable PD** (Postuma et al., 2015).

Physical and neurological evaluation by a neurologist will carefully be carried out, including analysis of the medical history, current and past medication patterns as some can mimic PD signs. Following, the medical professional will quantify the results, mainly according to the Unified Parkinson's Disease Rating Scale (UPDRS), a universal scale used by

neurologists and specialists to comprehensively evaluate and report the exam of a with PD patient. This scale can be used as a baseline, to assess the effect of medication, and to track the advances of the disease during follow-up appointments. If the diagnosis is positive, the patient may start a medication to help replace dopamine or increase its effect in the brain, as levodopa, and, consequently, mitigate the symptoms (Postuma et al., 2015).

Nonmotor manifestation should be taken into account and interpreted as possible "clues" – as explained before – see topic symptoms and clinical phenotypes (Postuma et al., 2012).

1.2.7 Braak staging

In 2003, Braak and collegues defined a degree of pathology staging system for PD based on the quantitative evaluation of LBs localization/distribution, by performing *postmortem* studies with large autopsy sections. Until today, this grading system is still one of the most used **(Figure 1.7)**. According to this scale, at Braak stages 1 and 2, LBs are most found in the olfactory bulb and medulla oblongata. However, stage 2 is also characterized by abnormal levels of α-synuclein in the adjacent structures, including caudal raphe nuclei and the locus coeruleus. A patient in these initial stages might present early nonmotor features, but normally, is still considered asymptomatic or presymptomatic (Braak et al., 2003).

At **stage 3**, LB pathology reaches SNpc, which is followed by neuronal loss, also extending to the basal forebrain and the amygdala, subsequently affecting temporal lobe structures at **stage 4**. During **Braak stages 5** and **6**, the pathology reaches all of neocortex and clinical wise, the patients develops severe PD (Braak et al., 2003).

Denote, Braak Staging system doesn't consider neuronal loss or its progression and more recent revisions of this work have, for example, suggested that α-synuclein pathology might initiate in nasal and intestinal mucosal sites, concretely in the olfactory bulb and enteric cell plexuses (Hawkes et al., 2007) without following the Braak staging path. Also, a considerable amount of studies failed to correlate their results with Braak´s (Jellinger, 2009; Kalaitzakis et al., 2008; Parkkinen et al., 2008). For all these reasons, the scale should always be used and interpreted cautiously.

Therefore, clinicians combine information from various systems such as the UPDRS, the Bayesian naïve classifer, which is a statistical method based on probability rates and thresholds comparisons to estimate the likelihood of a individuals developing PD, and Hoehn and Yahr scale, which are clinical assessment tools to monitor PD progression that assess both motor disability and impairment (Bhidayasiri & Tarsy, 2012; Disease, 2003). Although,

the clear existing level of subjectivity in the process highlights the urgency of biomarkers research as an auxiliary tool to achieve accurate, objective, and earlier diagnosis.

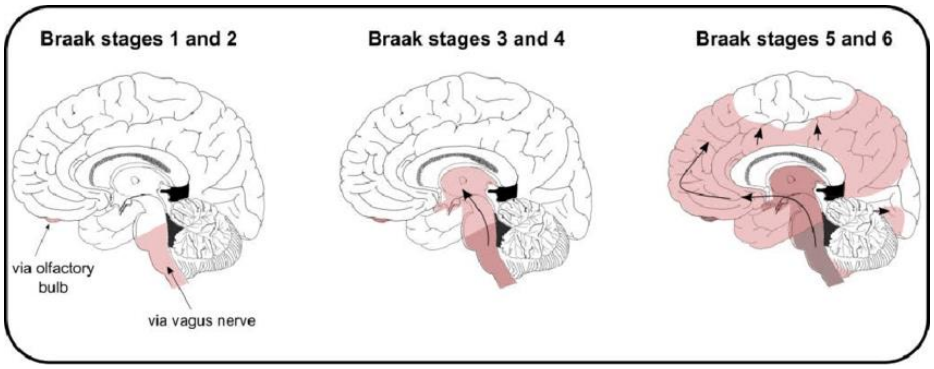


Figure 1.7 - - Braak Staging scale – scheme of the LBs deposition evolution throughout the Braak stages (Georgiopoulos, 2019).

1.2.8 PD spectrum: the clinical challenge

Diseases in the spectrum of PD: PD itself, PDD, DLB are characterized pathologically by neuronal loss and LBs deposition. However, in PDD and DLB amyloid-beta (Aß) deposits can be found, which are typical AD hallmarks. The presence of αsyn aggregates can increase the likelihood of Aß and tau deposition and the synergy of LBs and AD-type pathology can exacerbate disease to more severe levels as compared to when only LBs or AD pathology are present in isolation (Aarsland, 2016).

PDD and DLB patients suffer from cognitive impairment, which is defined by a cognitive dysfunction that once it reaches a certain threshold of a functional deficit leads to diagnosis of dementia. Around 30% of all PD cases are diagnosed with cognitive impairment and 80%, over the disease course, develop dementia – PDD, commonly 3-4 years after initial detection. Overall the risk of dementia among PD patients is 25%-50% higher than for cognitively healthy elderly individuals (Perez et al., 2012).

As a consequence of cognitive deficits, combined with motor impairment, patients become more disable, directly causing lower quality of life, incapacity of living independently and lower survivance periods (Mack & Marsh, 2017).

Clinical distinction between DLB and PDD presents challenges. DLB patients face cognitive decline either followed by or simultaneously with parkinsonism, while in PDD cases normally motor symptoms manifest earlier and after revealing cognitive deficits it is verified a significant decline, calling into question a clear distinguish of the pathologies (Lippa et al., 2007).

That said, clinically PDD and DLB often are indistinguishable, so diagnosis is assigned considering the timing of the impairment onset, using the so-called “1 year rule” between the onset of dementia and parkinsonism (McKeith, 2006). When dementia occurs before or within one year after the onset of parkinsonism patients are classified as DLB and if dementia is developed more than 1 year after initial motor symptoms patients are diagnosed with PDD, in spite of the pathological complexity of numerous features of the 3 pathologies (Yamada et al., 2020).

Among many scales available, the Mini-Mental State Examination (MMSE) and the Montreal Cognitive Assessment battery (MoCA) are most used for identifying impairment and characterizing cognitive profiles. Standardized scores of common features such as visual hallucinations, depression, fluctuating cognition, parasomnias, autonomous disturbance and apathy will help in the diagnosis and management of patients with PD and DLB (Aarsland, 2016).

Regarding symptomatic, PDD patients frequently struggle with lack of attention, executive functioning, visuospatial processing. Memory loss can be presented at different levels, associated with frontal pathology in advanced stages of the disease. Mild cognitive impairment (MCI) might be detected through early signs as forgetting small daily things, losing track of thought, repeating yourself, having trouble following a conversation. Despite the blurry clinical line between PD-MCI and PDD, factors such as greater age, more severe motor symptoms, visual hallucinations, biomarkers levels assessment – (e.g., Cerebrospinal fluid (CSF) value of Aß 42), and hippocampal and parietal cortical atrophy can be taken in consideration (Aarsland, 2016).

On the other hand, DLB patients deal with features including fluctuating cognition, recurrent detailed visual hallucinations, and parkinsonism, behavioral disorders - REM sleep, neuroleptic sensitivity, repeated falls, dysautonomia, delusions, and depression. 70%–90% of DLB present similar severe parkinsonism as PD, although usually symmetric (Broski et al., 2014).

Therefore, given the similarities and clinical challenges previously described new approaches to tackle the clinical heterogeneity of PD have been strongly explored with great focus on biomarkers.

A study which evaluated the burden of LBs, Aß and tau by performing neuropathological assessment (immunohistochemistry), evidences that the combination of the three reaches the strongest model at predicting PDD, although any one of these three pathological

features isolated showed a good statistical association, indicating that assessing the 3 characteristics provide the better diagnosing method of this pathology (Compta et al., 2011).

Other studies suggest other biomarkers as auspicious diagnostic tools: cortical LB/LN pathology highly correlates with severity scores PDD (Irwin et al., 2012) , AD CSF biomarker signature (that is, increased levels of total tau and decreased levels of Aß42) was found in half of PDD cases but only in one third of PD cases (Montine et al., 2010), increased number of striatal Aß plaques in DLB, compared to PDD (Halliday et al., 2011), among many others.

Moreover, supplementary tests show various promising results: such as **dopamine transporter Single-photon emission computed tomography (SPECT) imaging** - reduced dopamine uptake in caudate has been found to be associated with cognitive impairment, **CSF** – low Aß42 levels have shown a correlation with MCI and memory damage, **structural imaging** - atrophy of cortical and subcortical structures, associated with dementia and also MCI, **PET- fluorodeoxyglucose (FDG)** - characteristic pattern of reduced cortical metabolism associated with cognitive impairment in PD, **amyloid imaging using Pittsburgh Compound B (PIB)** - amyloid pathology is more common in DLB than in PDD and rare in non-demented PD patients (Shi et al., 2010).

To sum up, despite promising results and efforts in the field there is no tool currently available that allows clinicians to provide a definitive diagnosis, leading to the conclusion that combining different imaging modalities, and even imaging and CSF biomarkers looks the leading option for the future advances (Aarsland, 2016).

1.3 - Neuroinflammation

Neuroinflammation plays a major role in the progression and spread of neurodegenerative diseases. The process is mediated by glial cells. Glial cells are non-neuronal cells which cohabitate with neurons. Their main function is to keep homeostasis and maintain the strength of the immune system, proving to be fundamental in the context of pathology in the brain. Glial cells of the central nervous system (CNS) can be divided into: into macroglia (astroglia, NG-2 cells and oligodendroglia) and microglia, according to origin (Verkhratsky et al., 2019).

Under pathological conditions, glia becomes readily reactive and release modulators that will trigger neuroinflammation. In general, inflammation is a protective and defensive process, acting as a response against a variety of exogenous insults. However, as age advances can become upregulated and uncontrolled. Chronic neuroinflammation leads to detriment of the tissue and functional loss with persistent microglial activation, sustained

increases in proinflammatory cytokines, and elevated levels of oxidative stress (Verkhratsky et al., 2019).

This scenario is a common phenomenon to all neurodegenerative disorders, although parameters as how it starts, progresses and its specific causes and consequences are specific to each pathology.

Neuroinflammatory response shows high relevance in PD pathogenesis and development (Croisier & Graeber, 2006; Miklossy et al., 2006; Rizor et al., 2019). Animal studies show microglial activation in SN and cortical regions before cell loss, providing evidences that neuroinflammation is prior to neurodegeneration and cloud be an early disease biomarker for PD (Duffy et al., 2018).

Astrocytes have been a "hot target" in the field of biomarker development, since astrogliosis is shown to be an initial event in PD course (Booth et al., 2017; Koprich et al., 2008) and studies show astrocytic capacity to take up αsyn as an attempt to fight pathology (Wakabayashi et al., 2000), to protect non-SN brain regions from oxidative stress and mitochondrial damage (Mythri et al., 2011). A review suggests that reactive astrocytes are involved in two phases of the disease progression, being the first even before neuronal loss starts (Halliday & Stevens, 2011).

However, it was also shown that, αsyn-induced activated microglia enhances dopaminergic neurodegeneration and nigral neuronal damage and that aggregated αsyn released to SN activates microglial production of proinflammatory mediators, causing persistent and progressive neurodegeneration in PD (Isik et al., 2023).

Hereupon, seems that astrocytes show a first defensive mechanism reaction, although eventually the pathology reaches a threshold that glia cell can't fight, converting their action to harmful.

Besides that, factors such as disease stage, co-morbidities and cases-dependency may explain the discrepancies in the results regarding this mechanism. Further investigation in patients is still required to elucidate how neuroinflammation and glial cells behave as disease progresses and their role at different disease stages – from prodromal disease to advanced severe state.

1.4 - Astrocytes & Astrogliosis

Astrocytes – Brief history

In 1895, Michael von Lenhossék named the first subpopulation of glia - astrocytes, the star shaped neuroglia, that outnumber neurons in the human brain (Andriezen, 1893; Lenhossék, 1893).

Astrocytes are the most populous glia subtype, representing 20-40% of all the glia cells. Furthermore, astrocytes, as innate immune cells, play a critical role for brain functions and neuronal health: homeostasis regulation – to maintain levels of ions, pH, neurotransmitters; structural and metabolic support for the brain and spinal cord; defense against oxidative and nitrosative stress; transferring neuronal information; maintenance of the brain-blood barrier (BBB) integrity and water transport, synaptic plasticity, connectivity (Fakhoury, 2018; Jäkel & Dimou, 2017; Vasile et al., 2017; Verkhratsky et al., 2021).

Despite significant heterogeneity in morphology, functions, developmental origin, and regional expression there are two main categories of astrocytes:

- **Protoplasmic astrocytes** which are cortical and subcortical, do not present positive immunoreactivity for Glial fibrillary acidic protein (GFAP) in normal brain conditions, can be found in the grey matter both in the brain and spinal cord and present a distinctive "spongioform" appearance **(Figure 1.8A)**.
- **Fibrous astrocytes** which are localized in the white matter and are GFAP immunoreactive **(Figure 1.8B)** (Oberheim et al., 2009; Verkhratsky et al., 2021).

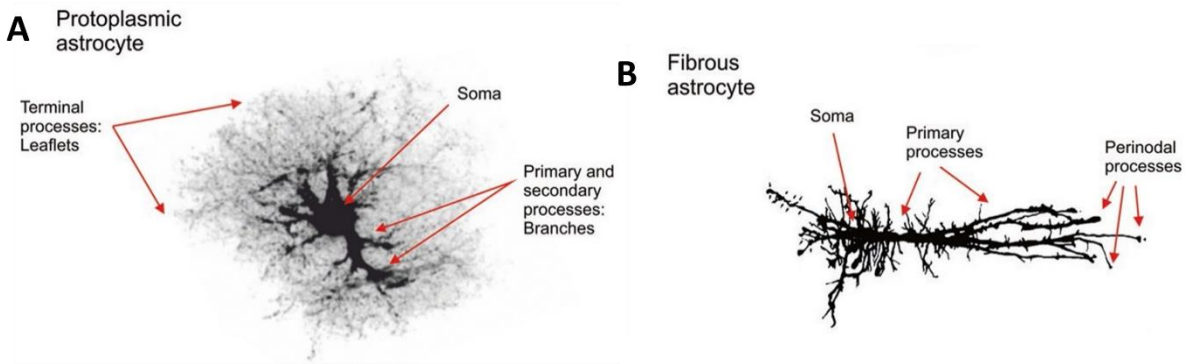


Figure 1.8 -Protoplasmic Astrocytes **(A);** Fibrous Astrocytes **(B)** adapted from (Verkhratsky et al., 2021).

How & why do Astrocytes become reactive?

First observed in the 19th century, as a response to brain damage, astrocytes become reactive, presenting various changes. Thereby, astrocytes assume two states: reactive and non-reactive/resting (Escartin et al., 2021).

The resting state astrocytes respond to physiological stimulus, manifest high plasticity, and keep brain homeostasis. These can be found in healthy CNS conditions **(Figure 1.9 – left side)** (Pekny & Pekna, 2014).

While the reactive state constitutes a response to pathology or is triggered by changes in brain homoeostasis (for instance, in ageing or CNS injury) **(Figure 1.9 – right side).** As recently uniformized, *'is a process whereby, astrocytes engage in molecularly defined programmes involving changes in transcriptional regulation, as well as biochemical, morphological, metabolic, and physiological remodelling, which ultimately result in gain of new function(s) or loss or up-regulation of homeostatic ones, in response to pathology'* (Escartin et al., 2021).

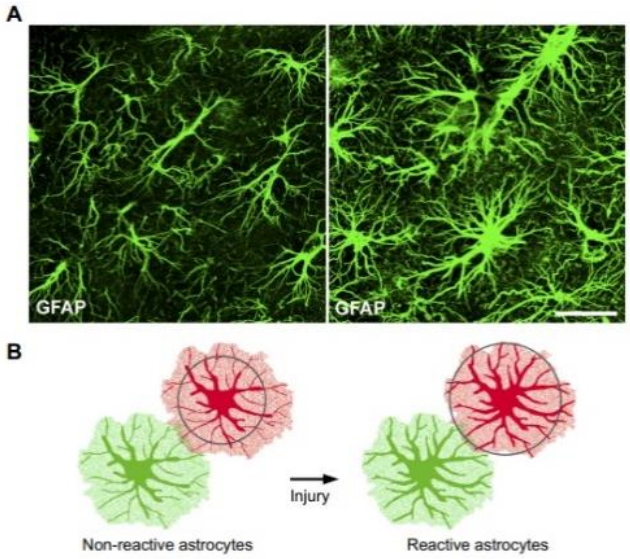


Figure 1.9 - Non-reactive/ resting astrocytes vs reactive astrocytes - GFAP marked **(A)** and respective illustration **(B)** (Pekny et al., 2014).

Morphologically, astrocytes show a projection that extends to the pre- and post-synaptic terminals for regulatory support but also present a second defense arm that functions to combat pathogens and harmful agents, molecules, cells. Under these conditions, a activation process named, according to recent consensus, **reactive astrogliosis** is triggered (Escartin et al., 2019, 2021).

Reactive astrogliosis show hypertrophy, overexpression of GFAP, formation of a non-functional structure that limits the site of damage: a scar border, promotion of post-injury neuronal function recovery, upregulation of homeostatic functions, recruitment of immune cells, release of extracellular molecules, such as neurotrophic factors, for example brain-derived neurotrophic factor (BDNF) and vascular endothelial growth factor (VEGF), inflammatory factors, including IL-1β, TNF-α, prostaglandins (PGE), nitric oxide (NO) and cytotoxins (such as Lcn2), present either a neuroprotective (IL-6, TGF-β) or neurotoxic (IL-1β, TNF-α) role (by causing neuroinflammation or provoking/aggravating damages), among many others (Escartin et al., 2019, 2021; Jäkel & Dimou, 2017; Liddelow & Barres, 2017; Pekny et al., 2016; Pekny & Pekna, 2016; Sofroniew & Vinters, 2010).

1.5 - Biomarkers

Biomarkers are objective measures of a biological processes and can be highly relevant to help diagnosing diseases before symptomatic manifestations, to monitor disease progression, to select patients for clinical trials, to drug and medical devices development, to evaluate treatment response, ideally with sensitivity, reproducibility and in a non-invasive way (Strimbu & Tavel, 2010).

CSF can reflect the molecular changes occurring in the brain, constituting an indirect contact with the extracellular space of the brain, highlighting the potential of CSF biomarkers for neurodegenerative diseases. Furthermore, the leakage of these factors can also be detected in the blood and collecting blood is an inexpensive, non-painful and easily executed technique, which shed light on this possibility as well (Mattsson, 2011).

For AD, biomarker research has been truly fruitful in the last past years. CSF Aß42, total tau (t-tau) and phosphorylated tau (p-tau) are well established markers that translate reliably early disease-related changes, even before clinical manifestations. This information allowed the field to bring a new operational diagnosing criterion, bringing confidence, objectiveness, and effectiveness to the diagnosing process, which is an urgent clinical need for all neurodegenerative diseases (Schoonenboom et al., 2004). The AT(N) framework is a biomarker-driven classification based on these pivotal features of AD – Aß (A), tau pathology (T) and neurodegeneration (N) (Hampel et al., 2021).

However, as the field progresses, more biomarkers rise and show breakthrough results, leading to open the possibility of a new framework – ATX(N), where X stands for a new biomarker candidate (Hampel et al., 2021). Recently, reactive astrocytes have already been suggested has a suitable applicant (Fontana et al., 2023).

Despite the lack of equally accurate biomarkers for PD, this highlights the importance of understanding which combination of biomarkers can be trusted to reflect the pathology in prodromal stages, since it begins considerably before motor complications.

On one hand, inflammatory markers such as cytokines - interleukin (IL)-1ß, IL-2, IL-6, IL-10, tumor necrosis factor (TNF)-α and molecules α-synuclein, DJ-1, Aß42, tau, and lysosomal enzymes in the CSF and blood have provided indication that might be valid fluid biomarkers for PD (Hong et al., 2010; Parnetti et al., 2013).

On another hand, as previously mentioned, neuroinflammation can be reflected by astrocytic markers, which have been showing auspicious results for many diseases, as it will be explored in a further topic.

1.6 - Astrocytic Markers

GFAP

Glial fibrillary acidic protein is an intermediate filament (IF) III protein found primarily in astrocytes of the CNS and responsible for cytoskeleton structure of glia cells and maintenance of their mechanical strength. GFAP protein and its metabolites are rapidly released into biofluids when a spinal injury, stroke or brain trauma occurs, making it easily detected (Z. Yang & Wang, 2015).

When reactive astrocytes go through structural (thickened, elongated, hypertrophy) changes intermediate filaments, GFAP and Vimentin, assure such structural flexibility with consequent increased expression (Z. Yang & Wang, 2015).

Brain injuries provoke releasing of GFAP break down products (GFAP-BDP) to the interstitial fluid where these proteins equilibrate into the CSF and then release to the circulating blood either by direct venous drainage (glymphatic pathway) or by following the CSF flow and eventually enter the circulation by diffusing pass the compromised BBB (Liddelow & Barres, 2017; Z. Yang & Wang, 2015).

That said, GFAP has been extensively studied for many neurodegenerative diseases, allowing to understand relevant phenomenon: in AD, GFAP-positive astrocytes surround plaques to limit neurotoxicity (Perez-Nievas & Serrano-Pozo, 2018), internalize Aß (Nagele et al., 2003) , and many investigations show great importance of Plasma GFAP as tool to identify cognitively normal adults at risk of AD (Chatterjee et al., 2021), to predict conversion from MCI to AD (Cicognola et al., 2021), to catch early Aß (Pereira et al., 2021), among many others.

Additionally, You *et al*. showed plasma GFAP correlation with neurofilament light protein (NfL) in HD (You et al., 2021), Benninger and colleagues found increased CSF-GFAP concentrations in ALS patients (Benninger et al., 2016) and in Oeckl *et al*. serum GFAP reveals capacity to be the first blood-based biomarker to differentiate AD and FTD (Oeckl et al., 2019), which call attention to the potential of GFAP as a biomarker for a broad range of neurological diseases.

Evidences show elevation of CSF and serum GFAP of PD patients compared to healthy controls (CN) (Oeckl et al., 2019; Su et al., 2012; Takahashi et al., 2015), high levels of hypophosphorylation and overexpression of enteric GFAP in PD patients compared to CN and atypical parkinsonism (MSA and PSP) (Clairembault et al., 2014). Besides, a recent study

examined Plasma GFAP and suggests potential to distinguish PDD and foretell MCI shift to dementia (Tang et al.,2023) and an extensive analysis of GFAP and other markers expression showed increased total GFAP levels in caudate nucleus and frontal cortex of PD patients, compared to controls (Tong et al., 2015).

Despite GFAP levels alignment with severity of the damage (Escartin et al., 2019) and all the positive already stated results, GFAP basal levels are region-dependent, vary with external factors, as the environment and physical activity and a consensus states that **overall GFAP alone cannot be considered a global astrocytic marker**, since it does not represent the full extension of what is happening (Escartin et al., 2021).

Vimentin is other non-epithelial IF protein from the same class (III) as GFAP and is expressed in astrocytes and glial precursors (Schnitzer et al., 1981). Vimentin plays a role in glial scar formation, affects GFAP expression, participates in reactive gliosis, it is highly increased in context of damaged CNS. Depletion in vimentin expression leads to decrease in GFAP in glial scar formation (Avola, 2010). Total vimentin was found to be significantly elevated in SN, elevated in caudate nucleus and slightly higher in frontal cortex and putamen of PD individuals, in comparison to healthy subjects (Tong et al., 2015).

S100B is an acidic protein, part of the S100 family, it is involved in Ca2+ regulation in various biological functions (enzyme activities, protein phosphorylation, cell differentiation and proliferation, inflammation) and it is mostly expressed in astrocytes with low expression none in neurons. Increased levels of S100B have been detected in AD, amyotrophic lateral sclerosis (ALS), depression, cerebral stroke (Avola, 2010) and was reported to correlate with PD symptoms severity (Schaf et al., 2005).

These important findings show that GFAP, vimentin and S100B are valuable astrocytic markers which might offer further improvement by being combined among them and with others (for instance, Hsp27, proliferation markers - Ki67, PCNA, and BrdU incorporation). However, not so motivating results which demonstrate absence of reactive astrocytes or suggest suppression of astrocytes by α-syn in PD, (Tong et al., 2015) underline the *need of further investigation* either to elucidate the field's knowledge or to move on to different/new targets.

MAO-B

Monoaminoxidase (MAO) is responsible for the catalyzes of dopamine, serotonin, and noradrenaline in the CNS, which are neurotransmitters implicated in a broad range of brain functions. It has been identified two types of MAO: MAO-A and MAO-B (80% of total MAO

activity) in the human brain with different biological functions, regional distribution and substrate selectivity, revealing distinct clinical relevance (Tan et al., 2022).

MAO-B is in the outer membrane of the mitochondria and can be found both in neurons and glial cells with abundant expression in astrocytes. This is a major dopamine degradation enzyme which plays an important role in regulating free intraneuronal concentration of dopamine and in metabolizing dopamine taken up by glial cells. However, can wrongly catabolize dopamine that is not being used, causing dopamine-deficiency. For that reason, MAO-B inhibitors can block this effect, enhancing levels of available dopamine in the synaptic cleft (Tan et al., 2022).

Thereby, Monoamine oxidase-B (MAO-B) inhibitors are commonly used for the symptomatic treatment of Parkinson's disease (PD) and have shown efficacy and safety during early stages of PD, since the motor symptoms are caused by the loss of the ability to produce dopamine, due to neuronal death (Binde et al., 2018), as explored above.

Interestingly, a study with iPSC neurons from twins one without and one with PD showed higher MAO-B by almost 1.5-fold in PD-affected persons compared to their unaffected twin (Woodard et al., 2014).

Moreover, due to astrocytic MAO-B overexpression in a variety of brain regions, was detected a 33% increase of this protein in FC of PD **(Figure 1.10)** (Tong et al., 2017). The very first study measuring MAO-B in PD reported that neuronal contribution is reduced around 45-55% and 200% increase of MAO-B positive glia in SN (Damier et al., 1996). Altogether, these results prove the specificity of this target to visualize reactive astrocytes.

Additionally, more recently, Tong et al., also investigates PSP and MSA, showing increase in MAO-B levels in some of the regions mentioned before and finding different patterns of expression that might be useful to differentiate patients (Tong et al., 2017).

	Control (n = 10–16)	PD (n = 10–11)
Substantia nigra pars compacta		
MAOB	4.46 ± 0.20	4.67 ± 0.28
Putamen		
MAOB	2.64 ± 0.19	3.41 ± 0.20
Caudate		
MAOB	3.14 ± 0.13	3.51 ± 0.15
Frontal cortex		
MAOB	1.18 ± 0.08	1.56 ± 0.10*

Figure 1.10 - Levels of MAO-B in PD and CN brains, adapted from (Tong et al., 2017).

Imidazoline-2 Binding Sites

Imidazoline receptors are a family of nonadrenergic high-affinity binding sites for clonidine, idazoxan, and allied drugs, with three subcategories. I_1 receptors, which show capacity to regulate blood pressure, the I_2 receptors, which are mitochondrial proteins and have diversified functions, such as an effective analgesic for persistent and chronic painful conditions (inflammatory, neuropathic and postoperative pain) (Li, 2017) and, finally, I_3 that are located in the pancreatic cells and regulate insulin secretion (Head & Mayorov, 2006).

Imidazoline I_2 receptors or I_2 binding sites (I_2BS) are located in the outer membrane of the mitochondria and are expressed in astrocytes and neurons, albeit in a much lower density. These receptors are constituted by a group of, at least, four biologically diverse heterogenous proteins - molecular weight in rat brains ~30, ~45, ~66, ~85 kDa and the expression level of these proteins can vary depending on the pathology (Li, 2017). The molecular identities are still poorly understood, only one of the proteins shows strong evidence to be brain creatine kinase (~45 kD protein band) (Kimura et al., 2009). However, the properties of I_2BS can vary at molecular level between astrocytes and neurons, between brain regions and pathologies (Li, 2017).

Regarding the expression of I_2BS on reactive astrocytes, De Vos *et al.* shown levels of positive expression in cortex, hippocampus, basal ganglia and brainstem of the human brain, therefore, validating these receptors as reflectors of reactive astrogliosis (De Vos et al., 1991, 1994).

Activation of I_2 receptors can increase the expression of GFAP in astrocytes, producing a neuroprotective effect (Qiu & Zheng, 2006). Moreover, these receptors are involved in the

regulation of GFAP expression (Olmos et al., 1994; Sastre & García-Sevilla, 1993) and a preclinical investigation that treated rats with imidazoline antagonists showed an increase in both I_2BS and GFAP parallelly in AD, suggesting biological interaction between them (García-Sevilla et al., 1998).

Besides, a *postmortem* study performed in CN and AD brain tissue, by testing ^{3}H-idazoxan in the presence of adrenaline to inhibit α_2- adrenoceptor binding and finding a 63% increase in I_2BS density in AD *postmortem* brain tissues, demonstrated that I_2BS expression reliably reflect astrocytes in pathological and non-pathological conditions (Ruiz et al., 1993). In the same year, a study showed imidazoline receptors upregulation in ageing individuals and a positive correlation with MAO-B levels (Sastre & García-Sevilla, 1993).

However, I_2BS expression in PD brain regions is not explored yet, which is fundamental to better understand its expression patterns.

1.7 - PET Imaging

PET (Positron emission tomography) is a nuclear powerful non-invasive imaging technique that enables to access in vivo information about multiple brain functions, proving a high clinical impact in different medicine fields with sensitivity and accuracy to aid diagnose, therapy, monitor disease progression, treatment effect and explore new therapy targets (Vaquero & Kinahan, 2015). Other neuroimaging non-invasive techniques are also widely used and provide relevant information, such SPECT, Magnetic resonance imaging (MRI), transcranial brain sonography (TCS) (Pavese and Brooks, 2009).

Despite the lack of a single test capable of diagnosing a neurodegenerative disease alone, a combination of tests can help narrow the differential diagnosis.

Currently, patients with Parkinsonian Syndromes can go through structural and functional imaging.

For structural evaluation an MRI is performed, and it is expected that most PD patients show a normal MRI, eventually with diffuse atrophy. Nevertheless, MSA, PSP, DLB and corticobasal degeneration (CBD) patients normally have structural alterations, so this exam can be useful as a distinguishing tool (Broski et al., 2014)

FDG-PET images regional glucose metabolism, since about 95% of the adenosine triphosphate (ATP) needed for brain function is derived from glucose, so its intake can provide information about neuronal activity. In PD, it is verified a decrease in striatal glucose consumption. FDG-PET in the field is FDA – Food and drug administration approved for differentiating AD from frontotemporal dementia (Broski et al., 2014).

^{11}C-PiB and ^{18}F-florbetapir PET, which evaluates amyloid-binding is expected to be negative in PD patients, so positive results can, combined with other tests, help diagnosing DLB, preventing PD-misdiagnosis (Broski et al., 2014).

Finally, ^{123}I-ioflupane SPECT can help diagnosing idiopathic PD and distinguish it from secondary parkinsonism syndromes (which have intact dopamine activity) due to assessment of dopamine transporters. This image can confirm neuronal loss by reflecting DA transporters expression, albeit fails to differentiate PD from other parkinsonian syndromes, since all present pre-synaptic dysfunction (Broski et al., 2014).

Hereupon, a tracer or a combination of tracers capable to distinguish PD and other parkinsonian syndromes would improve the diagnosis accuracy in early stages and change course of the treatment – as dopamine agonist therapy, is only effective for PD, but many patients take it for lack of certainty in the diagnosis, despite not showing any improvements later (Broski et al., 2014).

A panoply of tracers has been studied in concern of PD pathology, targeting different neuronal structures or systems: monoaminergic, cholinergic and glucose metabolism, however the field still needs proofs of clinical value/benefit to bring new criteria to the picture and overcome medical challenges.

Considering all the information presented above, reactive astrogliosis is a robust candidate and early biomarker to be assessed by PET imaging. Therefore, there is already a few tracers developed, namely Deprenyl, which binds irreversibly to MAO-B and BU99008, a more recent radiotracer that targets I_2BS (Fowler et al., 2015; Kealey et al., 2013; Tyacke et al., 2012a, 2018).

Denote there are also two more compounds developed – SL25.1188 and SMBT-1, although, despite the possible potential, there is still a low number of studies and none of them were focused on PD.

^{11}C-deuterium-L-deprenyl (^{11}C-Deprenyl/DED) has been extensively explored in different modalities of studies with AD (Schöll et al., 2015) and also in many other diseases, such as Creutzfeldt-Jakob disease, ALS, focal epilepsy (Engler et al., 2003; Johansson et al., 2007; Kumlien et al., 2001).

^{11}C-Deprenyl has brought remarkable findings and developments in concern of AD comprehension, showing reactive astrocytes are crucial in AD progression and an early event of the disease course, once Deprenyl reveals high binding levels in MCI patients (Carter et al., 2012), even preceding amyloid plaques (Rodriguez-Vieitez et al., 2015). In addition, Choo and colleagues reported a significant correlation between ^{11}C-Deprenyl binding and grey matter density in prodromal AD cases, suggesting an early link to cellular

loss (Choo et al., 2014). Finally, besides the link with Aß, Lemoine *et al.*, found a correlation between reactive astrocytes and tau deposits (Lemoine et al., 2017), another hallmark of the disease.

Postmortem study with sporadic AD assessed the regional binding pattern of microglia reactive astrocytes and shows that, unlike microglia, astrogliosis correlates with Aß plaques (Ni et al., 2021). However, a different study also using ^{3}H-Deprenyl and ^{3}H-PIB performed autoradiography and demonstrated that astrocytes are significantly expressed not only in brain regions with high Aß plaques number but also other regions, leading to the theory of coexistence of different subpopulations of this glia cells in AD brain regions (Marutle et al., 2013).

In familiar cases, an in vivo multi-tracer approach found elevated ^{11}C-Deprenyl binding in Autosomal dominant-AD cases (Rodriguez-Vieitez et al., 2016; Schöll et al., 2015) and exhibited a decrease in reactive astrocytes later during the disease progression, as the Aß burden gets more pronounced (Rodriguez-Vieitez et al., 2016).

As a result of combing a wide panoply of relevant findings, Kumar and colleagues recently proposed a two-wave theory for reactive astrogliosis course in AD. The first wave is caused by "an increased DED binding at preclinical /prodromal stages", followed by a depression – "lower DED binding (at AD dementia)" and finally the second wave "at advanced/end stage of AD dementia (*postmortem*)", reflected by the "increase again in DED/BU99008 binding" **(Figure 1.11A)** (Kumar et al., 2023). Later, a review about astrocytic signature, based on PET results for BU99008, Deprenyl and SMBT-1 reinforced this theory **(Figure 1.11B)** (Fontana et al., 2023).

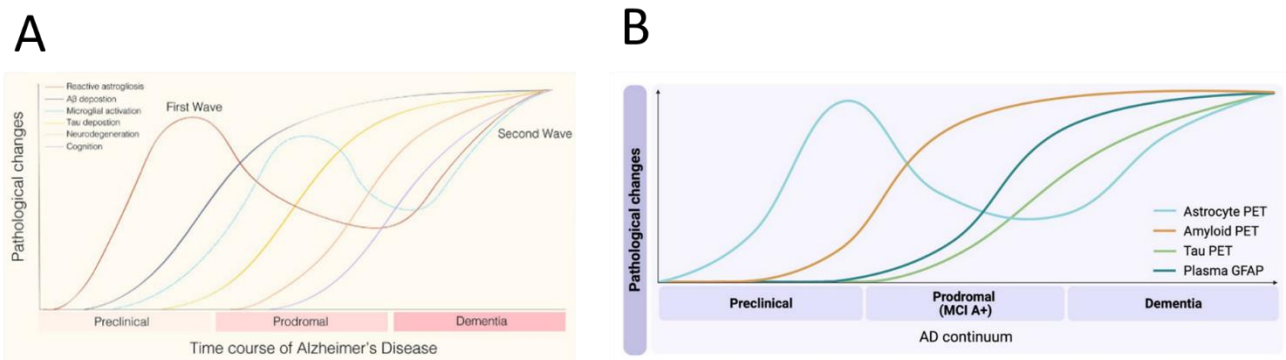


Figure 1.11 - The 'first (early)' and 'second (late)' wave of reactive astrogliosis in AD pathology adapted from (Kumar et al., 2023) **(A)** and from (Fontana et al., 2023) **(B)**.

In conclusion, all these results corroborate that Deprenyl is a promising and selective PET imaging biomarker of reactive astrogliosis.

However, despite studies showing increased reactive astrocytes in PD and the correlation between astrocytic MAO-B and various pathological features of PD (Mallajosyula et al., 2008), there is a paucity of studies with Deprenyl in PD patients.

To the best of our knowledge, only one recent study PD (2 patients), among other pathologies - AD, MSA, PSP, using ^{18}F-Deprenyl. The results indicate a similar increased level of MAO-B expression in both PD cases, but without control baseline levels to compare it with, limiting conclusions. The participants were diagnosed 1.7- and 4.8-years before the study, although their age difference is not significant (1 year), neither is their stage of the disease, according to the disease severity indices presented. Thus, new studies need to be performed with a wider range of ages, disease stages, higher number of subjects and inclusion of controls, as mentioned by the authors (Ballweg et al., 2023).

Despite validation and specificity to reflect reactive astrocytes, Deprenyl is not presenting all the panorama and developing new tracers to complement the existing can bring more and new information to the frame, which led BU99008 to emerge.

BU99008 targets imidazoline type-2 binding sites and was reported to cause reduction of available I_2 receptors, due to irreversible binding (Tyacke et al., 2002). The preclinical assessment of ^{11}C-BU99008 determinates appropriated proprieties for the tracer: reversible kinetics, specificity, selectivity, brain penetration and distribution (Tyacke et al., 2012b), later confirmed with an animal evaluation (Kealey et al., 2013; Parker et al., 2014). Brain distribution evaluation proved to be in accordance to the literature, validating ^{11}C-BU99008 as a promising reactive astrogliosis biomarker (Kealey et al., 2013; Parker et al., 2014; Tyacke et al., 2018). Additionally, BU99008 showed capacity to detect small changes caused by endogenous or exogenous ligands with specific binding for I_2 receptors (Kawamura et al., 2017).

Despite demonstrated specificity, BU99008 also has an allosteric binding site in MAO-B that should be considered (Tesson et al., 1995). In spite of that, MAO knockout mice express non-MAO I_2BS, rhesus pretreated with selective I_2BS inhibitor (BU224) presented significantly decreased binding and additional blocking studies in rhesus monkeys and healthy CNs corroborated its high selectivity and specificity, showing that BU99008 signal is mostly provided by non-MAO-B I_2BS (Parker et al., 2014; Remaury et al., 2000; Tyacke et al., 2012a).

Recent AD *postmortem* studies validated ^{3}H-BU99008 as a surrogate biomarker for reactive astrogliosis in AD. The authors demonstrated that ^{3}H-BU99008 could detect multiple binding sites in AD with different levels of affinity (super high, high, low), showed that Deprenyl is incapable of majorly blocking BU99008 binding and that their binding

behaviors in CN and AD tissues, vary compared to ^{3}H-Deprenyl. In consequence, the Kumar *et al.* confirms BU99008 specificity and suggests that the two used tracers are targeting distinct coexistent subpopulations or phenotypes of astrocytes to explain the presented results (Kumar et al., 2021).

On top of that, in vitro binding studies in AD and CN tissues showed, on one hand, higher specific binding in AD sections compared to CN and spatial overlap of higher binding regions with GFAP immunohistochemistry and, on another hand, the incapacity of both PiB and florbetaben to displace BU99008, proven no off target binding (Calsolaro et al., 2021). A PET imaging in vivo pilot study with older cognitively impaired (CI) individuals and aged-matched CN, evidence higher uptake levels of ^{11}C-BU99008 in Aß-positive MCI and AD subjects. ^{18}F-florbetaben (reflects Aß plaques) also demonstrated a relationship with ^{11}C-BU99008 binding patterns in these Aß-positive individuals. Although the same link was presented by 3 out of 11 Aß-negative patients, suggesting that reactive astrogliosis can begin before Aß plaque deposition, as previously proposed and supported by Nordberg group at Karolinska Institutet (Calsolaro et al., 2021).

Lastly, a multi-tracer study analysed two groups of cognitively impaired subjects: one with AD or related dementia and one with MCI patients and demonstrated that astrogliosis reactivity is increased in frontal, parietal and occipital areas of Aß-positive patients, assessed by ^{11}C-BU99008 uptake. When compared MCI and AD, in MCI patients the binding was even higher, leading the authors to propose that reactive astrocytes biomarkers are elevated in pre-symptomatic stages and then decline in early AD phase, assuming also the possibility of the lower detected binding being caused by a phenotype switch during the disease progression (Livingston et al., 2022), as preciously suggested by Kumar (Kumar et al., 2023). Although, note that the model suggested by Livingston *et al.* diverges in advanced AD/dementia.

Investigation of regional astrogliosis and the role of aging on regional I_2BS distribution, compared PDD patients with two groups of healthy controls, a younger and older was performed. The results point out no significant difference between PDD patients and older CN, which might suggest the higher binding is a consequence of aging (Mohamed et al., 2022).

Interestingly, another study that also performed regional distribution binding in CN, in comparison to two groups of PD patients – one early stages of the disease and one in moderate/ advanced stages, found that the volume of distribution assessed using ^{11}C-BU99008 is around 52% higher in the brain stem of patients with early onset. In contrast,

the moderate/advanced PD patients show decreased binding levels of BU99008 both in cortical and subcortical regions (Wilson et al., 2019). These results point us towards a possibly theory: reactive astrocytes actions are more pronounced in the beginning of the disease and there is a loss later during the progression of pathology, albeit more data being necessary.

SMBT-1 is recent PET tracer which also targets MAO-B. Despite few published results (Harada et al., 2021; Villemagne et al., 2022), SMBT-1 shows promising capacity to help understand astrocytes' behavior and, by comparison with BU99008 and Deprenyl, might help understand heterogeneity in different subpopulations.

According to the first in human evaluation of the tracer, it is highly selective to MAO-B and binds reversibly (Villemagne et al., 2022). In addition, an in vitro comparison of ^{18}F-SMBT-1 binding with regional MAO-B expression in the brain proved accordance. The same study shows, through autoradiography assays in AD and CN, a higher binding levels in AD. Moreover, competition assays with selective MAO-B inhibitor lazabemide confirmed high selectivity and low non-specific binding (Harada et al., 2021). Most recently, Fontana and colleagues demonstrated that SMBT-1 has a similar behavior to Deprenyl, competing for the same sites and is also capable of displacing BU99008 albeit with much lower power, suggesting a possible interaction with BU99008 site at the catalytic entrance of MAO-B (Fontana et al., 2022).

^{11}C-SL25.1188 is a reversible imaging agent used in the human brain. Initial studies with rat brains demonstrated favorable specificity, no abnormal retention rate, good biodistribution and metabolic stability (Dahl et al., 2017). First results point out appropriated characteristics in preclinical assessments with animal studies - primate brain (Saba et al., 2010) and with human subjects - AD patients (Dahl et al., 2017) and major depressive disorders (Moriguchi et al., 2019). Although there is few evidence of its properties and, for that reason, needs additional studies.

Lastly, ^{8}F-THK5351, a tracer originally developed to target tau protein (Harada et al., 2016) has reveal later capacity to bind reversibly to MAO-B with a high level of selectivity (Harada et al., 2018, 2021; Ng et al., 2017).

Both AD and PD are diseases strongly characterized by progressive dysfunction, neurodegeneration, protein misfolding and pathological aggregation – proteinopathies, although for PD the reactive astrogliosis neuroimaging field is underdeveloped compared to AD. Hence, all these AD findings accomplished should also stimulate to widen the panoply of diseases to be explored, namely PD.

To sum up, altogether these findings clearly show that there is still no biomarker which can alone be sufficient to deliver an accurate diagnose and monitoring of PD, which leads to considering an approach with multiple factors the most promising.

1.8 - Summary and Motivation

New approaches to understand the role of various pathological hallmarks in PD course timeline are needed to ensure clinicians, monitor therapeutic interventions, and develop alternate therapeutic strategies and targets. Exploring reactive astrogliosis signature from a biomarker point of view, since it shows a great correlation with early stages of the pathology, can bring better understanding of the disease continuum and broadly impact PD clinical frame in terms of diagnosis and treatment.

Therefore, the *main goal* of the present thesis is **'to employ the innovative mixed battery of multi-PET tracer approach and translational *postmortem* brain imaging to visualize and explore reactive astrogliosis signature in the etiology of PD'**.

1.9 - Research aims and strategy

To achieve our main objectives, we propose a pioneer, presumably the first *postmortem* study of reactive astrogliosis in PD brain tissues, using both ^{3}H-Deprenyl and ^{3}H-BU99008 PET tracers.

Specifically, the *aims* include:

Aim 1: Evaluation of ^{3}H-BU99008 and ^{3}H-Deprenyl binding site density and affinity in PD and CN brains with Saturation binding assays.

Aim 2: Identify the number of binding sites of ^{3}H-BU99008 and ^{3}H-Deprenyl in PD and CN brains with Competition binding assays in the presence of unlabeled BU99008 and Deprenyl.

Aim 3: Comparative interactions studies between ^{3}H-BU99008 and ^{3}H-Deprenyl.

Aim 4: Assessment of ^{3}H-BU99008 and ^{3}H-Deprenyl regional binding distribution patterns in PD and CN brains.

Chapter 2

2. Materials & Methods

This chapter provides information regarding the materials and techniques used to conduct this project. Each section addresses different steps of the experimental process:

- Materials;
- Clinical information & Brain tissue selection;
- Sectioning;
- Brain Homogenates and subcellular fractions preparation;
- Saturation Binding Assays;
- Competition Binding Assays;
- Regional distribution Binding;
- In vitro autoradiography studies.

Note that the protocol followed in the experiments presented in this sectioned is an inhouse optimized protocol (Kumar et al., 2021).

1.1 Chemicals

^{3}H-BU99008 (Specific Activity (SA) = 83 Ci/mmol), ^{3}H-Deprenyl (SA = 82 Ci/mmol), ^{3}H-Deprenyl (SA = 83 Ci/mmol) and unlabeled BU99008 and Deprenyl were custom synthesized by Novandi Chemistry AB (Södertälje, Sweden). Chemicals (sodium chloride (NaCl), potassium chloride (KCl2), calcium chloride (CaCl2), Tris base, magnesium chloride (MgCl2), disodium phosphate (Na2HPO4) and potassium dihydrogen phosphate (KH2PO4)) were purchased from Sigma-Aldrich AB, Sweden.

1.2 Methods

Brain Tissue - Clinical information analysis & Brain tissue Selection

Human frozen *postmortem* tissue from Parkinson's disease - PD and Healthy Controls Cases - CN brains obtained from the Netherlands Brain Bank (NBB – Amsterdam, Netherlands) were available for the study. Regarding the brain tissue from the 4 PD cases, 4 regions were selected in all cases, 2 cortical regions: frontal cortex and temporal cortex (TC) and striatum regions: caudate nucleus and putamen, allowing to compare different brain regions affected in different stages of the disease development – cortical regions are only affected later/ in more advanced stages. Thus, a cautious analysis of the clinical information of each patient allowed us to select the most suitable cases and the same regions of interest from all of them for comparison in the project. Regarding the CN, we selected the cases that allowed the analysis of the same brain regions from the in-house inventory. Factors such as age, sex, amyloid pathology, tau deposits, comorbidities, duration of the disease, medication and education were also considered. **Table 2.1** provides a summary of clinical and demographic information about the patients and controls from which brain tissues were used in this study.

Table 2.1 - Clinical demographic information of the patients whose brains were used in the experiments presented in this document.

	Sex	Age (years)	Braak Stage	BS LBs	H&Y	*DD*	PMD (h:min)	Observations
Controls								
CN 1	M	82	2	3	-	-	05:55	Leukemia, depression, morphine *
CN 2	F	89	1	0	-	-	13:00	Phenobarbital *
CN 3	F	82	1	0	-	-	07:45	Morphine, Paroxetine *
CN 4	F	77	1	0	-	-	02:55	Depression, morphine*
CN 5	M	82	2	0	-	-	05:45	Thiopental, rocuronium*
CN 6	F	55	1	0	-	-	07:30	Valprioc acid *
CN 7	M	77	2	0	-	-	04:50	Euthanasia, levodopa, motor impairment *
Mean	**3M/4F**	**77.7±10.8**	**1-2**	**0-3**	**-**	**-**	**6.54±3.3**	

Parkinson´s Disease								
PD 1	F	83	1	5	4	24	10:35	Euthanasia, rasagiline, levodopa
PD 2	M	74	2	6	-	7	06:10	Short term mild memory impairment, levodopa
PD 3	F	66	-	6	4	16	05:00	Euthanasia, levodopa
PD 4	M	68	1	5	2	24	04:05	Cognitive decline, selegiline, levodopa
Mean	**2M/2F**	**72.7±7.6**	**1-2**	**5-6**	**2-4**	**17.8±8.1**	**6.4±2.9**	

Bold values represent the number of male and female cases from control and PD used in this study as well as the mean ± standard deviation (SD) for the age, Braak stage tau, Braak stage Lewy bodies and *postmortem* delay of these individuals. BS LBs – Braak Stage Lewy Bodies; H&Y - Hoehn and Yahr Scale; DD – Disease duration; PMD -*postmortem* delay. * All these cases suffered from some of the following comorbidities: pneumonia, various types of cancer, hypertension, diabetes, cardiac problems, among others. Many of these are considered aged-related complications.

Sectioning

Small frozen *postmortem* brain sections (thickness: 20 µm) **(Figure 2.1)** kept at -80ºC were sectioned using a cryostat (Microm HM500M, Cellab) at -20ºC, coated on glass slides (Epredia – Superfrost Plus Adhesion Microscope Slides) and kept frozen at -4ºC. All regions and cases were sectioned under the same conditions.

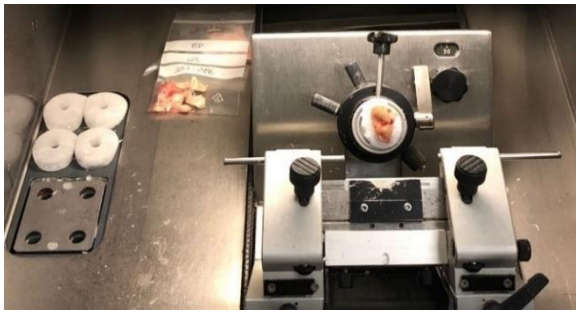


Figure 2.1- Cryostat with small frozen *postmortem* brain tissue mounted and prepared to be sectioned.

Brain Homogenates and subcellular fractions preparation

The human brain tissue was homogenized in phosphate buffer saline (PBS – pH 7.4) with additional 0.1% bovine serum albumin (BSA; 250 mg/mL) and protease/ phosphatase inhibitors (10 µL/mL) and were stored at −80 °C in aliquots until use in binding experiments.

For subcellular fractions preparation, the brain homogenates were centrifuged at 4°C for 10 min at 2800-3200 rpm. From the first pellet was obtained the P1 – nuclear fraction - by diluting it in 8mL PBS Buffer with protease/ phosphatase inhibitors. The supernatant was centrifugated again at 4°C for 20-25 min at 11000-12000 rpm. The second pellet corresponds to P2 – Synaptosomal/ membrane fraction – which was diluted in 2-4mL PBS Buffer with

protease/ phosphatase inhibitors, according to the pellet volume. The S2 fractions are the resultant supernatant **(Figure 2.2)**. After, the protein concentration was calculated using the Kit DC Protein Assay from Bio-Rad and by reading the absorbance in ELISA plate reader. All the subcellular fractions were stored at −80 °C in aliquots until use in binding experiments.

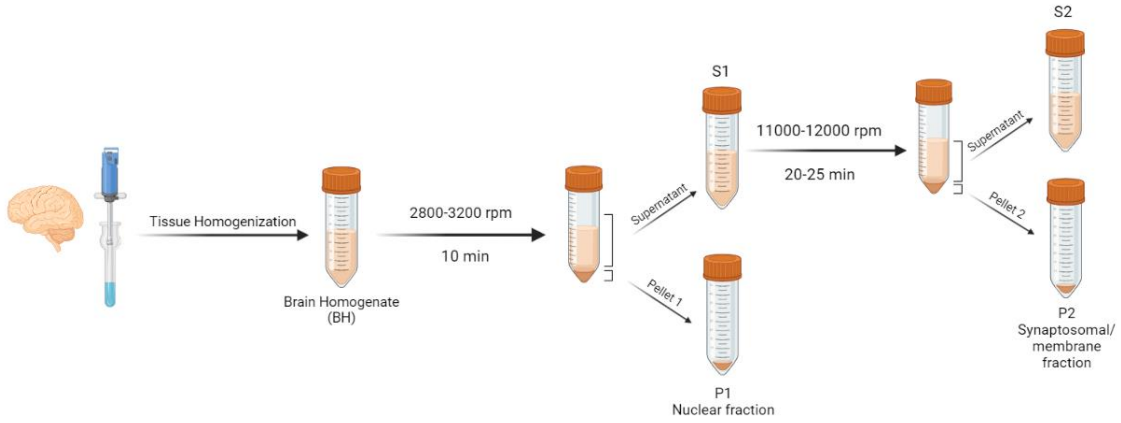


Figure 2.2 - Illustration shows the subcellular fractionation protocol for the preparation of P1 nuclear, P2 synaptosomal/membrane and S2 microsome/cytosolic proteins fractions from brain homogenates.

Saturation Binding Assays

Saturation binding assays using ^{3}H-BU99008 **(Figure 2.3)** were performed in 3 PD (PD1, PD2, PD4) and one CN cases for two brain regions – frontal cortex (Cortical region) and caudate nucleus (Subcortical) (CN2 for FC and CN1 for caudate). Tissue from the brain homogenates (0.5 mg) of all the cases was incubated with an increasing range of concentrations - 0.59nM to 30nM - of ^{3}H-BU99008 in 50 mM Tris-HCl binding buffer pH 7.4 (50 mM Tris-base, 140 mM NaCl, 1.5 mM MgCl2, 5 mM KCl, 1.5 mM CaCl2) for 90 minutes, at 37 °C. Non-specific (NSP) binding was determined with 1 µM unlabeled BU99008.

Saturation binding assays **(Figure 2.3)** using ^{3}H-Deprenyl were performed in 3 PD (PD1, PD2, PD4) and one CN (CN1) cases for 2 brain regions – frontal cortex and caudate nucleus. In ^{3}H-Deprenyl assays were incubated 0.1 mg of tissue from the brain homogenates of all the cases with increasing concentrations - 0.78nM to 40nM - in Na-K phosphate buffer pH 7.4 for 1h, at 37 °C. NSP binding was determined with 1 µM unlabeled Deprenyl.

For all the assays, the binding reaction was terminated by filtering through glass fibre filters (pre-soaked for 2–3 h in 0.3% polyethylenimine), followed by three quick rinses with cold binding buffer and overnight incubation of the filter in the scintillation liquid. The radioactivity in the tubes with reaction filters was counted on the day after with a beta

radiation scintillation counter since the radioactive source used was tritium (^{3}H) (PerkinElmer Tri-Carb 2910TR).

The Bmax – density of binding sites and Kd - affinity were determined by using the non-linear regression competitive-binding model of GraphPad Prism 9 software.

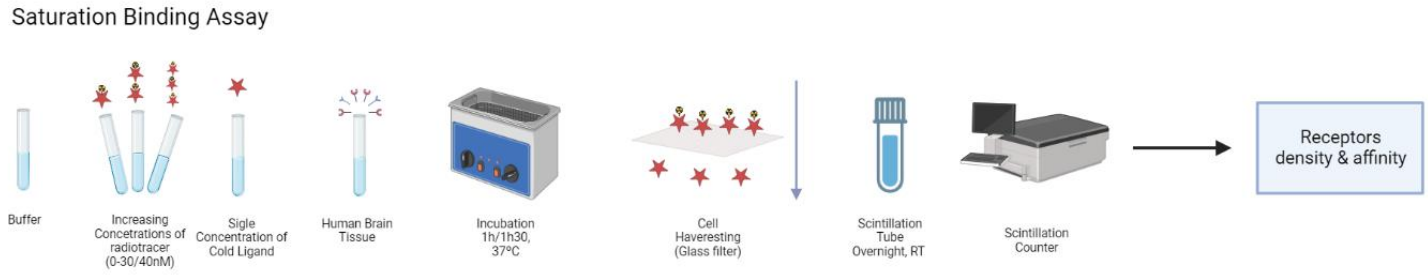


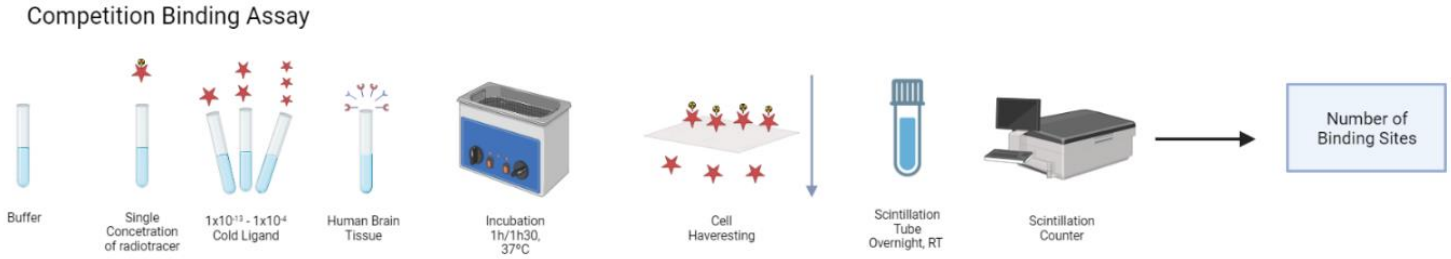
Figure 2.3 - Illustration of Saturation binding assay protocol steps.

Competition Binding Assays

Competitive binding assays **(Figure 2.4)** on two PD and two CN brains homogenates for 2 brain regions: frontal cortex and caudate nucleus were performed with two PET tracers.

Firstly, competition binding assays with 1nM of ^{3}H-BU99008 and increasing concentrations ($1x10^{-13}$ M to $1x10^{-5}$ M) of unlabeled BU99008 (PD1, PD4 & CN1, CN2) and Deprenyl (PD1 & CN3) were accomplished by incubating the compounds with 0.5mg of tissue in binding buffer (50 mM Tris-HCl) for 90 minutes, 37ºC.

Competition studies were also performed by incubating 0.1mg of tissue with 3nM ^{3}H-



Deprenyl along with increasing concentrations ($1x10^{-13}$ M to $1x10^{-4}$ M) unlabeled Deprenyl (PD1, PD4 & CN1, CN2) and BU99008 (PD1 & CN3) in binding buffer (50 mM Na-K phosphate buffer) for 1h at 37ºC.

Figure 2.4 - Illustration of Competition binding assay protocol steps.

For all the experiments, after incubation a similar protocol as saturation binding assay was done and the binding was quantified using the scintillation counter.

The half-maximal inhibitory concentration (IC50) was determined by using the non-linear regression competitive-binding model of GraphPad Prism 9 software.

Regional Distribution Binding Assays

Regional binding studies were performed on the frontal cortex, temporal cortex, caudate nucleus, and putamen brain homogenates (0.5 mg tissue) from four CNs and four AD patients, using 1nM ^{3}H-BU99008 and incubating 90 minutes, at 37ºC. The binding was quantified using the beta scintillation counter. Non-specific (NSP) binding was determined with 1 µM unlabeled BU99008.

Regional binding studies **(Figure 2.5)** were performed on the frontal cortex, temporal cortex, caudate nucleus, and putamen brain homogenates (0.1 mg tissue) from four CN (CN1-4) and four PD patients, using 3nM ^{3}H-Deprenyl by incubating 1h, at 37ºC. The binding was quantified using the beta scintillation counter. Non-specific (NSP) binding was determined with 1 µM unlabeled Deprenyl.

Caudate was not available for CN 3 and putamen was not available for CN 1 and CN 4. The binding data was analysed using GraphPad Prism 9 software and presented in graphs as specific binding (fmol/mg).

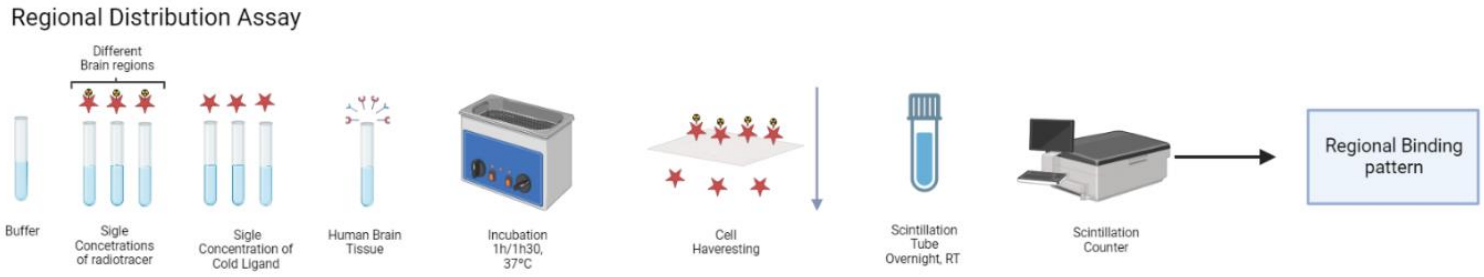


Figure 2.5 - Illustration of Regional distribution binding assay protocol steps.

In Vitro Autoradiography studies

^{3}H-BU99008 and ^{3}H-Deprenyl autoradiography studies were performed on small frozen *postmortem* brain sections from 7 CN and 4 PD patients, using all available brain regions.

The frozen sections were allowed to dry at room temperature (RT) for 20–30 mins, followed by 1 h incubation with either ^{3}H-BU99008 (1 nM) or ^{3}H-Deprenyl (3 nM) at RT or with unlabeled BU99008 (1µM) or Deprenly (1µM) for the NSP sections. Afterwards, the sections were rinsed for 5 mins three times in cold buffer (50 mM Tris-HCl buffer, pH 7.4 for ^{3}H-

BU99008; 50 mM Na-K phosphate buffer, pH 7.4 for ^{3}H-Deprenyl), followed by a quick dip in cold distilled water.

^{3}H-BU99008 vs unlabeled Deprenyl autoradiography was performed on small frozen *postmortem* brain sections from four CN and seven PD patients, using all available brain regions.

The frozen sections were allowed to dry at room temperature (RT) for 20–30 mins. After, proceed to pre-blocking with unlabeled Deprenyl (1uM) at RT for 30 minutes, followed by 2 rinses of 5 minutes with cold buffer (50 mM Tris-HCl buffer, pH 7.4 for ^{3H}-BU99008). Afterwards, sections were incubated 1 h with 1nM of ^{3}H-BU99008 at RT and, finally, were rinsed for 5 minutes three times in cold buffer followed by a quick dip in cold nanopure water.

All the sections were allowed to dry at RT for 24 h and were then apposed together with a tritium standard (Larodan Fine Chemicals AB, Mälmo, Sweden) on a phosphor-plate for 4 and 7 days for ^{3}H-Deprenyl and ^{3}H-BU99008, respectively, and then imaged using a BAS-2500 phosphor imager (Fujifilm, Tokyo, Japan). The semiquantitative analyses was performed by drawing manually the regions of interest (ROI), using the multigauge software on the autoradiogram and the photo stimulated luminescence per square millimetre (PSL/mm2). The obtained values were transformed with the standard curve to fmol/mg, allowing to determine the total, NSP and specific binding of ^{3}H-BU99008 and ^{3}H-Deprenyl in the ROI.

Chapter 3

3. Results

3.1 Saturation Binding Studies

^{3}H-BU99008 saturation binding studies in CN and PD brain homogenates

The results of the saturation binding studies performed in FC and the respective saturation curves are presented in Figure **3.1A** and **3.1B**. For CN, saturation occurred at a Bmax1 of 59.1 fmol/mg and a Kd of 2.97 nM. For PD, two binding sites were observed. $Bmax_1$= 51.6 fmol/mg, Kd_1= 2.31 nM and the second binding site, which was drawn manually in the Scatchard Plot (**Figure 3.1** – Red line) shows higher affinity Kd_2= 0.75 nM and a $Bmax_2$= 25.5 fmol/mg. For caudate nucleus, the results and the respective saturation curves are illustrated in **Figure 3.1C** and **Figure 3.1D**. In this brain region, was only detected one binding site in both CN and PD tissue. For CN, saturation occurred at a Bmax of 36.3 fmol/mg and a Kd of 2.77 nM, while for PD it showed a Bmax of 110.0 fmol/mg and at a Kd of 3.47 nM, showing a 3-fold higher Bmax, compared to CN.

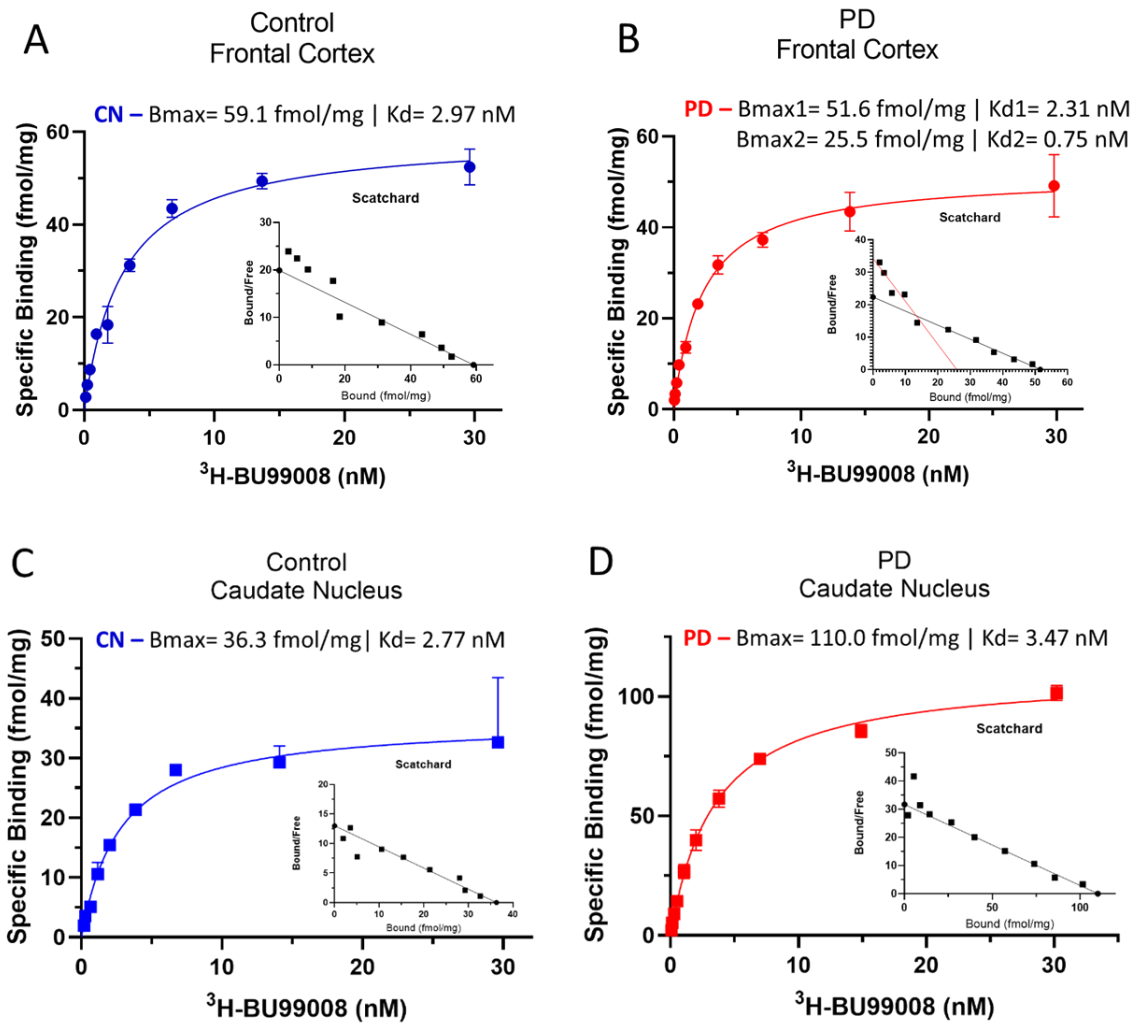


Figure 3.1 - ^{3}H-BU99008 Saturation Binding Assay in CN and PD brains. This study was performed in Frontal Cortex **(A, B)** brain homogenates from one CN and one PD case and in Caudate nucleus **(C,D)** in one CN and two PD cases, using increasing concentrations of ^{3}H-BU99008 (0-30nM). A,B,C,D show saturation binding curves for CN (82yo) and PD (83,68yo) cases, respectively, along with the corresponding Scatchard plot. The second binding site presented was drawn manually. Data are presented as means ± SEM of three experiments in duplicate. Kd- dissociation constant; Bmax - density of binding sites.

^{3}H-Deprenyl saturation binding studies in CN and PD brain homogenates

^{3}H-Deprenyl saturation in FC **(Figure 3.2A)** was reached saturation at a Bmax 190.1 fmol/mg and a Kd of 6.04 nM for CN, while the values for PD are 237.2 fmol/mg and 5.9 nM, respectively, revealing only one binding site with nM affinity and a 1.2-fold higher Bmax for PD. For caudate nucleus of CN (**Figure 3.2B**) ^{3}H-Deprenyl saturated at a Bmax of 366.6 fmol/mg and a Kd of 4.45 nM. PD saturation curve also exhibits one binding site - Bmax value of 321.1 fmol/mg and Kd 4.08 nM.

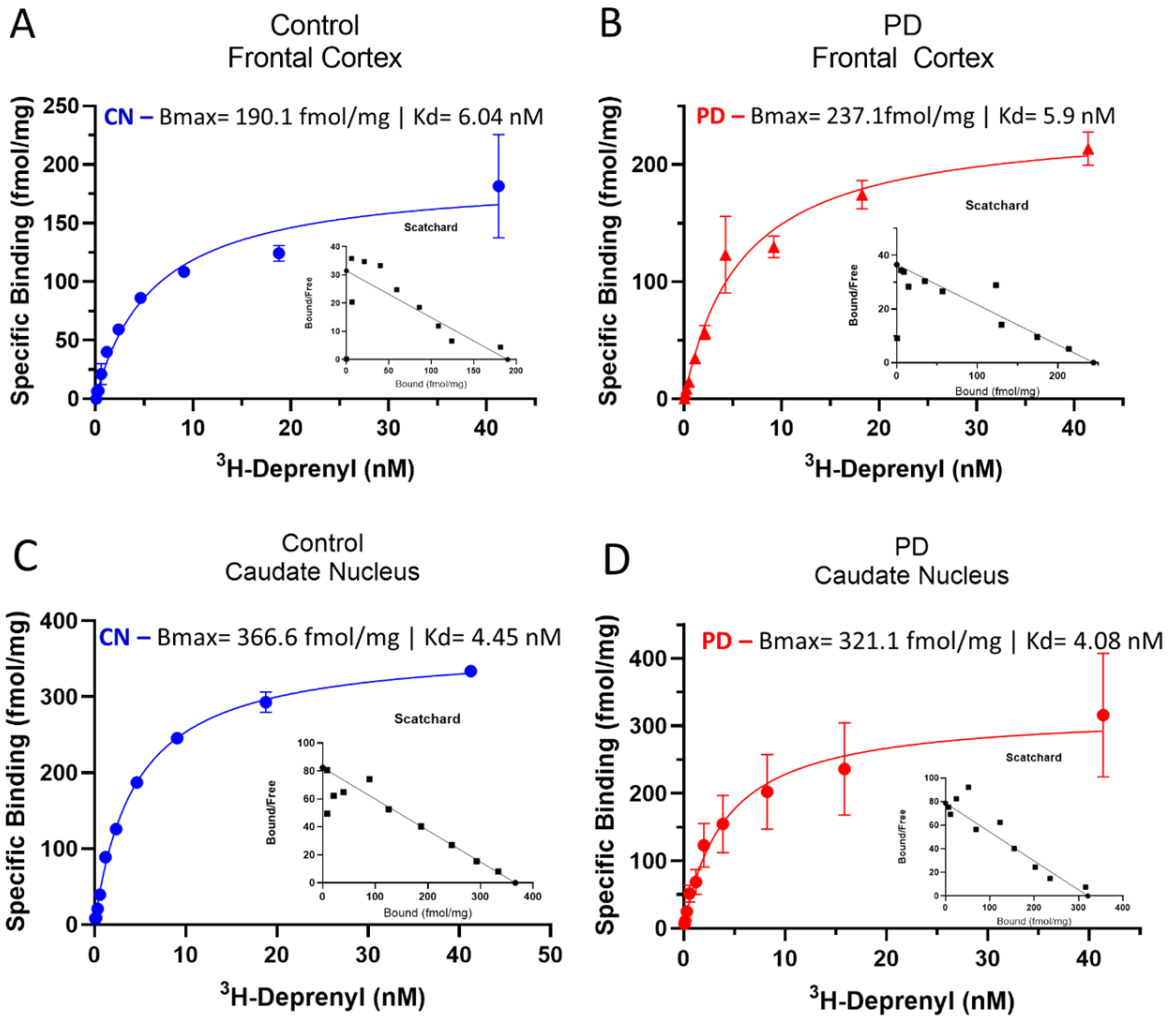


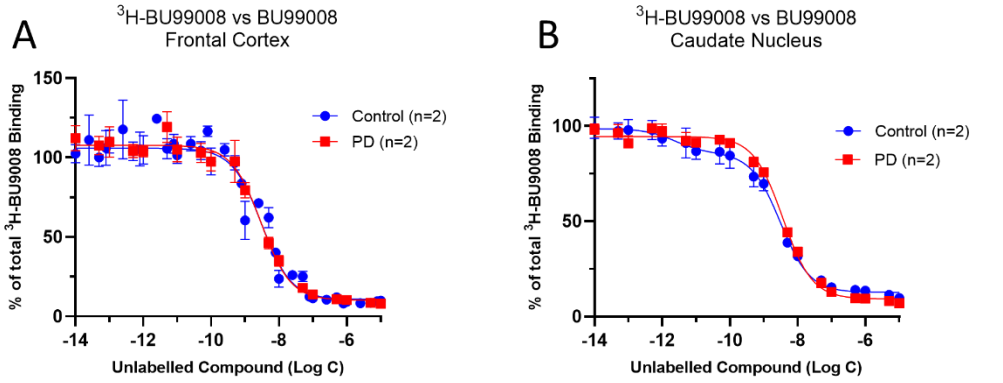
Figure 3.2 - ^{3}H-Deprenyl Saturation Binding Assay in CN and PD brains. This study was performed in Frontal Cortex **(A, B)** brain homogenates from one CN and three PD case and in Caudate nucleus **(C,D)** in one CN and three PD cases, using increasing concentrations of ^{3}H-Deprenyl (0-40nM). A,B,C,D show saturation binding curves for CN (82yo) and PD (66,68,83yo) cases, respectively, along with the corresponding Scatchard plot. Data are presented as means ± SEM of two experiments in duplicate. Kd- dissociation constant; Bmax - density of binding sites.

3.2 Competition Binding Studies

To further characterize the binding behaviour of ^{3}H-BU99008 and ^{3}H-Deprenyl competition binding assays were performed.

^{3}H-BU99008 competition binding studies with unlabeled BU99008 in CN and PD brain homogenates

Competition binding studies with ^{3}H-BU99008 vs BU99008 (**Figure 3.3**) show one binding site for CN and PD in frontal cortex **(Fig. 3.3A)** with respective binding affinities of 3.06 nM and 2.97 nM, 2 binding sites for CN in caudate nucleus ($IC50_1$= 2.3pm and $IC50_2$= 3.12nM) and one binding site for PD in caudate nucleus an IC50 value of 3.62nM **(Fig. 3.3B).** However, the proportion of second binding site found in PD caudate nucleus only represents 14%.



CN - IC50 = 3.06 nM | R^2 = 0.91
PD - IC50 = 2.97 nM | R^2 = 0.91

CN - $IC50_1$ = 2.3 pM | $IC50_2$ = 3.12 nM | R^2 = 0.93
PD - IC50 = 3.62 nM | R^2 = 0.97

Figure 3.3 - ^{3}H-BU99008 competition binding assay with unlabeled BU99008 in Frontal Cortex **(A)** and Caudate nucleus **(B)** brain homogenates of two CN (82 and 89 years old) cases. A single concentration of ^{3}H-BU99008 (1nM) was used along with increasing concentrations of BU99008 (10^{-5}-10^{-14}). Data are presented as means ± SEM of three experiments in duplicate for each CN and PD. IC50 – half-maximal inhibitory concentration.

^{3}H-Deprenyl competition binding studies with unlabeled Deprenyl in CN and PD brain homogenates

^{3}H-Deprenyl in the presence of unlabeled Deprenyl (**Figure 3.4**), for both CN and PD demonstrated one binding site in FC **(Fig. 3.4A)** with IC50 values of 8.85 nM and 11.9

nM, respectively. One binding site for CN and PD in caudate nucleus **(Fig. 3.4B)** was found ($IC50_{CN}$: 10.9nM, $IC50_{PD}$: 11.4 nM). CN and PD binding sites in frontal cortex as well as in caudate nucleus present similar affinities.

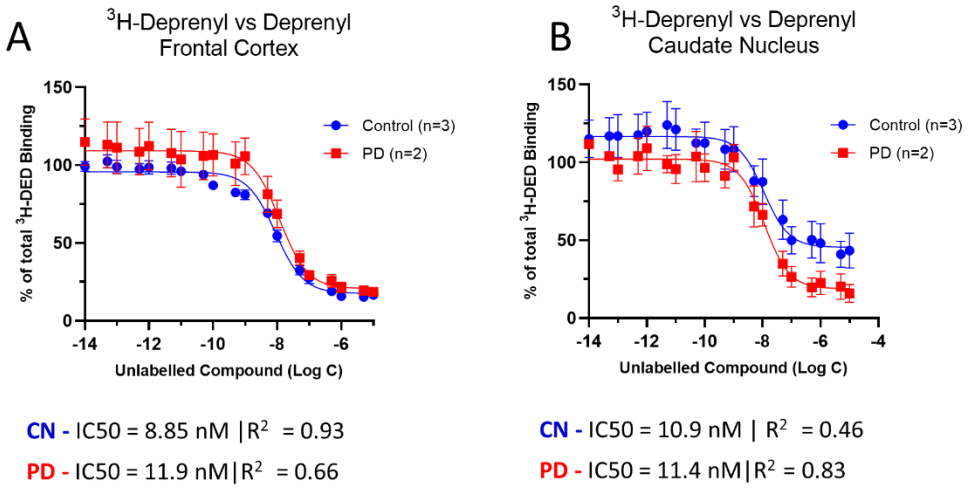
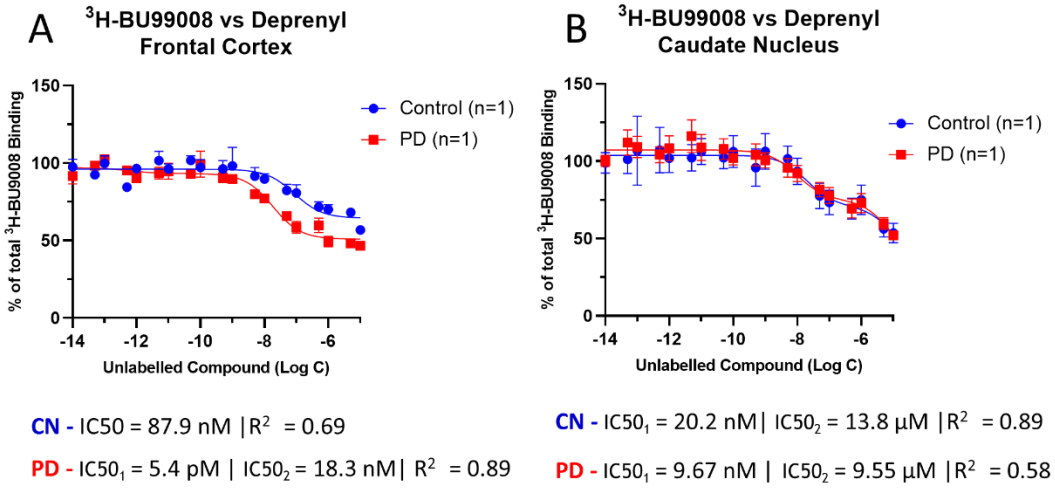


Figure 3.4 - ^{3}H-Deprenyl competition binding assay with unlabeled Deprenyl in Frontal Cortex **(A)** and Caudate nucleus **(B)** brain homogenates of three CN (82, 82, 77 years old) and two PD (82 and 89 years old) cases. A single concentration of ^{3}H-Deprenyl (3nM) was used along with increasing concentrations of Deprenyl (10^{-5}-10^{-14}). Data are presented as means ± SEM of three experiments in duplicate for each CN and PD. IC50 – half-maximal inhibitory concentration.

^{3}H-BU99008 competition binding studies with unlabeled Deprenyl in CN and PD brain homogenates

The results for the ^{3}H-BU99008 competition binding studies with unlabeled Deprenyl, presented in **Figure 3.5**, show one binding site for CN with an IC50 of 87.9 nM and two for PD in frontal cortex ($IC50_1$= 5.4 pM - 8% and $IC50_2$= 18.3 nM - 92 %) **(Fig. 3.5A).** On another hand, in caudate nucleus two binding sites were found for CN with 20.2 nM and 13.8 µM values of IC50 with 42% and 58% proportions of binding, respectively. PD also showed two binding sites in caudate nucleus ($IC50_1$= 9.67 nM and $IC50_2$= 9.55 µM) **(Fig. 3.5B).** The second binding site found caudate nucleus of PD represents a 40% proportion of binding.



CN - IC50 = 87.9 nM |R^2 = 0.69

PD - $IC50_1$ = 5.4 pM | $IC50_2$ = 18.3 nM| R^2 = 0.89

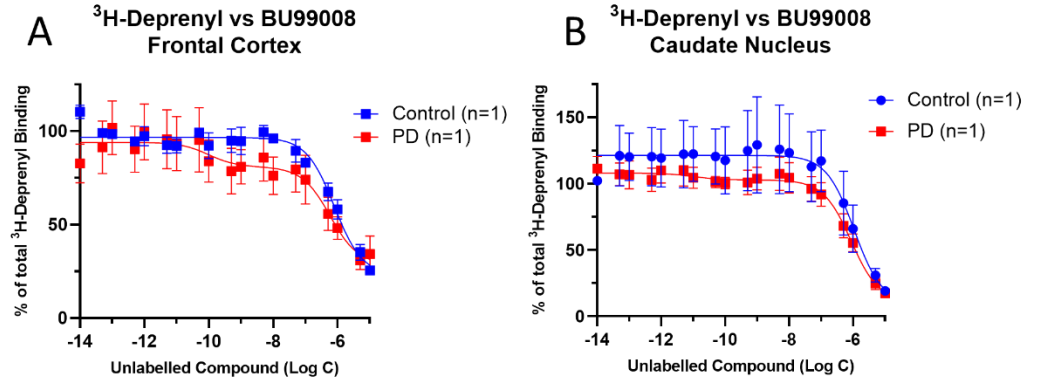
CN - $IC50_1$ = 20.2 nM| $IC50_2$ = 13.8 µM |R^2 = 0.89

PD - $IC50_1$ = 9.67 nM | $IC50_2$ = 9.55 µM |R^2 = 0.58

Figure 3.5 - ^{3}H-BU99008 competition binding assay with unlabeled Deprenyl in Frontal Cortex **(A)** and Caudate nucleus **(B)** brain homogenates of one CN (82 years old) and one PD (83 years old) case. A single cocentration of ^{3}H-BU99008 (1nM) was used along with increasing concentrations of Deprenyl (10^{-5}-10^{-14}). Data are presented as means ± SEM of three experiments in duplicate for each CN and PD. IC50 – half-maximal inhibitory concentration.

^{3}H-Deprenyl competition binding studies with unlabeled BU99008 in CN and PD brain homogenates

^{3}H-Deprenyl in the presence of BU99008 (**Figure 3.6**) revealed one binding site in FC of CN case **(Fig. 3.6A)** with IC50 values of 0.78 µM. PD showed two binding sites for FC $IC50_1$ = 98.1 pM and $IC50_2$ = 0.58 µM. In caudate nucleus of CN one binding site was found (IC50: 1.08 µM). On another hand, in PD two binding sites were detected $IC50_1$ = 9.72 pM and $IC50_2$ = 0.87 µM **(Figure 3.6B)**.



CN - IC50 = 0.78 µM |R^2 = 0.89

PD - $IC50_1$ = 98.1 pM| $IC50_2$ = 0.58 µM |R^2 = 0.55

CN - IC50 = 1.08 µM | R^2 = 0.82

PD - $IC50_1$ = 9.72 pM| $IC50_2$ = 0.87 µM |R^2 = 0.83

Figure 3.6 - ^{3}H-Deprenyl competition binding assay with unlabeled BU99008 in Frontal Cortex **(A)** and Caudate nucleus **(B)** brain homogenates of one CN (82 years old) and one PD (83 years old) case. A single cocentration of ^{3}H-Deprenyl (3nM) was used along with increasing concentrations of BU99008 (10^{-5}-10^{-14}). Data are presented as means ± SEM of three experiments in duplicate for each CN and PD. IC50 – half-maximal inhibitory concentration.

That said, it is possible to group the binding sites detected into three categories considering their IC50 values: Super high-affinity ($10^{-13 \text{ to } -11}$ M) - SHA, High-affinity ($10^{-10 \text{ to } -9}$ M) - HA and Low-affinity ($10^{-7 \text{ to } -5}$ M) – LA binding sites. A schematic was drawn to simplify the analysis and critical comprehension of the results of each tracer: ^{3}H-BU99008 **(Figure 3.7)** and ^{3}H-Deprenyl **(Figure 3.8)**.

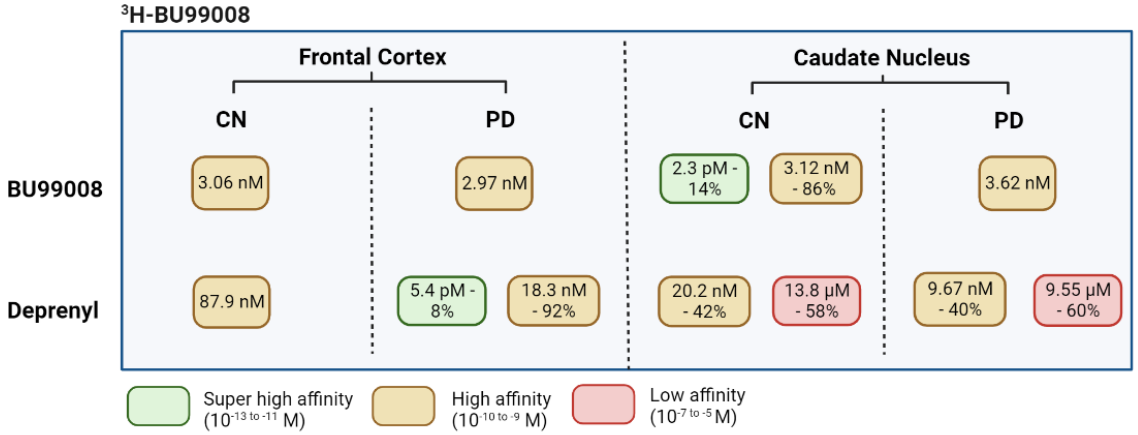


Figure 3.7 - Affinities of the various binding sites revealed for **^{3}H-BU99008** competition assays with unlabeled BU99008 and Deprenyl in *postmortem* CN and PD brain tissue in FC and caudate nucleus. When two binding sites are detected the proportion (%) of each site is presented next to its affinity. SH- Super high-affinity binding sites, SHA- super high-affinity, HA- high-affinity, LA- low-affinity binding sites.

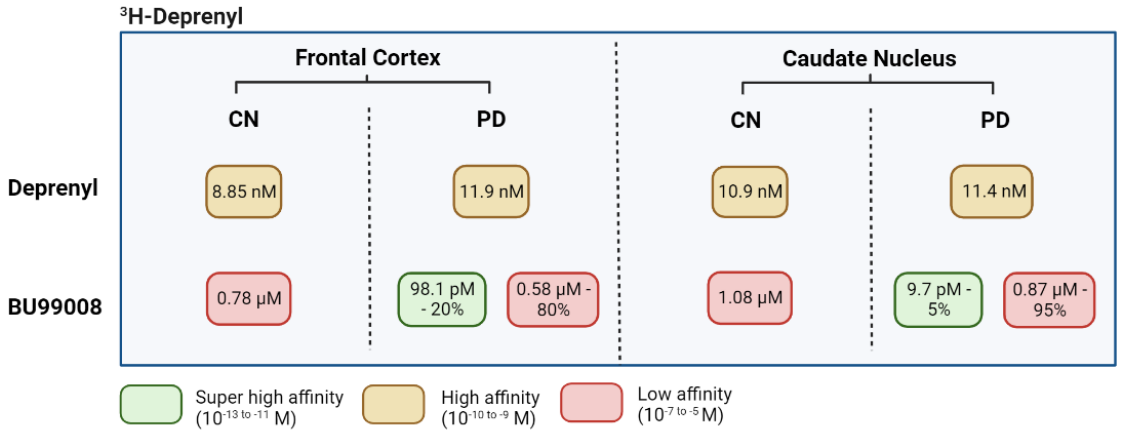
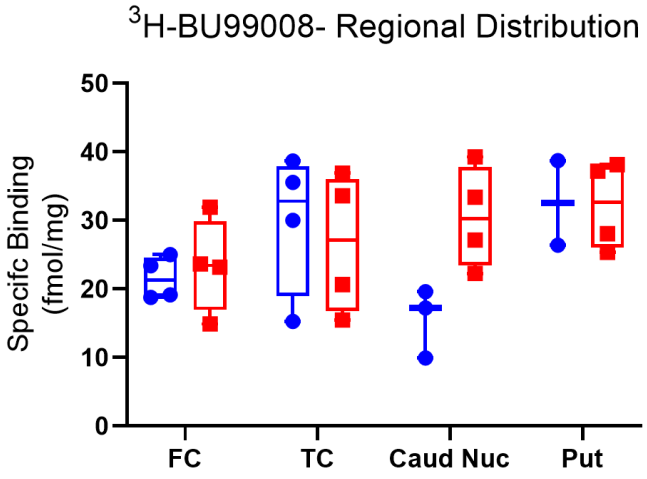


Figure 3.8 - Affinities of the various binding sites revealed for **^{3}H-Deprenyl** competition assays with unlabeled Deprenyl and BU99008 in *postmortem* CN and PD brain tissue in FC and caudate nucleus. When two binding sites are detected the proportion (%) of each site is presented next to its affinity. SH- Super high-affinity binding sites. SHA- super high-affinity, HA- high-affinity, LA- low-affinity bind sites.

3.1 Regional Distribution Binding Studies

^{3}H-BU99008 regional distribution binding studies in CN and PD brain homogenates

^{3}H-BU99008 (1 nM) regional distribution binding was performed in four brain regions (FC, TC, Caud. Nuc., Put.) from 4 CN and 4 PD individuals **(Figure 3.9).** A higher ^{3}H-BU99008 binding was observed in the FC and caudate nucleus. The increase of binding in caudate nucleus is evidentially the most significant (~50%). However, a lower and similar binding was observed in TC and putamen, respectively.



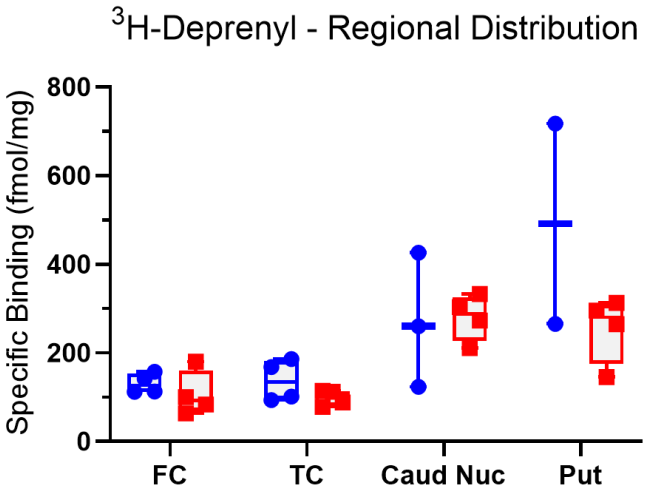
	^{3}H-BU99008 (fmol/mg)	
	CN	PD
FC	21.6	23.4
TC	29.9	26.7
Caud Nuc	15.6	30.5
Put	32.6	32.2

Figure 3.9 - ^{3}H-BU99008 regional distribution binding in *postmortem* homogenates of CN and PD individuals in four brain regions (FC, TC, Caud. Nuc., Put.), using a single concentration of ^{3}H-BU99008 of 1nM and 1 µM of unlabeled BU99008 to determine NSP binding. The **graph (left side)** shows a comparison between the specific binding results of CN and PD cases for each evaluated region and respective quantitative results are presented on the **table (right side).** Data are presented as box and whiskers plots and each point represents a mean of three experiments performed in duplicate for each case. FC – Frontal Cortex, TC – Temporal Cortex, Caud Nuc – Caudate nucleus, Put – Putamen.

^{3}H-Deprenyl regional distribution binding studies in CN and PD brain homogenates

^{3}H-Deprenyl (3 nM) regional distribution binding was performed in four brain regions (FC, TC, Caud. Nuc., Put.) from 4 CN and 4 PD individuals **(Figure 3.10)**. ^{3}H-Deprenyl binding was slightly higher in caudate nucleus of PD cases (3.6%), although for FC, TC and putamen we observed lower binding. Decrease in binding in cortical regions was ~ 23% and 40%, for FC

and TC, respectively. However, in putamen was verified a significant decrease in binding of PD, compared to CN - ~93%.



	3H-Deprenyl (fmol/mg)	
	CN	PD
FC	131.1	106.9
TC	137.7	98.5
Caud Nuc	270.2	280.2
Put	491.6	254.8

Figure 3.10 - ^{3}H-Deprenyl regional distribution binding in *postmortem* homogenates of CN and PD individuals in four brain regions (FC, TC, Caud. Nuc., Put.), using a single concentration of ^{3}H-Deprenyl of 3nM and 1 µM of unlabeled Deprenyl to determine NSP binding. The **graph (left side)** shows a comparison between the specific binding results of CN and PD cases for each evaluated region and respective quantitative results are presented on the **table (right side).** Data are presented as box and whiskers plots and each point represents a mean of three experiments performed in duplicate for each case. FC – Frontal Cortex, TC – Temporal Cortex, Caud Nuc – Caudate nucleus, Put – Putamen.

3.2 Autoradiography studies

^{3}H-BU99008 Autoradiography studies in CN and PD brains

^{3}H-BU99008 (1nM) regional binding autoradiography on small frozen brain sections (20µm) was assessed in four brain regions (FC, TC, caudate nucleus, putamen) of CN and PD tissue. The **Figure 3.11** presents the total binding (on the left) and non-specific binding (on the right) – co-incubation with 1µM of unlabeled BU99008 and on the left corner note the standard scale – hotter colors correspond to higher binding. Note also that all the NSP regions that are shown as a square is due to impossibility to distinguish the NSP section area from the background of the image.

As shown by the **Figure 3.11**, visual analysis revealed a high total binding in ROI of ^{3}H-BU99008 and a relatively low nonspecific binding (~0-4%) (See supplementary data – **Table S1**). Visual assessment of the autoradiography results allows to detect higher binding in PD cases, compared to CN. Although, it also highlights that the CN 1 showed higher general binding, compared to CN 2,3 and 4 and PD 4 also showed an increase in the total binding, compared to the other 3 PD cases.

Moreover, the semi-quantitative analysis of the specific binding in the ROI is presented in **Figure 3.12**, which demonstrates a global increment in the binding of PD patients, compared to CN. The TC and caudate nucleus are the two regions that show greatest difference in specific binding (81.4% and 78.0% increase) – **Figure 3.12B**.

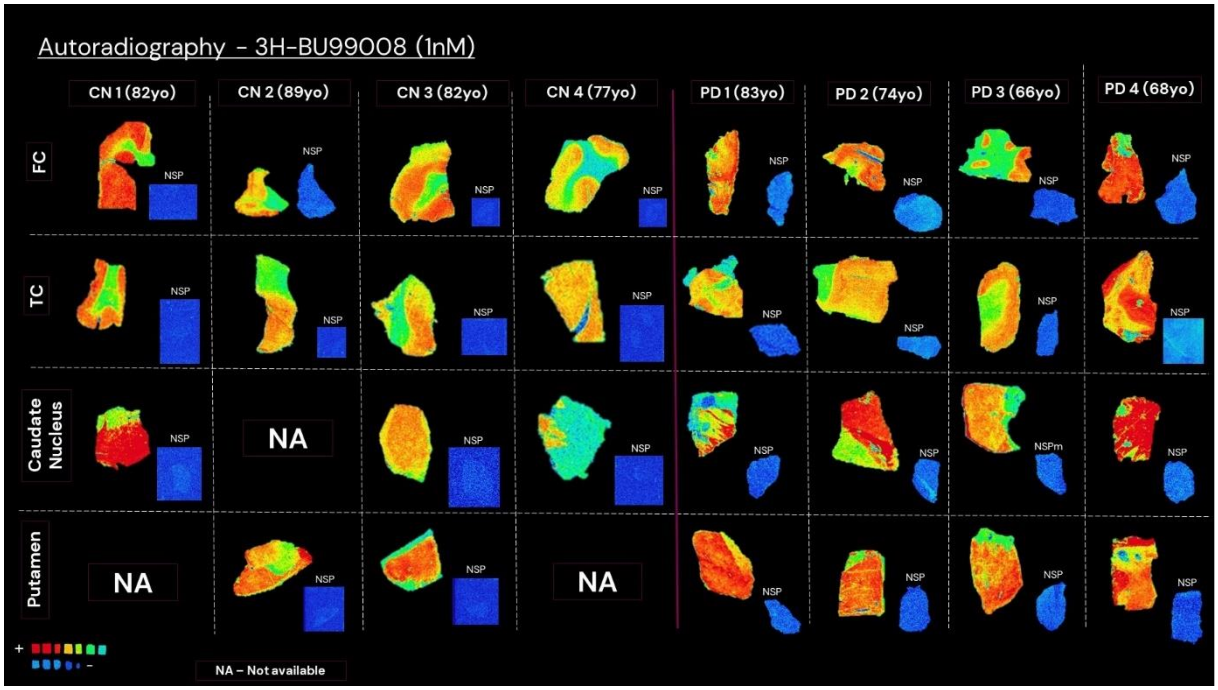
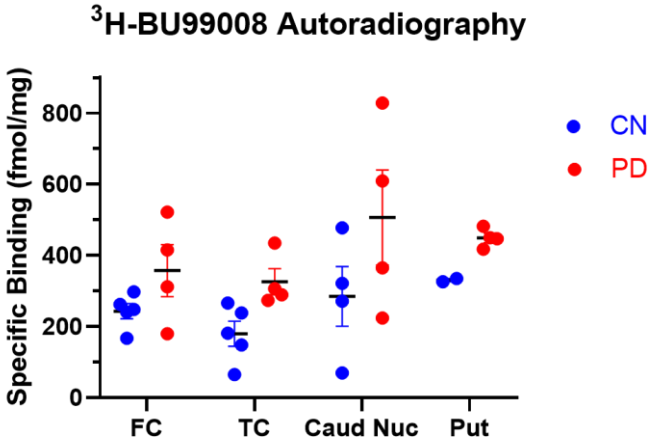


Figure 3.11 - ^{3}H-BU99008 autoradiography on small frozen brain sections (20µm) for PD and CN cases. The figure displays the result of a total binding of 1nM of ^{3}H-BU99008 and non-specific binding of 1 µM unlabeled BU99008 (identified as NSP in white). Standards are representative of the binding scale: + = 2915-2957 fmol/mg, − = 0.83-0.85 fmol/mg. The autoradiography color/brightness threshold level was set on 50629 from the raw images (16 bits: 0–65,535 (color scale). Regions of interest as shown in the figures were drawn manually using Multigauge software to calculate the specific, non-specific and total binding values in fmol/mg. NA – not available.

A



B

	Specific Binding (fmol/mg)		
	CN	PD	% Increase
FC	242.8	357.1	47.1%
TC	179.6	325.9	81.4%
Caudate Nucleus	284.7	506.7	78.0%
Putamen	330.4	449.0	35.9%

Figure 3.12 - Semiquantitative analysis of Autoradiography presented in figure above (Figure 3.11) **(A)** and percentage of increase of the specific binding in PD compared to CN, reflecting the results of the autoradiography presented in Figure 3.11 **(B).**

^{3}H-BU99008 autoradiography studies in CN and PD brains after pre-blocking with unlabeled Deprenyl

^{3}H-BU99008 autoradiography using CN and PD brain sections was performed to evaluate the possible contribution of additional off-target I_2BS on MAO-B for ^{3}H-BU99008 (see section above -I_2BS introduction – for further explanation).

^{3}H-BU99008 (1nM) regional binding autoradiography on small frozen brain sections (20µm) was assessed in four brain regions (FC, TC, caudate nucleus, putamen) of CN and PD tissue. **Figure 3.13** shows the total binding (on the left) and non-specific binding (on the right) – co-incubation with 1µM of unlabeled BU99008 and on the left corner note the standard scale. All the NSP regions that are shown as a square are due to impossibility to distinguish the NSP section area from the background of the imaging plate.

Visual comparison of **Figure 3.11** and **Figure 3.13** demonstrates a global decrease of total binding, confirmed by the Table on **Figure 3.14C**, with still low values of NSP binding (~0-4.5%) (See supplementary data – **Table S2**). Nevertheless, PD still showed higher binding (verified in semi-quantitative analysis - **Figure 3.14B**), compared to CN with the biggest increased levels in striatum (~462% in caudate nucleus and ~85% in putamen). Moreover, for PD, the decrease shown was around ~50-60% for all regions, compared to the previous autoradiography results (**Figure 3.14C)**. For CN the decrease in binding varies in FC, TC and putamen between ~31–68%, however in caudate the decrease is more pronounced (~87%).

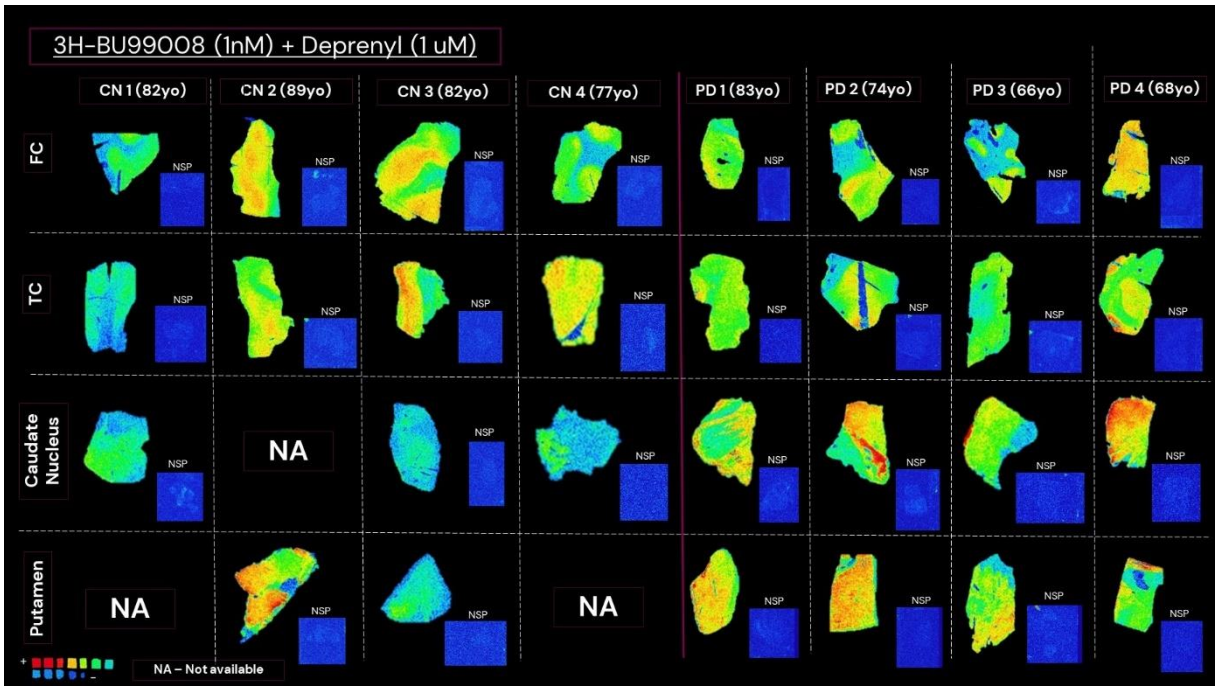
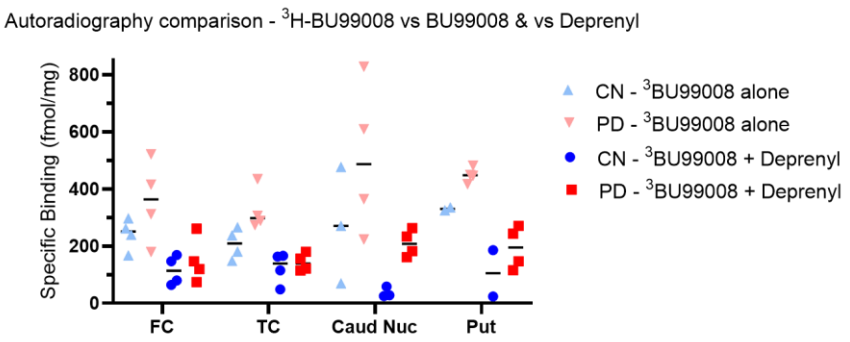


Figure 3.13 - ^{3}H-BU99008 autoradiography on small frozen brain sections (20µm) for PD and CN cases with pre-incubation with 1 µM unlabeled Deprenyl. The figure displays the result of the posterior total binding of 1nM of ^{3}H-BU99008 and Non-specific binding of 1 µM unlabeled BU99008 (identified as NSP in white). Standards are representative of the binding scale: + = 2915 fmol/mg, – = 0.83 fmol/mg. The autoradiography color/brightness threshold level was set on 50629 from the raw images (16 bits: 0–65,535 (color scale). Regions of interest as shown in the figures were drawn manually to calculate the specific, non-specific, and total binding values in fmol/mg. NA – Not available.

A



B

Specific Binding (fmol/mg)

	CN	PD	% Increase
FC	115.1	150.5	30.7%
TC	123.2	143.1	16.2%
Caud	37.4	210.0	462.1%
Put	105.0	194.2	85.1%

C

% Binding Decrease

	CN	PD
FC	**53%**	**58%**
TC	**31%**	**56%**
Caud	**87%**	**59%**
Put	**68%**	**57%**

Figure 3.14 - Semiquantitative analysis of Autoradiography presented in figure above (Figure 3.14) **(A);** percentage of increase of the specific binding in PD compared to CN, reflecting the results of the autoradiography presented in Figure 3.14 **(B);** percentage of increase of the specific binding in PD and CN presented in autoradiography Figure 3.11, compared to the previous autoradiography ^{3}H-BU99008 against BU99008 – Figure 3.9 **(C).**

^{3}H-Deprenyl autoradiography studies in CN and PD brains

^{3}H-Deprenyl (3nM) regional binding autoradiography on small frozen brain sections (20µm) was assessed in four brain regions (FC, TC, caudate nucleus, putamen) of CN and PD tissue. The **Figure 3.14** displays the total binding (on the left) and non-specific binding (on the right) – co-incubation with 1µM of unlabeled Deprenyl and on the left corner the standard scale is shown. Note that all the NSP regions that are shown as a square is due to impossibility to distinguish the NSP section area from the background of the image NSP (~0-4.6% of total) (See supplementary data – **Table S3**).

Figure 3.15 reveals a high heterogeneity in the specific binding, mostly in caudate and putamen. ^{3}H-Deprenyl binds more to PD (~8-27% increase), compared to CN **(Figure 3.15A)**. However, the binding increase **(Figure 3.15B)** from CN to PD is lower compared to ^{3}H-BU99008 results.

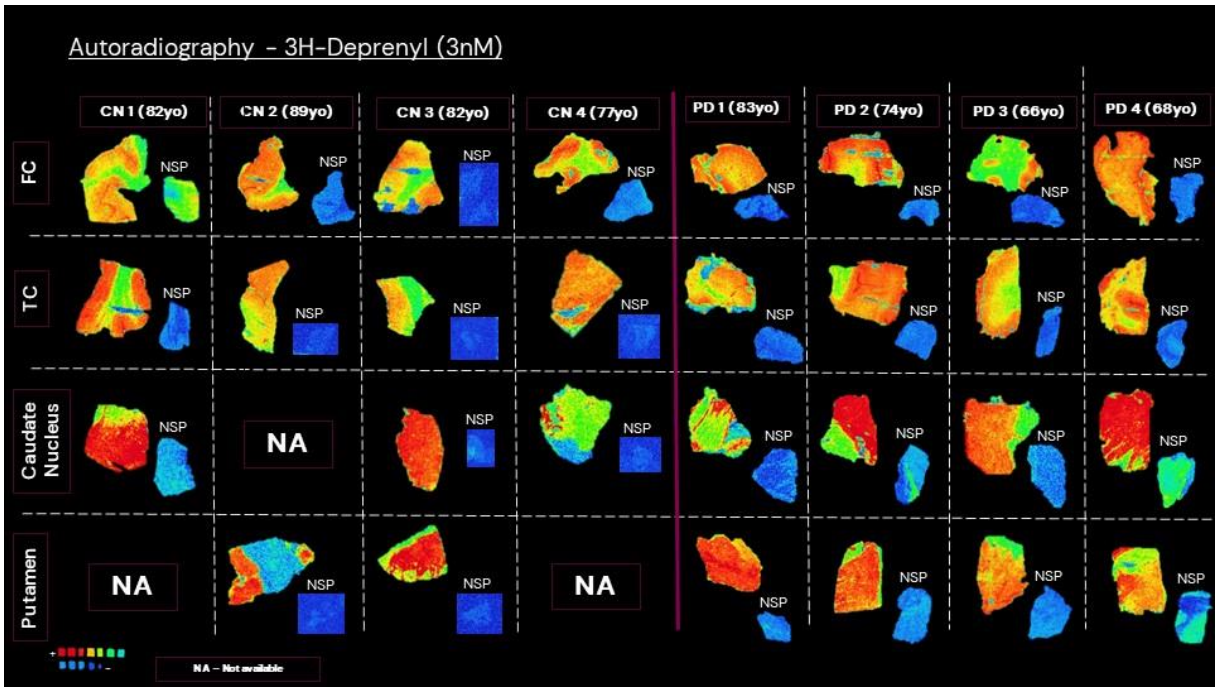
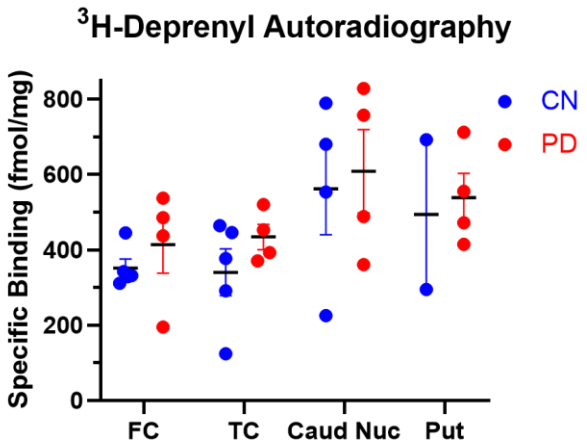


Figure 3.15 - ^{3}H-Deprenyl autoradiography on small frozen brain sections (20µm) for PD and CN cases. The figure displays the result of a total binding of 3nM of ^{3}H-Deprenyl and Non-specific binding of 1 µM unlabeled Deprenyl (identified as NSP in white). Standards are representative of the binding scale: + = 2913–2959 fmol/mg, − = 0.83-0.85 fmol/mg. The autoradiography color/brightness threshold level was set on 50629 from the raw images (16 bits: 0–65,535 (color scale). Regions of interest as shown in the figures were drawn to calculate the specific, non-specific and total binding values in fmol/mg. NA – Not available.

A



B

	Specific Binding (fmol/mg)		
	CN	PD	% Increase
FC	352.0	413.7	17.5%
TC	340.6	434.2	27.5%
Caudate Nucleus	562.2	608.7	8.3%
Putamen	493.8	538.7	9.1%

Figure 3.16 - Semiquantitative analysis of Autoradiography presented in figure above (Figure 3.15) **(A);** percentage of increase of the specific binding in PD compared to CN, reflecting the results of the autoradiography presented in Figure 3.15 **(B).**

Autoradiography - Analysis of age and sex influence on reactive astrogliosis of PD cases

As previously explored, reactive astrogliosis is a phenomenon triggered by natural ageing (Escartin et al., 2021). To evaluate a possible correlation between the collected data and age, the autoradiography results previously presented were sorted considering the age of the patient and by region.

Autoradiography results were chosen for this analysis in order to understand if there is not only gender-dependency but also if this factor affects binding equally, or not, among various regions.

No clear correlation between binding of either the PET tracers and age was found in any of the assessed brain regions **(Figure 3.17A** and **3.17B).** In putamen, is possible to detect a tendency of higher binding in the older cases (74 and 83 years old) seen with both tracers.

Regarding sex influence, as discussed above, sex can affect many features of Parkinson's disease (see Sex differences topic of introduction) **(Figure 3.17C and 3.17D)**. That said, to better understand the possibility of sex-associated changes in reactive astrogliosis of PD patients, autoradiography data was separately analysed, creating a female (n=2) and male (n=2) subgroup of the pathology.

Autoradiography results were chosen for this analysis in order to allow understanding if the binding regional pattern and binding levels are gender dependent.

Male cases show a tendency to be higher than female binding levels for both ^{3}H-BU99008 and ^{3}H-Deprenyl **(Figure 3.17C and 3.17D)**.

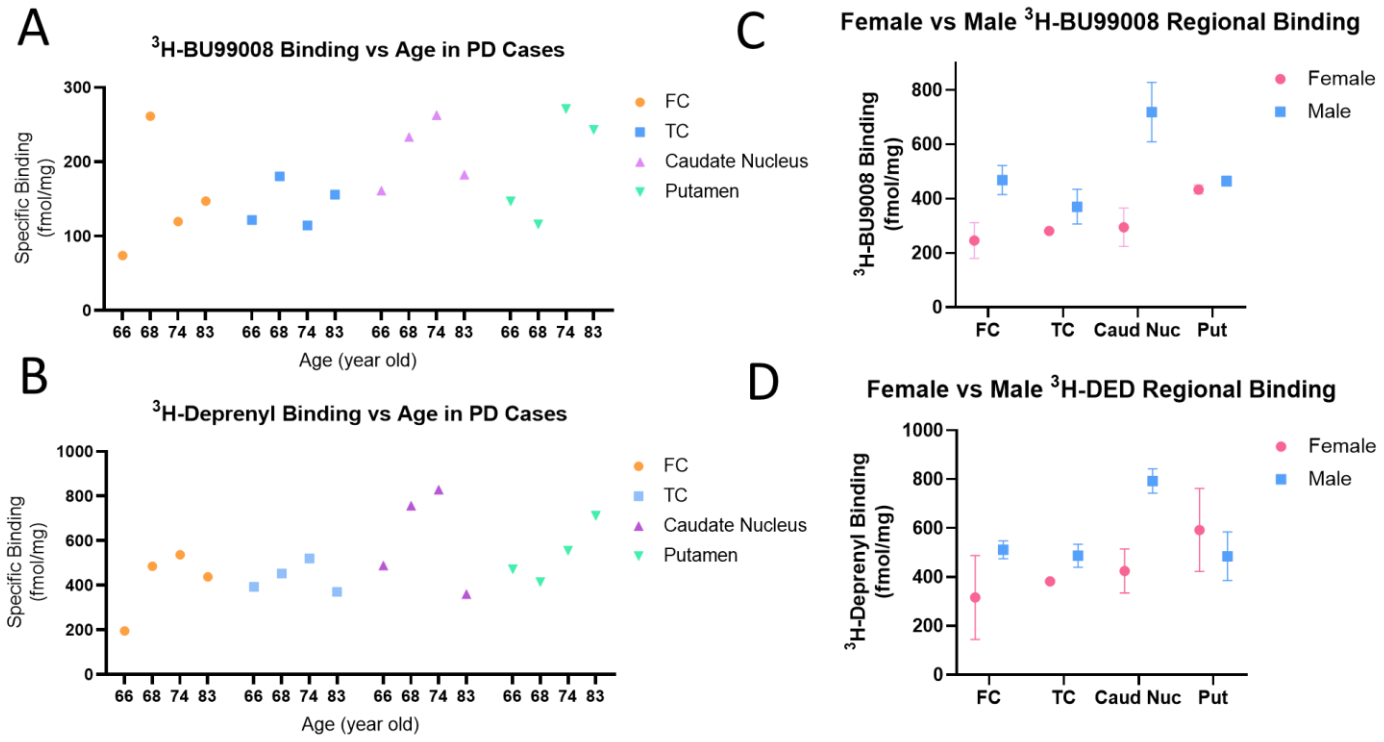


Figure 3.17 - Analysis of age and sex-influence on binding of ^{3}H-BU99008 and ^{3}H-Deprenyl. ^{3}H-BU99008 autoradiography results compared with age of the individuals per each assessed brain region **(A);** ^{3}H-Deprenyl autoradiography results compared with age of the individuals per each assessed brain region **(B);** ^{3}H-BU99008 autoradiography results separated by sex of the individuals per each assessed brain region **(C);** ^{3}H-Deprenyl Autoradiography results separated by sex of the individuals per each assessed brain region **(D).**

Chapter 4

4. Discussion

Astrocytes, the star-shaped glial cells, identified in 1895 by Micheal von Lenhossék, can reliably reflect neuroinflammation, a central feature of neuronal damage (Lenhossék, 1893). Despite their regional heterogeneity and pathology-dependency, astrocytes have been in the spotlight for biomarker development for multiple neurodegenerative diseases. Early in the time course of the changes associated with these diseases, astrocytes go under a panoply of alterations and become reactive, which can be a sign of brain abnormalities. That said, novel specific astrocytic PET tracers are currently a high interest for the field to monitor the function of glial-neuronal network and bring better knowledge about the disease progression (Escartin et al., 2021).

In this study we assess, for the first time, the binding behavior of BU99008 and Deprenyl, in order to explore reactive astrogliosis signature in the etiology and progression of PD, using a multi-PET tracer approach and translational *postmortem* brain imaging techniques.

From previous research, it is known that reactive astrogliosis correlates positively with age, mostly in the striatum (O'Callaghan & Miller, 1991) and that in moderate/advanced Parkinson's cases I_2BS expression is decreased in cortical and subcortical areas (Wilson et al., 2019), however the evaluation of reactive astrogliosis at the end stages of the disease had not been performed before with neither of the tracers: BU99008 and Deprenyl.

^{3}H-BU99008 saturation assays in FC of PD demonstrates two binding sites, being the second one (Kd=0.75) of higher affinity. In FC, the Bmax of the one binding site detected in CN and the binding site with less affinity for PD are similar, $Bmax_{CN}$= 59.1 fmol/mg and $Bmax_{PD}$= 51.6 fmol/mg. In caudate, PD shows only one binding site with 3-fold higher Bmax than CN, indicating a significant increase in the density of available sites ($Bmax_{PD}$=110 fmol/mg > $Bmax_{CN}$=36.3).

The differences detected between PD and CN can be attributed to heterogeneity of astrocytic types found in different contexts, such as pathological vs non-pathological. The

distinct number of binding sites reported in FC and caudate may be explained by the well documented knowledge that physiological and morphological properties of astrocytes can vary from region to region (Liddelow & Barres, 2017). Note that in Kumar *et al*, ^{3}H-BU99008 showed two binding sites in TC of a control (Kumar et al., 2021), while our results detected one binding site both in FC and caudate nucleus, reinforcing this regional-dependency concept.

Our ^{3}H-BU99008 competition studies with unlabeled ligands for I_2BS – BU99008 and for MAO-B – Deprenyl results show an array of binding sites in different levels of affinity (SHA, HA, LA) **(Figure 3.7)**. ^{3}H-BU99008 vs BU99008 results clearly indicate that this radiotracer can target a main binding site in the nM range – HA, which shows in PD and CN major proportions of binding (86-100%) in the two tested regions. These findings are in accordance with the *postmortem* study by Kumar and colleagues that reports 75.2% of binding of ^{3}H-BU99008 to a HA site in Control and 78.4% of binding of ^{3}H-BU99008 in AD (Kumar et al., 2021).

On the other hand, ^{3}H-BU99008 in the presence of unlabeled deprenyl showed two binding sites for PD FC and caudate nucleus and for CN caudate nucleus. In every evaluated context, the binding sites found do not coincide with the detected sites in the previous experiment with most of the binding to LA site in caudate and to HA site in FC.

However, is highly relevant to observe that ^{3}H-BU99008 vs BU99008 curves (**Figure 3.3)** show 100% or close displacement, opposing to ^{3}H-BU99008 vs deprenyl curves, which shows Deprenyl capability of displacing only ~50% of ^{3}H-BU99008.

Therefore, ^{3}H-BU99008 shows a high affinity site with majority of binding with which deprenyl is incapable of interfering, suggesting that this is the I_2BS, targeted by ^{3}H-BU99008 with high specificity.

As reported, when ^{3}H-BU99008 was forced to compete with unlabeled deprenyl, new binding sites were revealed, bringing some possible explanations:

1) These array of binding sites other than the specific site are dynamic and transient, meaning that these sites are nor permanent and might not always be available due to *structural versatility* of the protein containing the receptor, triggered by multiple factors (Perkins et al., 2010).

2) Another explanation is that the binding of the tracer to one site available can open access to a new site, previously not detected in the absence of deprenyl because MAO B inhibitors might interact directly with BU99008 and subsequently interfere with its binding and the extent of interference might depend on the binding mechanism of the ligand (see Edmondson et al., 2009). Possibly, the presence of different endogenous

ligands, which we do not control or purposely manipulated in the experiment, can induce structural transformation of the protein, leading the binding site to become available or easily accessible by the radioactive compound.

3) Lastly, these results can also be explained with the differences in binding proportions presented, pointing that these sites only detected in the presence of a different competitor and have such low proportion of binding that become imperceptible in the assay, masked by the significant displacement of the main binding site.

^{3}H-Deprenyl saturation assays demonstrated one binding site with a Kd in the nM range (FC: Kd= 6.04, caudate nucleus Kd=4.45) for CN. PD ^{3}H-Deprenyl saturation results also show only one binding site in both brain regions with similar Kds (FC: Kd= 5.9, caudate nucleus Kd=4.08). Regarding the density of the binding sites, Bmax in caudate> Bmax in FC. In FC of PD, Bmax is 1.2-fold higher than CN, showing higher density of binding sites. In caudate nucleus, Bmax value was lower as compared to CN. However, note that the three tested cases for saturation in caudate nucleus show a wide variety of binding sites density ($Bmax_{PD1}$: 322.7 fmol/mg; $Bmax_{PD2}$: 255.6 fmol/mg; $Bmax_{PD4}$: 515.2 fmol/mg) values, indicating that case heterogeneity might be influencing this combined result.

When competition between ^{3}H-Deprenyl and unlabeled deprenyl was performed, one binding site was detected in all evaluated circumstances with similar affinities, varying from 8.85 nM to 11.9 nM. The four presented curves **(Figure 3.4)** show a displacement of approximately 90-100%. Together, these results lead to the conclusion that this site is without doubt the MAO-B binding site located in the mitochondrial membrane, which deprenyl is targeting with high affinity and specificity.

Furthermore, when ^{3}H-Deprenyl is challenged by competing with BU99008, similar to ^{3}H-BU99008 vs Deprenyl competition results, new binding sites are detected. All the cases assessed displayed 80-95% of binding in the LA range with affinities between 0.58-1.08μM, showing a probability of changes in Deprenyl binding behavior in the presence of BU99008 or the presence of dynamic and transient sites (provoked or not by a third compound involved – BU99008 or another endogenous ligand), as discussed above. The results demonstrated that BU99008 is capable of displacing around 75% in FC and 85% in caudate nucleus, showing a strong interaction between the tracers and suggesting that Deprenyl might be binding to I_2BS in MAO-B, at which BU99008 can interact and displace Deprenyl at high concentrations, leading to high levels of displacement. However, note that the displacement is not total (as seen in ^{3}H-Deprenyl vs Deprenyl), assuring that the main site of Deprenyl in MAO-B remains selective and a target with intact binding, not influenced by the competitor.

The second binding sites seen in PD, both FC and caudate, might be explained by the same reasons as presented and explained before for ^{3}H-BU99008 vs Deprenyl competition results.

To understand to a greater extent the influence of region dependency and explore the regional pattern of the two tracers, regional binding assays were performed. Additionally, to complement and find a more robust conclusion regarding this aim autoradiographies were also performed, which provided semi-quantitative data generated by a technique that analyses the tissue and all its structures in a more preserved state and allows to study the binding properties in detail.

^{3}H-BU99008 regional distribution demonstrates similar binding levels to all regions in PD (23 to 32 fmol/mg) and in CN (FC: 21 fmol/mg, TC: 30 fmol/mg, putamen: 33 fmol/mg). Although, in caudate of CN the binding of the tracer is lower: 15 fmol/mg, suggesting a 2.13-fold higher binding in PD in this region in comparison to CN. These findings further complemented our ^{3}H-BU99008 saturation binding data.

^{3}H-Deprenyl regional binding distribution data in the PD FC and caudate showed inconsistency as compared to saturation findings, which was surprising and could be attributed to experimental differences and variability in the cases. However, ^{3}H-BU99008 and ^{3}H-Deprenyl both showed similar binding patterns in regional distribution studies with highest binding increase in caudate as compared to CNs.

Autoradiography comparative studies suggested similar binding patterns of low unspecific binding, overall high specific levels for the four brain regions tested and a clear tendency of the two tracers to bind significantly less to white matter (Supplementary **Tables S1, S2 and S3**).

^{3}H-BU99008 autoradiography suggests a strong regional binding with higher binding in the striatum (caudate: 506 fmol/mg; putamen: 449 fml/mg), as supported by saturation (PD: $Bmax_{Caud}$>$Bmax_{FC}$). However, when considered the % of increase in the binding compared to our baseline – CN levels, there is a relevant difference in all the regions, revealing an increased reactive astrogliosis with most impact in TC and caudate.

As discussed before, is likely that ^{3}H-BU99008 might have off-target binding to MAO-B, due to the existence of I_2BS in MAO-B (check I_2BS topic of introduction), so to assure that high binding seen in the first autoradiography **(Figure 3.11)** is specifically reflecting the expression of I_2BS on astrocytes a new autoradiography was performed on the pre-blocked sections with MAO-B inhibitor Deprenyl. These results **(Figure 3.13)** show that blocking MAO-B affects ^{3}H-BU99008 binding, causing a depletion in binding levels for all regions, although highlights BU99008 specificity, since the binding results in deprenyl presence are relevant,

showing that off-target effect only represents a part of BU99008 signal, as corroborated by the competition results discussed above. Moreover, the differentiation between PD and CN is still clear, showing general increased values, highlighting the gap by approximately 462% in caudate and 85% in putamen. Additionally, the decrease in binding expression between the two autoradiographies consistently rounds 50-60% throughout all PD regions, while in CN the % values of decrease vary from 53% and 31% for cortical regions and 87% and 68% for subcortical regions. Two possibilities can explain the variance. The reduction in CN might be caused by the fact the BU99008 also can target neurons and partly of the off-target binding is neuronal and this reduction is lower in PD patients because this subjects suffer 45-55% neuronal loss in the striatum (Damier et al., 1996). Another justification could be that in cognitively healthy controls BU99008 shows a biggest propensity to MAO-B off-target binding site which was also highlighted by our ^{3}H-BU99008 vs BU99008 competition studies, due, for instance, to conformation variation of the protein. Independently of the reason, the specific I_2BS signal provided by BU99008, after guarantying MAO-B blockage, shows even greater disparity in the binding of PD cases, compared to CN, reflecting a promising capacity to distinguish or identify the pathology and trace reactive astrogliosis.

^{3}H-Deprenyl autoradiography demonstrates again group differences with higher binding in PD with a range of increased binding from 8% to 27% for PD, compared to CN. Contrary to ^{3}H-BU99008 autoradiography, ^{3}H-Deprenyl reveals a different regional binding specificity. The higher increase in Cortical regions – FC and TC (18% and 27% of increase in binding of PD vs CN) than subcortical regions accentuates the possibility that the tracers are binding to different subpopulations of astrocytes, as suggested before in Kumar *et al*. also in a *postmortem* study with the two compounds (Kumar et al., 2021).

The differences between regional distribution and autoradiography results could be also explained by variances in the experimental setup and protocol, since regional distribution assess binding behavior using brain homogenates, while autoradiography is performed on intact frozen brain section that don't go through homogenization process and are more likely to preserve biological integrity of astrocytes and respective receptors.

According to the literature, reactive astrogliosis is triggered by ageing, besides brain damage, so it would be expected to detect higher binding of the PET tracers in older cases. However, other factors that interact with astrocytic reactivity and clinical features, such as disease duration of severity can influence reactive astrogliosis and, consequently, binding. For instance, in our study the case with 68 years old **(Figure 3.17)** shows high BU99008 binding in FC and TC, higher than the two older cases, however, the patient has dealt with the disease for 24 years.

Regarding the differences found between sexes, additional studies and a larger sample size of individuals is needed to reach conclusions. Despite that, our results indicate a pattern of higher binding in males, in comparison to females, which can be explained by estrogen anti-inflammatory effect (Yun et al., 2018), as explored above (Introduction - sex differences section).

Chapter 5

5. Conclusions

PET imaging shows great promise in contributing to understanding the role of different pathological hallmarks of a broad spectrum of neurodegenerative diseases and their timelines. In addition, this innovative approach of mechanistic and translational molecular brain imaging research might lead to novel early diagnose and preventive measures, tools to monitor therapeutic interventions, and consequently improving the quality of life and care offered to various people suffering from neurological disorders, such as Parkinson's Disease. A range of technological advances have been made with the development of new biomarkers and novel PET tracers, aiming to prevent late or wrong diagnose, not prescribing the most effective medication, enrolling patients not suitable in clinical trials, lack of monitoring. However, the paucity of an accurate and objective methodology is still a big concern. To address this issue, the field keeps bringing new targets to the picture and evaluating them deeply both with *in vivo* and *in vitro* strategies.

This study, by performing the first *postmortem* analysis and comparison of ^{3}H-BU99008 and ^{3}H-Deprenyl binding behaviour in PD brain tissues, allows to conclude that both PET tracers: **1)** could interact at different sites (transient), **2)** demonstrate one highly specific binding site (HA site with nM range), **3**) might be targeting different subpopulations/subtypes of reactive astrocytes and **4)** reflect reactive astrogliosis at end stages of the disease.

In addition, our findings also highlight that ^{3}H-BU99008 might be targeting a more specific population of reactive astrocytes upregulated in the severely affected region (specifically caudate) during late stages of pathology, warrant further investigation. Although the possibility of combining the information provided by both tracers through a multi-PET tracer

approach it is still a viable option to achieve accurate diagnosis and better understanding of the role of reactive astrogliosis in PD and other neurodegenerative disorders.

Overall, present findings report, for the first time, detailed mechanistic insight into ^{3}H-BU99008 and ^{3}H-Deprenyl binding behavior in different regions of PD brains and highlight the potential of this imaging tool to reflect an extremely relevant biomarker – Reactive Astrogliosis – in PD, in order to complement and enhance the field's knowledge on the topic and expedite clinical application.

Limitations of the study

Postmortem studies present a few limitations that should be acknowledged. The experiments were performed on a small number of cases, and it would be interesting to further explore these tracers in larger sample sizes. In addition, only four brain regions were studied for PD and less in some CN cases due to lack of all the correspondent brain regions which constitutes a limitation. However, it is important to keep in mind that brain tissues are rare material and difficult to acquire. Despite these limitations, the study presents conclusive data.

Future Perspectives

As future research, it is important, as mentioned above, to increase the number of individuals studied to achieve greater robustness to the conclusions. Moreover, a few relevant questions remain elusive. Is the population of reactive astrocytes detected at end stages still trying to fight pathology by maintaining brain homeostasis? Is this phenomenon purely caused by other pathological features, such as Lewy Bodies or neurodegeneration or is it aggravating them? To address these questions, further understating of the correlation between these hallmarks is needed.

Furthermore, as mentioned before, the diagnosis and differentiation of PD and PD-like diseases is a crucial clinical challenge. That said, performing the same pipeline of work for diseases as PDD and DLD could provide important information about how reactive astrocytes behave in these different pathologies and, possibly, help distinguish them.

Finally, considering the final and main objective, it is also fundamental to test both tracers in clinical environment, conducting studies with a large sample size in order to achieve reliable conclusions and comparisons with CN subjects and contribute to the debate around this topic.

Ethical approval

Ethical permissions were obtained from the regional human ethics committee in Stockholm (permission number 2011/962/31-1), the medical ethics committee of the VU Medical Center for the Netherlands Brain Bank tissue (permission number 1998-06/5). Informed consent Informed consent was obtained from Netherlands Brain Bank tissue for all cases investigated.

References

Aarsland, D. (2016). Cognitive impairment in Parkinson's disease and dementia with Lewy bodies. *Parkinsonism & Related Disorders*, *22*, S144–S148. https://doi.org/10.1016/j.parkreldis.2015.09.034

Andriezen, W. L. (1893). The Neuroglia Elements in the Human Brain. *British Medical Journal*, *2*(1700), 227–230.

Ascherio, A., & Schwarzschild, M. A. (2016). The epidemiology of Parkinson's disease: Risk factors and prevention. *The Lancet. Neurology*, *15*(12), 1257–1272. https://doi.org/10.1016/S1474-4422(16)30230-7

Avola, R. (2010). Biomarkers of glial cell proliferation and differentiation in culture. *Frontiers in Bioscience*, *S2*(2), 558–570. https://doi.org/10.2741/s85

Balestrino, R., & Schapira, A. h. v. (2020). Parkinson disease. *European Journal of Neurology*, *27*(1), 27–42. https://doi.org/10.1111/ene.14108

Ballweg, A., Klaus, C., Vogler, L., Katzdobler, S., Wind, K., Zatcepin, A., Ziegler, S. I., Secgin, B., Eckenweber, F., Bohr, B., Bernhardt, A., Fietzek, U., Rauchmann, B.-S., Stoecklein, S., Quach, S., Beyer, L., Scheifele, M., Simmet, M., Joseph, E., … Brendel, M. (2023). [18F]F-DED PET imaging of reactive astrogliosis in neurodegenerative diseases: Preclinical proof of concept and first-in-human data. *Journal of Neuroinflammation*, *20*(1), 68. https://doi.org/10.1186/s12974-023-02749-2

Benninger, F., Glat, M. J., Offen, D., & Steiner, I. (2016). Glial fibrillary acidic protein as a marker of astrocytic activation in the cerebrospinal fluid of patients with amyotrophic lateral

sclerosis. *Journal of Clinical Neuroscience: Official Journal of the Neurosurgical Society of Australasia*, *26*, 75–78. https://doi.org/10.1016/j.jocn.2015.10.008

Bhatia, A., Lenchner, J. R., & Saadabadi, A. (2023). Biochemistry, Dopamine Receptors. Em *StatPearls*. StatPearls Publishing. http://www.ncbi.nlm.nih.gov/books/NBK538242/

Bhidayasiri, R., & Tarsy, D. (2012). Parkinson's Disease: Hoehn and Yahr Scale. Em R. Bhidayasiri & D. Tarsy (Eds.), *Movement Disorders: A Video Atlas: A Video Atlas* (pp. 4–5). Humana Press. https://doi.org/10.1007/978-1-60327-426-5_2

Binde, C. D., Tvete, I. F., Gåsemyr, J., Natvig, B., & Klemp, M. (2018). A multiple treatment comparison meta-analysis of monoamine oxidase type B inhibitors for Parkinson's disease. *British Journal of Clinical Pharmacology*, *84*(9), 1917–1927. https://doi.org/10.1111/bcp.13651

Booth, H. D. E., Hirst, W. D., & Wade-Martins, R. (2017). The Role of Astrocyte Dysfunction in Parkinson's Disease Pathogenesis. *Trends in Neurosciences*, *40*(6), 358–370. https://doi.org/10.1016/j.tins.2017.04.001

Braak, H., Tredici, K. D., Rüb, U., de Vos, R. A. I., Jansen Steur, E. N. H., & Braak, E. (2003). Staging of brain pathology related to sporadic Parkinson's disease. *Neurobiology of Aging*, *24*(2), 197–211. https://doi.org/10.1016/S0197-4580(02)00065-9

Breydo, L., Wu, J. W., & Uversky, V. N. (2012). α-Synuclein misfolding and Parkinson's disease. *Biochimica et Biophysica Acta (BBA) - Molecular Basis of Disease*, *1822*(2), 261–285. https://doi.org/10.1016/j.bbadis.2011.10.002

Broen, M. P. G., Leentjens, A. F. G., Hinkle, J. T., Moonen, A. J. H., Kuijf, M. L., Fischer, N. M., Perepezko, K., Bakker, A., & Pontone, G. M. (2018). Clinical Markers of Anxiety Subtypes in Parkinson Disease. *Journal of Geriatric Psychiatry and Neurology*, *31*(2), 55–62. https://doi.org/10.1177/0891988718757369

Broski, S. M., Hunt, C. H., Johnson, G. B., Morreale, R. F., Lowe, V. J., & Peller, P. J. (2014). Structural and Functional Imaging in Parkinsonian Syndromes. *Radiographics*, *34*(5), 1273–1292. https://doi.org/10.1148/rg.345140009

Calsolaro, V., Matthews, P. M., Donat, C. K., Livingston, N. R., Femminella, G. D., Guedes, S. S., Myers, J., Fan, Z., Tyacke, R. J., Venkataraman, A. V., Perneczky, R., Gunn, R., Rabiner, E.

A., Gentleman, S., Parker, C. A., Murphy, P. S., Wren, P. B., Hinz, R., Sastre, M., … Edison, P. (2021). Astrocyte reactivity with late-onset cognitive impairment assessed in vivo using 11C-BU99008 PET and its relationship with amyloid load. *Molecular Psychiatry*, *26*(10), Artigo 10. https://doi.org/10.1038/s41380-021-01193-z

Carter, S. F., Schöll, M., Almkvist, O., Wall, A., Engler, H., Långström, B., & Nordberg, A. (2012). Evidence for astrocytosis in prodromal Alzheimer disease provided by 11C-deuterium-L-deprenyl: A multitracer PET paradigm combining 11C-Pittsburgh compound B and 18F-FDG. *Journal of Nuclear Medicine: Official Publication, Society of Nuclear Medicine*, *53*(1), 37–46. https://doi.org/10.2967/jnumed.110.087031

Cerri, S., Mus, L., & Blandini, F. (2019). Parkinson's Disease in Women and Men: What's the Difference? *Journal of Parkinson's Disease*, *9*(3), 501–515. https://doi.org/10.3233/JPD-191683

Chatterjee, P., Pedrini, S., Stoops, E., Goozee, K., Villemagne, V. L., Asih, P. R., Verberk, I. M. W., Dave, P., Taddei, K., Sohrabi, H. R., Zetterberg, H., Blennow, K., Teunissen, C. E., Vanderstichele, H. M., & Martins, R. N. (2021). Plasma glial fibrillary acidic protein is elevated in cognitively normal older adults at risk of Alzheimer's disease. *Translational Psychiatry*, *11*(1), Artigo 1. https://doi.org/10.1038/s41398-020-01137-1

Choo, I. L. H., Carter, S. F., Schöll, M. L., & Nordberg, A. (2014). Astrocytosis measured by ^{11}C-deprenyl PET correlates with decrease in gray matter density in the parahippocampus of prodromal Alzheimer's patients. *European Journal of Nuclear Medicine and Molecular Imaging*, *41*(11), 2120–2126. https://doi.org/10.1007/s00259-014-2859-7

Cicognola, C., Janelidze, S., Hertze, J., Zetterberg, H., Blennow, K., Mattsson-Carlgren, N., & Hansson, O. (2021). Plasma glial fibrillary acidic protein detects Alzheimer pathology and predicts future conversion to Alzheimer dementia in patients with mild cognitive impairment. *Alzheimer's Research & Therapy*, *13*(1), 68. https://doi.org/10.1186/s13195-021-00804-9

Clairembault, T., Kamphuis, W., Leclair-Visonneau, L., Rolli-Derkinderen, M., Coron, E., Neunlist, M., Hol, E. M., & Derkinderen, P. (2014). Enteric GFAP expression and phosphorylation in

Parkinson's disease. *Journal of Neurochemistry*, *130*(6), 805–815. https://doi.org/10.1111/jnc.12742

Compta, Y., Parkkinen, L., O'Sullivan, S. S., Vandrovcova, J., Holton, J. L., Collins, C., Lashley, T., Kallis, C., Williams, D. R., de Silva, R., Lees, A. J., & Revesz, T. (2011). Lewy- and Alzheimer-type pathologies in Parkinson's disease dementia: Which is more important? *Brain: A Journal of Neurology*, *134*(Pt 5), 1493–1505. https://doi.org/10.1093/brain/awr031

Croisier, E., & Graeber, M. B. (2006). Glial degeneration and reactive gliosis in alpha-synucleinopathies: The emerging concept of primary gliodegeneration. *Acta Neuropathologica*, *112*(5), 517–530. https://doi.org/10.1007/s00401-006-0119-z

Cullity, E. R., Madsen, H. B., Perry, C. J., & Kim, J. H. (2019). Postnatal developmental trajectory of dopamine receptor 1 and 2 expression in cortical and striatal brain regions. *Journal of Comparative Neurology*, *527*(6), 1039–1055. https://doi.org/10.1002/cne.24574

Dahl, K., Collier, T., Cheng, R., Svedberg, M., Toth, M., Das, A., Nag, S., Liang, S., Halldin, C., & Vasdev, N. (2017). Radiosynthesis of [11C]SL25.1188 via "in-Loop" [11C]CO2 Fixation: Pre-clinical Evaluation for MAO-B Activity in Alzheimer's Disease. *Journal of Nuclear Medicine*, *58*(supplement 1), 863–863.

Damier, P., Kastner, A., Agid, Y., & Hirsch, E. C. (1996). Does monoamine oxidase type B play a role in dopaminergic nerve cell death in Parkinson's disease? *Neurology*, *46*(5), 1262–1269. https://doi.org/10.1212/wnl.46.5.1262

De Vos, H., Bricca, G., De Keyser, J., De Backer, J.-P., Bousquet, P., & Vauquelin, G. (1994). Imidazoline receptors, non-adrenergic idazoxan binding sites and α2-adrenoceptors in the human central nervous system. *Neuroscience*, *59*(3), 589–598. https://doi.org/10.1016/0306-4522(94)90179-1

De Vos, H., Convents, A., De Keyser, J., De Backer, J.-P., Van Megen, I. J. B., Ebinger, G., & Vauquelin, G. (1991). Autoradiographic distribution of α2 adrenoceptors, NAIBS, and 5-HT1A receptors in human brain using [3H]idazoxan and [3H]rauwolscine. *Brain Research*, *566*(1), 13–20. https://doi.org/10.1016/0006-8993(91)91675-Q

Dickson, D. W. (2012). Parkinson's disease and parkinsonism: Neuropathology. *Cold Spring Harbor Perspectives in Medicine*, *2*(8), a009258. https://doi.org/10.1101/cshperspect.a009258

Disease, M. D. S. T. F. on R. S. for P. (2003). The Unified Parkinson's Disease Rating Scale (UPDRS): Status and recommendations. *Movement Disorders*, *18*(7), 738–750. https://doi.org/10.1002/mds.10473

Dorsey, E. R., & Bloem, B. R. (2018). The Parkinson Pandemic-A Call to Action. *JAMA Neurology*, *75*(1), 9–10. https://doi.org/10.1001/jamaneurol.2017.3299

Driver, J. A., Logroscino, G., Gaziano, J. M., & Kurth, T. (2009). Incidence and remaining lifetime risk of Parkinson disease in advanced age. *Neurology*, *72*(5), 432–438. https://doi.org/10.1212/01.wnl.0000341769.50075.bb

Duffy, M. F., Collier, T. J., Patterson, J. R., Kemp, C. J., Luk, K. C., Tansey, M. G., Paumier, K. L., Kanaan, N. M., Fischer, D. L., Polinski, N. K., Barth, O. L., Howe, J. W., Vaikath, N. N., Majbour, N. K., El-Agnaf, O. M. A., & Sortwell, C. E. (2018). Lewy body-like alpha-synuclein inclusions trigger reactive microgliosis prior to nigral degeneration. *Journal of Neuroinflammation*, *15*(1), 129. https://doi.org/10.1186/s12974-018-1171-z

Engler, H., Lundberg, P. O., Ekbom, K., Nennesmo, I., Nilsson, A., Bergström, M., Tsukada, H., Hartvig, P., & Långström, B. (2003). Multitracer study with positron emission tomography in Creutzfeldt-Jakob disease. *European Journal of Nuclear Medicine and Molecular Imaging*, *30*(1), 85–95. https://doi.org/10.1007/s00259-002-1008-x

Escartin, C., Galea, E., Lakatos, A., O'Callaghan, J. P., Petzold, G. C., Serrano-Pozo, A., Steinhäuser, C., Volterra, A., Carmignoto, G., Agarwal, A., Allen, N. J., Araque, A., Barbeito, L., Barzilai, A., Bergles, D. E., Bonvento, G., Butt, A. M., Chen, W.-T., Cohen-Salmon, M., … Verkhratsky, A. (2021). Reactive astrocyte nomenclature, definitions, and future directions. *Nature neuroscience*, *24*(3), 312–325. https://doi.org/10.1038/s41593-020-00783-4

Escartin, C., Guillemaud, O., & Carrillo-de Sauvage, M.-A. (2019). Questions and (some) answers on reactive astrocytes. *Glia*, *67*(12), 2221–2247. https://doi.org/10.1002/glia.23687

Fakhoury, M. (2018). Microglia and Astrocytes in Alzheimer's Disease: Implications for Therapy. *Current Neuropharmacology*, *16*(5), 508–518. https://doi.org/10.2174/1570159X15666170720095240

Fontana, I. C., Kumar, A., Okamura, N., & Nordberg, A. K. (2022). PET tracer SMBT-1 discriminates between BU99008 and Deprenyl binding sites on reactive astrocytes in Alzheimer's disease brains. *Alzheimer's & Dementia*, *18*(S3), e066484. https://doi.org/10.1002/alz.066484

Fontana, I. C., Scarpa, M., Malarte, M.-L., Rocha, F. M., Ausellé-Bosch, S., Bluma, M., Bucci, M., Chiotis, K., Kumar, A., & Nordberg, A. (2023). Astrocyte Signature in Alzheimer's Disease Continuum through a Multi-PET Tracer Imaging Perspective. *Cells*, *12*(11), Artigo 11. https://doi.org/10.3390/cells12111469

Fowler, J. S., Logan, J., Shumay, E., Alia-Klein, N., Wang, G.-J., & Volkow, N. D. (2015). Monoamine oxidase: Radiotracer chemistry and human studies. *Journal of Labelled Compounds and Radiopharmaceuticals*, *58*(3), 51–64. https://doi.org/10.1002/jlcr.3247

García-Sevilla, J. A., Escribá, P. V., Walzer, C., Bouras, C., & Guimón, J. (1998). Imidazoline receptor proteins in brains of patients with Alzheimer's disease. *Neuroscience Letters*, *247*(2–3), 95–98. https://doi.org/10.1016/s0304-3940(98)00265-1

Greenland, J. C., & Barker, R. A. (2018). The Differential Diagnosis of Parkinson's Disease. Em *Parkinson's Disease: Pathogenesis and Clinical Aspects [Internet]*. Codon Publications. https://doi.org/10.15586/codonpublications.parkinsonsdisease.2018.ch6

Haaxma, C. A., Bloem, B. R., Borm, G. F., Oyen, W. J. G., Leenders, K. L., Eshuis, S., Booij, J., Dluzen, D. E., & Horstink, M. W. I. M. (2007). Gender differences in Parkinson's disease. *Journal of Neurology, Neurosurgery & Psychiatry*, *78*(8), 819–824. https://doi.org/10.1136/jnnp.2006.103788

Halliday, G. M., Song, Y. J. C., & Harding, A. J. (2011). Striatal ß-amyloid in dementia with Lewy bodies but not Parkinson's disease. *Journal of Neural Transmission (Vienna, Austria: 1996)*, *118*(5), 713–719. https://doi.org/10.1007/s00702-011-0641-6

Halliday, G. M., & Stevens, C. H. (2011). Glia: Initiators and progressors of pathology in Parkinson's disease. *Movement Disorders: Official Journal of the Movement Disorder Society*, *26*(1), 6–17. https://doi.org/10.1002/mds.23455

Hampel, H., Cummings, J., Blennow, K., Gao, P., Jack, C. R., & Vergallo, A. (2021). Developing the ATX(N) classification for use across the Alzheimer disease continuum. *Nature Reviews Neurology*, *17*(9), Artigo 9. https://doi.org/10.1038/s41582-021-00520-w

Harada, C. N., Natelson Love, M. C., & Triebel, K. (2013). Normal Cognitive Aging. *Clinics in geriatric medicine*, *29*(4), 737–752. https://doi.org/10.1016/j.cger.2013.07.002

Harada, R., Hayakawa, Y., Ezura, M., Lerdsirisuk, P., Du, Y., Ishikawa, Y., Iwata, R., Shidahara, M., Ishiki, A., Kikuchi, A., Arai, H., Kudo, Y., Yanai, K., Furumoto, S., & Okamura, N. (2021). 18F-SMBT-1: A Selective and Reversible PET Tracer for Monoamine Oxidase-B Imaging. *Journal of Nuclear Medicine: Official Publication, Society of Nuclear Medicine*, *62*(2), 253–258. https://doi.org/10.2967/jnumed.120.244400

Harada, R., Ishiki, A., Kai, H., Sato, N., Furukawa, K., Furumoto, S., Tago, T., Tomita, N., Watanuki, S., Hiraoka, K., Ishikawa, Y., Funaki, Y., Nakamura, T., Yoshikawa, T., Iwata, R., Tashiro, M., Sasano, H., Kitamoto, T., Yanai, K., … Okamura, N. (2018). Correlations of 18F-THK5351 PET with Postmortem Burden of Tau and Astrogliosis in Alzheimer Disease. *Journal of Nuclear Medicine: Official Publication, Society of Nuclear Medicine*, *59*(4), 671–674. https://doi.org/10.2967/jnumed.117.197426

Harada, R., Okamura, N., Furumoto, S., Furukawa, K., Ishiki, A., Tomita, N., Tago, T., Hiraoka, K., Watanuki, S., Shidahara, M., Miyake, M., Ishikawa, Y., Matsuda, R., Inami, A., Yoshikawa, T., Funaki, Y., Iwata, R., Tashiro, M., Yanai, K., … Kudo, Y. (2016). 18F-THK5351: A Novel PET Radiotracer for Imaging Neurofibrillary Pathology in Alzheimer Disease. *Journal of Nuclear Medicine: Official Publication, Society of Nuclear Medicine*, *57*(2), 208–214. https://doi.org/10.2967/jnumed.115.164848

Hawkes, C. H., Del Tredici, K., & Braak, H. (2007). Parkinson's disease: A dual-hit hypothesis. *Neuropathology and Applied Neurobiology*, *33*(6), 599–614. https://doi.org/10.1111/j.1365-2990.2007.00874.x

Head, G. A., & Mayorov, D. N. (2006). Imidazoline receptors, novel agents and therapeutic potential. *Cardiovascular & Hematological Agents in Medicinal Chemistry*, *4*(1), 17–32. https://doi.org/10.2174/187152506775268758

Hong, Z., Shi, M., Chung, K. A., Quinn, J. F., Peskind, E. R., Galasko, D., Jankovic, J., Zabetian, C. P., Leverenz, J. B., Baird, G., Montine, T. J., Hancock, A. M., Hwang, H., Pan, C., Bradner, J., Kang, U. J., Jensen, P. H., & Zhang, J. (2010). DJ-1 and alpha-synuclein in human

cerebrospinal fluid as biomarkers of Parkinson's disease. *Brain: A Journal of Neurology*, *133*(Pt 3), 713–726. https://doi.org/10.1093/brain/awq008

Hou, Y., Dan, X., Babbar, M., Wei, Y., Hasselbalch, S. G., Croteau, D. L., & Bohr, V. A. (2019). Ageing as a risk factor for neurodegenerative disease. *Nature Reviews. Neurology*, *15*(10), 565–581. https://doi.org/10.1038/s41582-019-0244-7

Irwin, D. J., Lee, V. M.-Y., & Trojanowski, J. Q. (2013). Parkinson's disease dementia: Convergence of α-synuclein, tau and amyloid-β pathologies. *Nature reviews. Neuroscience*, *14*(9), 626–636. https://doi.org/10.1038/nrn3549

Irwin, D. J., White, M. T., Toledo, J. B., Xie, S. X., Robinson, J. L., Van Deerlin, V., Lee, V. M.-Y., Leverenz, J. B., Montine, T. J., Duda, J. E., Hurtig, H. I., & Trojanowski, J. Q. (2012). Neuropathologic substrates of Parkinson disease dementia. *Annals of Neurology*, *72*(4), 587–598. https://doi.org/10.1002/ana.23659

Ishihara, L. S., Cheesbrough, A., Brayne, C., & Schrag, A. (2007). Estimated life expectancy of Parkinson's patients compared with the UK population. *Journal of Neurology, Neurosurgery, and Psychiatry*, *78*(12), 1304–1309. https://doi.org/10.1136/jnnp.2006.100107

Isik, S., Yeman Kiyak, B., Akbayir, R., Seyhali, R., & Arpaci, T. (2023). Microglia Mediated Neuroinflammation in Parkinson's Disease. *Cells*, *12*(7), 1012. https://doi.org/10.3390/cells12071012

Jäkel, S., & Dimou, L. (2017). Glial Cells and Their Function in the Adult Brain: A Journey through the History of Their Ablation. *Frontiers in Cellular Neuroscience*, *11*, 24. https://doi.org/10.3389/fncel.2017.00024

Jellinger, K. A. (2009). A critical evaluation of current staging of α-synuclein pathology in Lewy body disorders. *Biochimica et Biophysica Acta (BBA) - Molecular Basis of Disease*, *1792*(7), 730–740. https://doi.org/10.1016/j.bbadis.2008.07.006

Johansson, A., Engler, H., Blomquist, G., Scott, B., Wall, A., Aquilonius, S.-M., Långström, B., & Askmark, H. (2007). Evidence for astrocytosis in ALS demonstrated by [11C](L)-deprenyl-D2 PET. *Journal of the Neurological Sciences*, *255*(1–2), 17–22. https://doi.org/10.1016/j.jns.2007.01.057

Kalaitzakis, M. E., Graeber, M. B., Gentleman, S. M., & Pearce, R. K. B. (2008). The dorsal motor nucleus of the vagus is not an obligatory trigger site of Parkinson's disease: A critical analysis of α-synuclein staging. *Neuropathology and Applied Neurobiology*, *34*(3), 284–295. https://doi.org/10.1111/j.1365-2990.2007.00923.x

Kalia, L. V., Brotchie, J. M., & Fox, S. H. (2013). Novel nondopaminergic targets for motor features of Parkinson's disease: Review of recent trials. *Movement Disorders: Official Journal of the Movement Disorder Society*, *28*(2), 131–144. https://doi.org/10.1002/mds.25273

Kawamura, K., Shimoda, Y., Yui, J., Zhang, Y., Yamasaki, T., Wakizaka, H., Hatori, A., Xie, L., Kumata, K., Fujinaga, M., Ogawa, M., Kurihara, Y., Nengaki, N., & Zhang, M.-R. (2017). A useful PET probe [11C]BU99008 with ultra-high specific radioactivity for small animal PET imaging of I2-imidazoline receptors in the hypothalamus. *Nuclear Medicine and Biology*, *45*, 1–7. https://doi.org/10.1016/j.nucmedbio.2016.10.005

Kealey, S., Turner, E. M., Husbands, S. M., Salinas, C. A., Jakobsen, S., Tyacke, R. J., Nutt, D. J., Parker, C. A., & Gee, A. D. (2013). Imaging imidazoline-I2 binding sites in porcine brain using 11C-BU99008. *Journal of Nuclear Medicine: Official Publication, Society of Nuclear Medicine*, *54*(1), 139–144. https://doi.org/10.2967/jnumed.112.108258

Killinger, B. A., Melki, R., Brundin, P., & Kordower, J. H. (2019). Endogenous alpha-synuclein monomers, oligomers and resulting pathology: Let's talk about the lipids in the room. *Npj Parkinson's Disease*, *5*(1), Artigo 1. https://doi.org/10.1038/s41531-019-0095-3

Kim, R., Lee, J., Kim, Y., Kim, A., Jang, M., Kim, H.-J., Jeon, B., Kang, U. J., & Fahn, S. (2018). Presynaptic striatal dopaminergic depletion predicts the later development of freezing of gait in de novo Parkinson's disease: An analysis of the PPMI cohort. *Parkinsonism & Related Disorders*, *51*, 49–54. https://doi.org/10.1016/j.parkreldis.2018.02.047

Kimura, A., Tyacke, R. J., Robinson, J. J., Husbands, S. M., Minchin, M. C. W., Nutt, D. J., & Hudson, A. L. (2009). Identification of an imidazoline binding protein: Creatine kinase and an imidazoline-2 binding site. *Brain Research*, *1279*, 21–28. https://doi.org/10.1016/j.brainres.2009.04.044

Koga, S., Sekiya, H., Kondru, N., Ross, O. A., & Dickson, D. W. (2021). Neuropathology and molecular diagnosis of Synucleinopathies. *Molecular Neurodegeneration*, *16*(1), 83. https://doi.org/10.1186/s13024-021-00501-z

Koprich, J. B., Reske-Nielsen, C., Mithal, P., & Isacson, O. (2008). Neuroinflammation mediated by IL-1beta increases susceptibility of dopamine neurons to degeneration in an animal model of Parkinson's disease. *Journal of Neuroinflammation*, *5*, 8. https://doi.org/10.1186/1742-2094-5-8

Kumagai, T., Nagayama, H., Ota, T., Nishiyama, Y., Mishina, M., & Ueda, M. (2014). Sex Differences in the Pharmacokinetics of Levodopa in Elderly Patients With Parkinson Disease. *Clinical Neuropharmacology*, *37*(6), 173. https://doi.org/10.1097/WNF.0000000000000051

Kumar, A., Fontana, I. C., & Nordberg, A. (2023). Reactive astrogliosis: A friend or foe in the pathogenesis of Alzheimer's disease. *Journal of Neurochemistry*, *164*(3), 309–324. https://doi.org/10.1111/jnc.15565

Kumar, A., Koistinen, N. A., Malarte, M.-L., Nennesmo, I., Ingelsson, M., Ghetti, B., Lemoine, L., & Nordberg, A. (2021). Astroglial tracer BU99008 detects multiple binding sites in Alzheimer's disease brain. *Molecular Psychiatry*, *26*(10), 5833–5847. https://doi.org/10.1038/s41380-021-01101-5

Kumlien, E., Nilsson, A., Hagberg, G., Långström, B., & Bergström, M. (2001). PET with 11C-deuterium-deprenyl and 18F-FDG in focal epilepsy. *Acta Neurologica Scandinavica*, *103*(6), 360–366. https://doi.org/10.1034/j.1600-0404.2001.103006360.x

Lemoine, L., Saint-Aubert, L., Nennesmo, I., Gillberg, P.-G., & Nordberg, A. (2017). Cortical laminar tau deposits and activated astrocytes in Alzheimer's disease visualised by 3H-THK5117 and 3H-deprenyl autoradiography. *Scientific Reports*, *7*(1), Artigo 1. https://doi.org/10.1038/srep45496

Lenhossék, M. (1893). *Der feinere Bau des Nervensystems im Lichte neuester Forschungen*. Fischer.

Li, J.-X. (2017). Imidazoline I2 receptors: An update. *Pharmacology & Therapeutics*, *178*, 48–56. https://doi.org/10.1016/j.pharmthera.2017.03.009

Liddelow, S. A., & Barres, B. A. (2017). Reactive Astrocytes: Production, Function, and Therapeutic Potential. *Immunity*, *46*(6), 957–967. https://doi.org/10.1016/j.immuni.2017.06.006

Lippa, C. F., Duda, J. E., Grossman, M., Hurtig, H. I., Aarsland, D., Boeve, B. F., Brooks, D. J., Dickson, D. W., Dubois, B., Emre, M., Fahn, S., Farmer, J. M., Galasko, D., Galvin, J. E., Goetz, C. G., Growdon, J. H., Gwinn-Hardy, K. A., Hardy, J., Heutink, P., … Wszolek, Z. K. (2007). DLB and PDD boundary issues: Diagnosis, treatment, molecular pathology, and biomarkers. *Neurology*, *68*(11), 812–819. https://doi.org/10.1212/01.wnl.0000256715.13907.d3

Livingston, N. R., Calsolaro, V., Hinz, R., Nowell, J., Raza, S., Gentleman, S., Tyacke, R. J., Myers, J., Venkataraman, A. V., Perneczky, R., Gunn, R. N., Rabiner, E. A., Parker, C. A., Murphy, P. S., Wren, P. B., Nutt, D. J., Matthews, P. M., & Edison, P. (2022). Relationship between astrocyte reactivity, using novel 11C-BU99008 PET, and glucose metabolism, grey matter volume and amyloid load in cognitively impaired individuals. *Molecular Psychiatry*, *27*(4), 2019–2029. https://doi.org/10.1038/s41380-021-01429-y

Mack, J., & Marsh, L. (2017). Parkinson's Disease: Cognitive Impairment. *Focus (American Psychiatric Publishing)*, *15*(1), 42–54. https://doi.org/10.1176/appi.focus.20160043

Mallajosyula, J. K., Kaur, D., Chinta, S. J., Rajagopalan, S., Rane, A., Nicholls, D. G., Di Monte, D. A., Macarthur, H., & Andersen, J. K. (2008). MAO-B Elevation in Mouse Brain Astrocytes Results in Parkinson's Pathology. *PLoS ONE*, *3*(2), e1616. https://doi.org/10.1371/journal.pone.0001616

Marras, C., Canning, C. G., & Goldman, S. M. (2019). Environment, lifestyle, and Parkinson's disease: Implications for prevention in the next decade. *Movement Disorders: Official Journal of the Movement Disorder Society*, *34*(6), 801–811. https://doi.org/10.1002/mds.27720

Martinez-Martin, P., Rodriguez-Blazquez, C., Kurtis, M. M., Chaudhuri, K. R., & NMSS Validation Group. (2011). The impact of non-motor symptoms on health-related quality of life of patients with Parkinson's disease. *Movement Disorders: Official Journal of the Movement Disorder Society*, *26*(3), 399–406. https://doi.org/10.1002/mds.23462

Marutle, A., Gillberg, P.-G., Bergfors, A., Yu, W., Ni, R., Nennesmo, I., Voytenko, L., & Nordberg, A. (2013). 3H-Deprenyl and 3H-PIB autoradiography show different laminar distributions of

astroglia and fibrillar ß-amyloid in Alzheimer brain. *Journal of Neuroinflammation*, *10*(1), 861. https://doi.org/10.1186/1742-2094-10-90

Mattsson, N. (2011). CSF biomarkers in neurodegenerative diseases. *Clinical Chemistry and Laboratory Medicine*, *49*(3), 345–352. https://doi.org/10.1515/CCLM.2011.082

McKeith, I. G. (2006). Consensus guidelines for the clinical and pathologic diagnosis of dementia with Lewy bodies (DLB): Report of the Consortium on DLB International Workshop. *Journal of Alzheimer's Disease: JAD*, *9*(3 Suppl), 417–423. https://doi.org/10.3233/jad-2006-9s347

Miklossy, J., Doudet, D. D., Schwab, C., Yu, S., McGeer, E. G., & McGeer, P. L. (2006). Role of ICAM-1 in persisting inflammation in Parkinson disease and MPTP monkeys. *Experimental Neurology*, *197*(2), 275–283. https://doi.org/10.1016/j.expneurol.2005.10.034

Mohamed, M. A., Zeng, Z., Gennaro, M., Lao-Kaim, N. P., Myers, J. F. M., Calsolaro, V., Femminella, G. D., Tyacke, R. J., Martin-Bastida, A., Gunn, R. N., Nutt, D. J., Edison, P., Piccini, P., & Roussakis, A.-A. (2022). Astrogliosis in aging and Parkinson's disease dementia: A new clinical study with 11C-BU99008 PET. *Brain Communications*, *4*(5), fcac199. https://doi.org/10.1093/braincomms/fcac199

Montine, T. J., Shi, M., Quinn, J. F., Peskind, E. R., Craft, S., Ginghina, C., Chung, K. A., Kim, H., Galasko, D. R., Jankovic, J., Zabetian, C. P., Leverenz, J. B., & Zhang, J. (2010). CSF Aß42 and tau in Parkinson's disease with cognitive impairment. *Movement Disorders*, *25*(15), 2682–2685. https://doi.org/10.1002/mds.23287

Moriguchi, S., Wilson, A. A., Miler, L., Rusjan, P. M., Vasdev, N., Kish, S. J., Rajkowska, G., Wang, J., Bagby, M., Mizrahi, R., Varughese, B., Houle, S., & Meyer, J. H. (2019). Monoamine Oxidase B Total Distribution Volume in the Prefrontal Cortex of Major Depressive Disorder: An [11C]SL25.1188 Positron Emission Tomography Study. *JAMA Psychiatry*, *76*(6), 634–641. https://doi.org/10.1001/jamapsychiatry.2019.0044

Mythri, R. B., Venkateshappa, C., Harish, G., Mahadevan, A., Muthane, U. B., Yasha, T. C., Srinivas Bharath, M. M., & Shankar, S. K. (2011). Evaluation of Markers of Oxidative Stress, Antioxidant Function and Astrocytic Proliferation in the Striatum and Frontal Cortex of Parkinson's Disease Brains. *Neurochemical Research*, *36*(8), 1452–1463. https://doi.org/10.1007/s11064-011-0471-9

Nagele, R. G., D'Andrea, M. R., Lee, H., Venkataraman, V., & Wang, H.-Y. (2003). Astrocytes accumulate A beta 42 and give rise to astrocytic amyloid plaques in Alzheimer disease brains. *Brain Research*, *971*(2), 197–209. https://doi.org/10.1016/s0006-8993(03)02361-8

Nalls, M. A., Blauwendraat, C., Vallerga, C. L., Heilbron, K., Bandres-Ciga, S., Chang, D., Tan, M., Kia, D. A., Noyce, A. J., Xue, A., Bras, J., Young, E., von Coelln, R., Simón-Sánchez, J., Schulte, C., Sharma, M., Krohn, L., Pihlstrøm, L., Siitonen, A., … International Parkinson's Disease Genomics Consortium. (2019). Identification of novel risk loci, causal insights, and heritable risk for Parkinson's disease: A meta-analysis of genome-wide association studies. *The Lancet. Neurology*, *18*(12), 1091–1102. https://doi.org/10.1016/S1474-4422(19)30320-5

Ng, K. P., Pascoal, T. A., Mathotaarachchi, S., Therriault, J., Kang, M. S., Shin, M., Guiot, M.-C., Guo, Q., Harada, R., Comley, R. A., Massarweh, G., Soucy, J.-P., Okamura, N., Gauthier, S., & Rosa-Neto, P. (2017). Monoamine oxidase B inhibitor, selegiline, reduces 18F-THK5351 uptake in the human brain. *Alzheimer's Research & Therapy*, *9*(1), 25. https://doi.org/10.1186/s13195-017-0253-y

Ni, R., Röjdner, J., Voytenko, L., Dyrks, T., Thiele, A., Marutle, A., & Nordberg, A. (2021). In vitro Characterization of the Regional Binding Distribution of Amyloid PET Tracer Florbetaben and the Glia Tracers Deprenyl and PK11195 in Autopsy Alzheimer's Brain Tissue. *Journal of Alzheimer's Disease*, *80*(4), 1723–1737. https://doi.org/10.3233/JAD-201344

Nuytemans, K., Theuns, J., Cruts, M., & Van Broeckhoven, C. (2010). Genetic etiology of Parkinson disease associated with mutations in the SNCA, PARK2, PINK1, PARK7, and LRRK2 genes: A mutation update. *Human Mutation*, *31*(7), 763–780. https://doi.org/10.1002/humu.21277

Oberheim, N. A., Takano, T., Han, X., He, W., Lin, J. H. C., Wang, F., Xu, Q., Wyatt, J. D., Pilcher, W., Ojemann, J. G., Ransom, B. R., Goldman, S. A., & Nedergaard, M. (2009). Uniquely hominid features of adult human astrocytes. *The Journal of Neuroscience: The Official Journal of the Society for Neuroscience*, *29*(10), 3276–3287. https://doi.org/10.1523/JNEUROSCI.4707-08.2009

O'Callaghan, J. P., & Miller, D. B. (1991). The concentration of glial fibrillary acidic protein increases with age in the mouse and rat brain. *Neurobiology of Aging*, *12*(2), 171–174. https://doi.org/10.1016/0197-4580(91)90057-q

Oeckl, P., Halbgebauer, S., Anderl-Straub, S., Steinacker, P., Huss, A. M., Neugebauer, H., von Arnim, C. A. F., Diehl-Schmid, J., Grimmer, T., Kornhuber, J., Lewczuk, P., Danek, A., German, C. for F. L. D., Ludolph, A. C., & Otto, M. (2019). Glial Fibrillary Acidic Protein in Serum is Increased in Alzheimer's Disease and Correlates with Cognitive Impairment. *Journal of Alzheimer's Disease*, *67*(2), 481–488. https://doi.org/10.3233/JAD-180325

Olmos, G., Alemany, R., Escriba, P. V., & García-Sevilla, J. A. (1994). The effects of chronic imidazoline drug treatment on glial fibrillary acidic protein concentrations in rat brain. *British Journal of Pharmacology*, *111*(4), 997–1002. https://doi.org/10.1111/j.1476-5381.1994.tb14842.x

Parker, C. A., Nabulsi, N., Holden, D., Lin, S., Cass, T., Labaree, D., Kealey, S., Gee, A. D., Husbands, S. M., Quelch, D., Carson, R. E., Nutt, D. J., Huang, Y., & Tyacke, R. J. (2014). Evaluation of 11C-BU99008, a PET ligand for the imidazoline2 binding sites in rhesus brain. *Journal of Nuclear Medicine: Official Publication, Society of Nuclear Medicine*, *55*(5), 838–844. https://doi.org/10.2967/jnumed.113.131854

Parkkinen, L., Pirttilä, T., & Alafuzoff, I. (2008). Applicability of current staging/categorization of α-synuclein pathology and their clinical relevance. *Acta Neuropathologica*, *115*(4), 399–407. https://doi.org/10.1007/s00401-008-0346-6

Parnetti, L., Castrioto, A., Chiasserini, D., Persichetti, E., Tambasco, N., El-Agnaf, O., & Calabresi, P. (2013). Cerebrospinal fluid biomarkers in Parkinson disease. *Nature Reviews. Neurology*, *9*(3), 131–140. https://doi.org/10.1038/nrneurol.2013.10

Pekny, M., & Pekna, M. (2014). Astrocyte reactivity and reactive astrogliosis: Costs and benefits. *Physiological Reviews*, *94*(4), 1077–1098. https://doi.org/10.1152/physrev.00041.2013

Pekny, M., & Pekna, M. (2016). Reactive gliosis in the pathogenesis of CNS diseases. *Biochimica et Biophysica Acta (BBA) - Molecular Basis of Disease*, *1862*(3), 483–491. https://doi.org/10.1016/j.bbadis.2015.11.014

Pekny, M., Pekna, M., Messing, A., Steinhäuser, C., Lee, J.-M., Parpura, V., Hol, E. M., Sofroniew, M. V., & Verkhratsky, A. (2016). Astrocytes: A central element in neurological diseases. *Acta Neuropathologica*, *131*(3), 323–345. https://doi.org/10.1007/s00401-015-1513-1

Pereira, J. B., Janelidze, S., Smith, R., Mattsson-Carlgren, N., Palmqvist, S., Teunissen, C. E., Zetterberg, H., Stomrud, E., Ashton, N. J., Blennow, K., & Hansson, O. (2021). Plasma GFAP is an early marker of amyloid-β but not tau pathology in Alzheimer's disease. *Brain: A Journal of Neurology*, *144*(11), 3505–3516. https://doi.org/10.1093/brain/awab223

Perez, F., Helmer, C., Foubert-Samier, A., Auriacombe, S., Dartigues, J.-F., & Tison, F. (2012). Risk of dementia in an elderly population of Parkinson's disease patients: A 15-year population-based study. *Alzheimer's & Dementia: The Journal of the Alzheimer's Association*, *8*(6), 463–469. https://doi.org/10.1016/j.jalz.2011.09.230

Perez-Lloret, S., & Barrantes, F. J. (2016). Deficits in cholinergic neurotransmission and their clinical correlates in Parkinson's disease. *Npj Parkinson's Disease*, *2*(1), Artigo 1. https://doi.org/10.1038/npjparkd.2016.1

Perez-Nievas, B. G., & Serrano-Pozo, A. (2018). Deciphering the Astrocyte Reaction in Alzheimer's Disease. *Frontiers in Aging Neuroscience*, *10*, 114. https://doi.org/10.3389/fnagi.2018.00114

Perkins, J. R., Diboun, I., Dessailly, B. H., Lees, J. G., & Orengo, C. (2010). Transient Protein-Protein Interactions: Structural, Functional, and Network Properties. *Structure*, *18*(10), 1233–1243. https://doi.org/10.1016/j.str.2010.08.007

Postuma, R. B., Aarsland, D., Barone, P., Burn, D. J., Hawkes, C. H., Oertel, W., & Ziemssen, T. (2012). Identifying prodromal Parkinson's disease: Pre-motor disorders in Parkinson's disease. *Movement Disorders: Official Journal of the Movement Disorder Society*, *27*(5), 617–626. https://doi.org/10.1002/mds.24996

Postuma, R. B., Berg, D., Stern, M., Poewe, W., Olanow, C. W., Oertel, W., Obeso, J., Marek, K., Litvan, I., Lang, A. E., Halliday, G., Goetz, C. G., Gasser, T., Dubois, B., Chan, P., Bloem, B. R., Adler, C. H., & Deuschl, G. (2015). MDS clinical diagnostic criteria for Parkinson's disease. *Movement Disorders: Official Journal of the Movement Disorder Society*, *30*(12), 1591–1601. https://doi.org/10.1002/mds.26424

Qiu, W.-W., & Zheng, R.-Y. (2006). Neuroprotective effects of receptor imidazoline 2 and its endogenous ligand agmatine. *Neuroscience Bulletin*, *22*(3), 187–191.

Remaury, A., Raddatz, R., Ordener, C., Savic, S., Shih, J. C., Chen, K., Seif, I., Maeyer, E. D., Lanier, S. M., & Parini, A. (2000). Analysis of the Pharmacological and Molecular Heterogeneity of I2-Imidazoline-Binding Proteins using Monoamine Oxidase-Deficient Mouse Models. *Molecular Pharmacology*, *58*(5), 1085–1090. https://doi.org/10.1124/mol.58.5.1085

Rizor, A., Pajarillo, E., Johnson, J., Aschner, M., & Lee, E. (2019). Astrocytic Oxidative/Nitrosative Stress Contributes to Parkinson's Disease Pathogenesis: The Dual Role of Reactive Astrocytes. *Antioxidants (Basel, Switzerland)*, *8*(8), 265. https://doi.org/10.3390/antiox8080265

Rodriguez-Vieitez, E., Ni, R., Gulyás, B., Tóth, M., Häggkvist, J., Halldin, C., Voytenko, L., Marutle, A., & Nordberg, A. (2015). Astrocytosis precedes amyloid plaque deposition in Alzheimer APPswe transgenic mouse brain: A correlative positron emission tomography and in vitro imaging study. *European Journal of Nuclear Medicine and Molecular Imaging*, *42*(7), 1119–1132. https://doi.org/10.1007/s00259-015-3047-0

Rodriguez-Vieitez, E., Saint-Aubert, L., Carter, S. F., Almkvist, O., Farid, K., Schöll, M., Chiotis, K., Thordardottir, S., Graff, C., Wall, A., Långström, B., & Nordberg, A. (2016). Diverging longitudinal changes in astrocytosis and amyloid PET in autosomal dominant Alzheimer's disease. *Brain: A Journal of Neurology*, *139*(Pt 3), 922–936. https://doi.org/10.1093/brain/awv404

Ruiz, J., Martín, I., Callado, L. F., Meana, J. J., Barturen, F., & García-Sevilla, J. A. (1993). Non-adrenoceptor [3H]idazoxan binding sites (I2-imidazoline sites) are increased in postmortem brain from patients with Alzheimer's disease. *Neuroscience Letters*, *160*(1), 109–112. https://doi.org/10.1016/0304-3940(93)90925-B

Saba, W., Valette, H., Peyronneau, M.-A., Bramoullé, Y., Coulon, C., Curet, O., George, P., Dollé, F., & Bottlaender, M. (2010). [(11)C]SL25.1188, a new reversible radioligand to study the monoamine oxidase type B with PET: Preclinical characterisation in nonhuman primate. *Synapse (New York, N.Y.)*, *64*(1), 61–69. https://doi.org/10.1002/syn.20703

Sastre, M., & García-Sevilla, J. A. (1993). Opposite age-dependent changes of alpha 2A-adrenoceptors and nonadrenoceptor [3H]idazoxan binding sites (I2-imidazoline sites) in the

human brain: Strong correlation of I2 with monoamine oxidase-B sites. *Journal of Neurochemistry*, *61*(3), 881–889. https://doi.org/10.1111/j.1471-4159.1993.tb03599.x

Schaf, D. V., Tort, A. B. L., Fricke, D., Schestatsky, P., Portela, L. V. C., Souza, D. O., & Rieder, C. R. M. (2005). S100B and NSE serum levels in patients with Parkinson's disease. *Parkinsonism & Related Disorders*, *11*(1), 39–43. https://doi.org/10.1016/j.parkreldis.2004.07.002

Schnitzer, J., Franke, W. W., & Schachner, M. (1981). Immunocytochemical demonstration of vimentin in astrocytes and ependymal cells of developing and adult mouse nervous system. *The Journal of Cell Biology*, *90*(2), 435–447. https://doi.org/10.1083/jcb.90.2.435

Schöll, M., Carter, S. F., Westman, E., Rodriguez-Vieitez, E., Almkvist, O., Thordardottir, S., Wall, A., Graff, C., Långström, B., & Nordberg, A. (2015). Early astrocytosis in autosomal dominant Alzheimer's disease measured in vivo by multi-tracer positron emission tomography. *Scientific Reports*, *5*(1), Artigo 1. https://doi.org/10.1038/srep16404

Schoonenboom, N. S. M., Pijnenburg, Y. a. L., Mulder, C., Rosso, S. M., Van Elk, E.-J., Van Kamp, G. J., Van Swieten, J. C., & Scheltens, P. (2004). Amyloid beta(1-42) and phosphorylated tau in CSF as markers for early-onset Alzheimer disease. *Neurology*, *62*(9), 1580–1584. https://doi.org/10.1212/01.wnl.0000123249.58898.e0

Shi, M., Huber, B. R., & Zhang, J. (2010). Biomarkers for Cognitive Impairment in Parkinson Disease. *Brain Pathology*, *20*(3), 660–671. https://doi.org/10.1111/j.1750-3639.2009.00370.x

Smith, L., & Schapira, A. H. V. (2022). GBA Variants and Parkinson Disease: Mechanisms and Treatments. *Cells*, *11*(8), 1261. https://doi.org/10.3390/cells11081261

Sofroniew, M. V., & Vinters, H. V. (2010). Astrocytes: Biology and pathology. *Acta Neuropathologica*, *119*(1), 7–35. https://doi.org/10.1007/s00401-009-0619-8

Strimbu, K., & Tavel, J. A. (2010). What are Biomarkers? *Current opinion in HIV and AIDS*, *5*(6), 463–466. https://doi.org/10.1097/COH.0b013e32833ed177

Su, W., Chen, H. B., Li, S. H., & Wu, D. Y. (2012). Correlational study of the serum levels of the glial fibrillary acidic protein and neurofilament proteins in Parkinson's disease patients. *Clinical Neurology and Neurosurgery*, *114*(4), 372–375. https://doi.org/10.1016/j.clineuro.2011.11.002

Takahashi, Y., Kanbayashi, T., Hoshikawa, M., Imanishi, A., Sagawa, Y., Tsutsui, K., Takeda, Y., Kusanagi, H., Nishino, S., & Shimizu, T. (2015). Relationship of orexin (hypocretin) system and astrocyte activation in Parkinson's disease with hypersomnolence. *Sleep and Biological Rhythms*, *13*(3), 252–260. https://doi.org/10.1111/sbr.12112

Takahashi-Niki, K., Niki, T., Taira, T., Iguchi-Ariga, S. M. M., & Ariga, H. (2004). Reduced anti-oxidative stress activities of DJ-1 mutants found in Parkinson's disease patients. *Biochemical and Biophysical Research Communications*, *320*(2), 389–397. https://doi.org/10.1016/j.bbrc.2004.05.187

Tan, Y.-Y., Jenner, P., & Chen, S.-D. (2022). Monoamine Oxidase-B Inhibitors for the Treatment of Parkinson's Disease: Past, Present, and Future. *Journal of Parkinson's Disease*, *12*(2), 477. https://doi.org/10.3233/JPD-212976

Tang, Y., Han, L., Li, S., Hu, T., Xu, Z., Fan, Y., Liang, X., Yu, H., Wu, J., & Wang, J. (2023). Plasma GFAP in Parkinson's disease with cognitive impairment and its potential to predict conversion to dementia. *NPJ Parkinson's Disease*, *9*, 23. https://doi.org/10.1038/s41531-023-00447-7

Tesson, F., Limon-Boulez, I., Urban, P., Puype, M., Vandekerckhove, J., Coupry, I., Pompon, D., & Parini, A. (1995). Localization of I2-Imidazoline Binding Sites on Monoamine Oxidases (∗). *Journal of Biological Chemistry*, *270*(17), 9856–9861. https://doi.org/10.1074/jbc.270.17.9856

Theillet, F.-X., Binolfi, A., Bekei, B., Martorana, A., Rose, H. M., Stuiver, M., Verzini, S., Lorenz, D., van Rossum, M., Goldfarb, D., & Selenko, P. (2016). Structural disorder of monomeric α-synuclein persists in mammalian cells. *Nature*, *530*(7588), Artigo 7588. https://doi.org/10.1038/nature16531

Tong, J., Ang, L.-C., Williams, B., Furukawa, Y., Fitzmaurice, P., Guttman, M., Boileau, I., Hornykiewicz, O., & Kish, S. J. (2015). Low Levels of Astroglial Markers in Parkinson's Disease: Relationship to α-Synuclein Accumulation. *Neurobiology of disease*, *82*, 243–253. https://doi.org/10.1016/j.nbd.2015.06.010

Tong, J., Rathitharan, G., Meyer, J. H., Furukawa, Y., Ang, L.-C., Boileau, I., Guttman, M., Hornykiewicz, O., & Kish, S. J. (2017). Brain monoamine oxidase B and A in human

parkinsonian dopamine deficiency disorders. *Brain: A Journal of Neurology*, *140*(9), 2460–2474. https://doi.org/10.1093/brain/awx172

Triarhou, L. C. (2013). Dopamine and Parkinson's Disease. Em *Madame Curie Bioscience Database [Internet]*. Landes Bioscience. https://www.ncbi.nlm.nih.gov/books/NBK6271/

Tyacke, R. J., Fisher, A., Robinson, E. S. J., Grundt, P., Turner, E. M., Husbands, S. M., Hudson, A. L., Parker, C. A., & Nutt, D. J. (2012a). Evaluation and initial in vitro and ex vivo characterization of the potential positron emission tomography ligand, BU99008 (2-(4,5-Dihydro-1H-imidazol-2-yl)-1- methyl-1H-indole), for the imidazoline2 binding site. *Synapse*, *66*(6), 542.

Tyacke, R. J., Fisher, A., Robinson, E. S. J., Grundt, P., Turner, E. M., Husbands, S. M., Hudson, A. L., Parker, C. A., & Nutt, D. J. (2012b). Evaluation and initial in vitro and ex vivo characterization of the potential positron emission tomography ligand, BU99008 (2-(4,5-dihydro-1H-imidazol-2-yl)-1- methyl-1H-indole), for the imidazoline$_2$ binding site. *Synapse (New York, N.Y.)*, *66*(6), 542–551. https://doi.org/10.1002/syn.21541

Tyacke, R. J., Myers, J. F. M., Venkataraman, A., Mick, I., Turton, S., Passchier, J., Husbands, S. M., Rabiner, E. A., Gunn, R. N., Murphy, P. S., Parker, C. A., & Nutt, D. J. (2018). Evaluation of 11C-BU99008, a PET Ligand for the Imidazoline2 Binding Site in Human Brain. *Journal of Nuclear Medicine: Official Publication, Society of Nuclear Medicine*, *59*(10), 1597–1602. https://doi.org/10.2967/jnumed.118.208009

Tyacke, R. J., Robinson, E. S. J., Nutt, D. J., & Hudson, A. L. (2002). 5-Isothiocyanato-2-benzofuranyl-2-imidazoline (BU99006) an irreversible imidazoline(2) binding site ligand: In vitro and in vivo characterisation in rat brain. *Neuropharmacology*, *43*(1), 75–83. https://doi.org/10.1016/s0028-3908(02)00074-6

Vaquero, J. J., & Kinahan, P. (2015). Positron Emission Tomography: Current Challenges and Opportunities for Technological Advances in Clinical and Preclinical Imaging Systems. *Annual review of biomedical engineering*, *17*, 385–414. https://doi.org/10.1146/annurev-bioeng-071114-040723

Vasile, F., Dossi, E., & Rouach, N. (2017). Human astrocytes: Structure and functions in the healthy brain. *Brain Structure & Function*, *222*(5), 2017–2029. https://doi.org/10.1007/s00429-017-1383-5

Vekrellis, K., Xilouri, M., Emmanouilidou, E., Rideout, H. J., & Stefanis, L. (2011). Pathological roles of α-synuclein in neurological disorders. *The Lancet Neurology*, *10*(11), 1015–1025. https://doi.org/10.1016/S1474-4422(11)70213-7

Verkhratsky, A., Ho, M. S., Zorec, R., & Parpura, V. (2019). The Concept of Neuroglia. *Advances in experimental medicine and biology*, *1175*, 1–13. https://doi.org/10.1007/978-981-13-9913-8_1

Verkhratsky, A., Parpura, V., Li, B., & Scuderi, C. (2021). Astrocytes: The Housekeepers and Guardians of the CNS. *Advances in neurobiology*, *26*, 21–53. https://doi.org/10.1007/978-3-030-77375-5_2

Villemagne, V. L., Harada, R., Doré, V., Furumoto, S., Mulligan, R., Kudo, Y., Burnham, S., Krishnadas, N., Bozinovski, S., Huang, K., Lopresti, B. J., Yanai, K., Rowe, C. C., & Okamura, N. (2022). First-in-Humans Evaluation of ^{18}F-SMBT-1, a Novel ^{18}F-Labeled Monoamine Oxidase-B PET Tracer for Imaging Reactive Astrogliosis. *Journal of Nuclear Medicine*, *63*(10), 1551–1559. https://doi.org/10.2967/jnumed.121.263254

Wakabayashi, K., Hayashi, S., Yoshimoto, M., Kudo, H., & Takahashi, H. (2000). NACP/α-synuclein-positive filamentous inclusions in astrocytes and oligodendrocytes of Parkinson's disease brains. *Acta Neuropathologica*, *99*(1), 14–20. https://doi.org/10.1007/PL00007400

Wilson, H., Dervenoulas, G., Pagano, G., Tyacke, R. J., Polychronis, S., Myers, J., Gunn, R. N., Rabiner, E. A., Nutt, D., & Politis, M. (2019). Imidazoline 2 binding sites reflecting astroglia pathology in Parkinson's disease: An in vivo11C-BU99008 PET study. *Brain: A Journal of Neurology*, *142*(10), 3116–3128. https://doi.org/10.1093/brain/awz260

Woodard, C. M., Campos, B. A., Kuo, S.-H., Nirenberg, M. J., Nestor, M. W., Zimmer, M., Mosharov, E. V., Sulzer, D., Zhou, H., Paull, D., Clark, L., Schadt, E. E., Sardi, S. P., Rubin, L., Eggan, K., Brock, M., Lipnick, S., Rao, M., Chang, S., … Noggle, S. A. (2014). IPSC-Derived Dopamine Neurons Reveal Differences between Monozygotic Twins Discordant for

Parkinson's Disease. *Cell Reports*, *9*(4), 1173–1182. https://doi.org/10.1016/j.celrep.2014.10.023

Xia, Q., Liao, L., Cheng, D., Duong, D. M., Gearing, M., Lah, J. J., Levey, A. I., & Peng, J. (2008). Proteomic identification of novel proteins associated with Lewy bodies. *Frontiers in Bioscience: A Journal and Virtual Library*, *13*, 3850–3856. https://doi.org/10.2741/2973

Yamada, M., Komatsu, J., Nakamura, K., Sakai, K., Samuraki-Yokohama, M., Nakajima, K., & Yoshita, M. (2020). Diagnostic Criteria for Dementia with Lewy Bodies: Updates and Future Directions. *Journal of Movement Disorders*, *13*(1), 1–10. https://doi.org/10.14802/jmd.19052

Yang, Y., Shi, Y., Schweighauser, M., Zhang, X., Kotecha, A., Murzin, A. G., Garringer, H. J., Cullinane, P. W., Saito, Y., Foroud, T., Warner, T. T., Hasegawa, K., Vidal, R., Murayama, S., Revesz, T., Ghetti, B., Hasegawa, M., Lashley, T., Scheres, S. H. W., & Goedert, M. (2022). *Cryo-EM structures of a-synuclein filaments from Parkinson's disease and dementia with Lewy bodies* (p. 2022.07.12.499706). bioRxiv. https://doi.org/10.1101/2022.07.12.499706

Yang, Z., & Wang, K. K. W. (2015). Glial Fibrillary acidic protein: From intermediate filament assembly and gliosis to neurobiomarker. *Trends in neurosciences*, *38*(6), 364–374. https://doi.org/10.1016/j.tins.2015.04.003

You, H., Wu, T., Du, G., Huang, Y., Zeng, Y., Lin, L., Chen, D., Wu, C., Li, X., Burgunder, J.-M., & Pei, Z. (2021). Evaluation of Blood Glial Fibrillary Acidic Protein as a Potential Marker in Huntington's Disease. *Frontiers in Neurology*, *12*, 779890. https://doi.org/10.3389/fneur.2021.779890

Yun, J., Yeo, I. J., Hwang, C. J., Choi, D.-Y., Im, H.-S., Kim, J. Y., Choi, W. R., Jung, M. H., Han, S.-B., & Hong, J. T. (2018). Estrogen deficiency exacerbates Aß-induced memory impairment through enhancement of neuroinflammation, amyloidogenesis and NF-κB activation in ovariectomized mice. *Brain, Behavior, and Immunity*, *73*, 282–293. https://doi.org/10.1016/j.bbi.2018.05.013

Zhang, J., Li, X., & Li, J.-D. (2019). The Roles of Post-translational Modifications on α-Synuclein in the Pathogenesis of Parkinson's Diseases. *Frontiers in Neuroscience*, *13*, 381. https://doi.org/10.3389/fnins.2019.00381

Zhou, J., Zhang, J., Li, Y., Du, L., Li, Z., Lei, F., Wing, Y.-K., Kushida, C. A., Zhou, D., & Tang, X. (2015). Gender differences in REM sleep behavior disorder: A clinical and polysomnographic study in China. *Sleep Medicine*, *16*(3), 414–418. https://doi.org/10.1016/j.sleep.2014.10.020

Supplementary Data

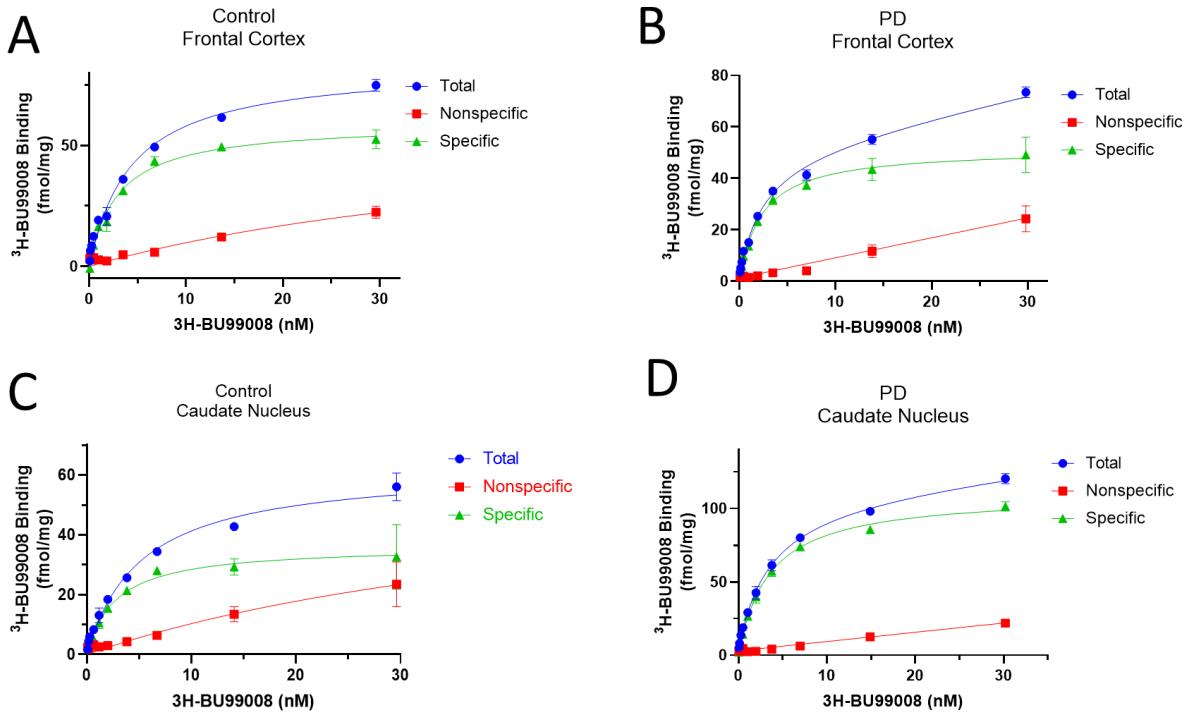


Figure S. 1 - ^{3}H-BU99008 Saturation Binding Assay. This study was performed in Frontal Cortex (A, B) brain homogenates from one CN and one PD case and in Caudate nucleus (C,D) in one CN and two PD cases, using increasing concentrations of ^{3}H-BU99008 (0-30nM). A,B,C,D show saturation binding curves for CN (82yo) and PD (83,68yo) cases, respectively, along with the correspondent Scatchard plot. The second binding sites presented were drawn manually. Data are presented as means ± SEM of three experiments in duplicate. Kd- dissociation constant; Bmax - density of binding sites.

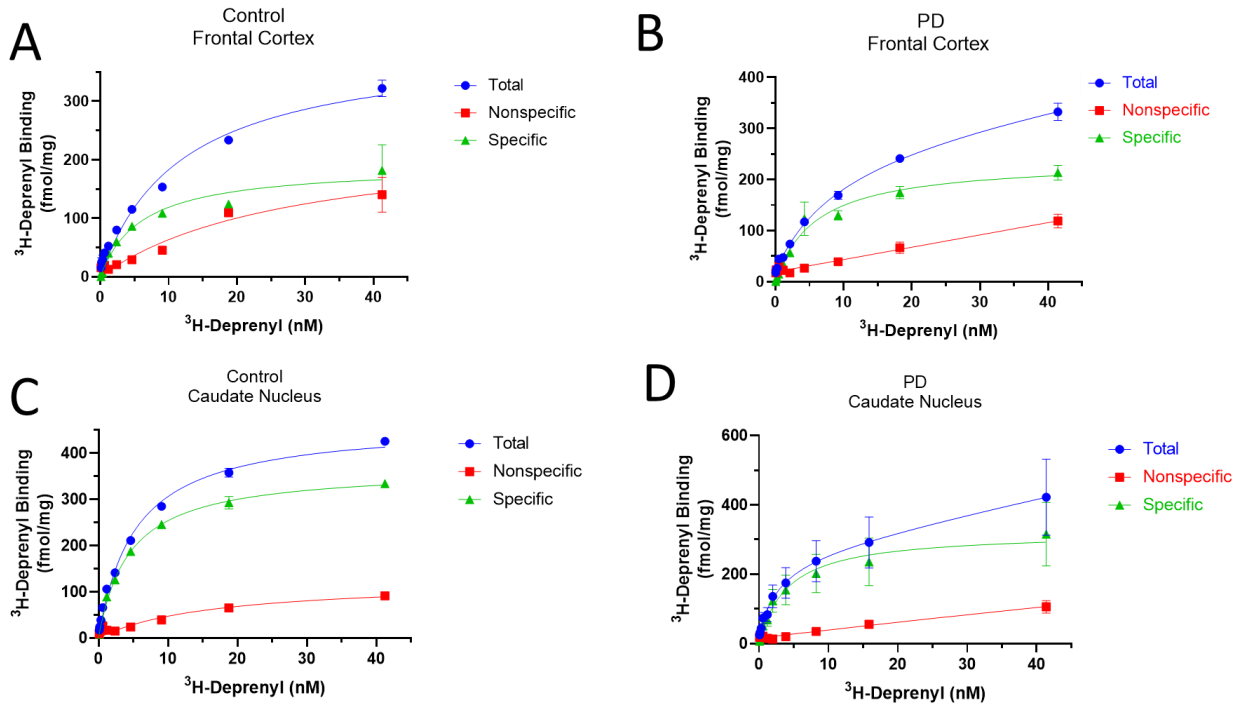


Figure S. 2 - ^{3}H-Deprenyl Saturation Binding Assay. This study was performed in Frontal Cortex (A, B) brain homogenates from one CN and three PD case and in Caudate nucleus (C,D) in one CN and three PD cases, using increasing concentrations of ^{3}H-Deprenyl (0-40nM). A,B,C,D show saturation binding curves for CN (82yo) and PD (66,68,83yo) cases, respectively, along with the correspondent Scatchard plot. The second binding sites presented were drawn manually. Data are presented as means ± SEM of two experiments in duplicate. Kd- dissociation constant; Bmax - density of binding sites.

Table S. 1 - ^{3}H-BU99008 autoradiography - Total, Non-specific and specific binding (fmol/mg) in PD and CN cases.

	^{3}H-BU99008 vs BU99008 ATRDG (fmol/mg)					
	PD			CN		
	Total	NSP	Specific	Total	NSP	Specific
FC	365.2	8.1	357.1	244.3	1.5	242.8
TC	338.1	12.3	325.9	179.6	0.0	179.6
Caudate nucleus	516.6	9.9	506.7	285.9	1.3	284.7
Putamen	456.7	7.7	449.0	330.4	0.0	330.4

Table S. 2 - ^{3}H-BU99008 in the presence of unlabeled Deprenyl autoradiography - Total, Non-specific and specific binding (fmol/mg) in PD and CN cases.

	^{3}H-BU99008 vs Deprenyl ATRDG (fmol/mg)					
	PD			CN		
	Total	NSP	Specific	Total	NSP	Specific
FC	152.0	1.6	150.5	115.4	0.3	115.1
TC	144.0	0.9	143.1	123.5	0.3	123.2
Caudate nucleus	212.3	2.3	210.0	39.2	1.8	37.4
Put	195.2	0.9	194.2	105.0	0.0	105.0

Table S. 3 - ^{3}H-Deprenyl autoradiography - Total, Non-specific and specific binding (fmol/mg) in PD and CN cases

	^{3}H-Deprenyl vs Deprenyl ATRDG (fmol/mg)					
	PD			CN		
	Total	NSP	Specific	Total	NSP	Specific
FC	413.7	0.0	413.7	353.9	1.9	352.0
TC	434.2	0.0	434.2	341.1	0.4	340.6
Caudate nucleus	638.2	29.5	608.7	566.7	4.5	562.2
Putamen	546.9	8.2	538.7	493.9	0.1	493.8